REACTOR MATERIALS

A Quarterly Technical Progress Review

Prepared for DIVISION OF TECHNICAL INFORMATION, U. S. ATOMIC ENERGY COMMISSION,
by BATTELLE MEMORIAL INSTITUTE, COLUMBUS LABORATORIES

ENGINEERING LIBRARY

Summer 1969

● VOLUME 12

● NUMBER 2

TECHNICAL PROGRESS REVIEWS

The United States Atomic Energy Commission publishes the Technical Progress Reviews to meet the needs of industry and government for concise summaries of current nuclear developments. Each journal digests and evaluates the latest findings in a specific area of nuclear technology and science. *Nuclear Safety* is a bimonthly journal; the other three are quarterly journals.

Isotopes and Radiation Technology
P. S. Baker, A. F. Rupp, and associates
Isotopes Information Center, Oak Ridge National Laboratory

Nuclear Safety
Wm. B. Cottrell, W. H. Jordan, J. P. Blakely, and associates
Nuclear Safety Information Center, Oak Ridge National Laboratory

Reactor and Fuel-Processing Technology

Reactor Materials
E. M. Simons and associates
Battelle Memorial Institute, Columbus Laboratories

All are available from the U. S. Government Printing Office. See the back cover for ordering instructions.

The views expressed in this publication do not necessarily represent those of the United States Atomic Energy Commission, its divisions or offices, or of any Commission advisory committee or contractor.

Availability of Reports Cited in This Review

United States Atomic Energy Commission (USAEC) reports are available at USAEC depository libraries and are sold by the Clearinghouse for Federal Scientific and Technical Information (CFSTI), National Bureau of Standards, U. S. Department of Commerce, Springfield, Va. 22151. All reports sold by CFSTI are $3.00 for printed copy and $0.65 for microfiche. Each separately bound part of a report is priced as a separate report. Some reports may not be available because of their preliminary nature; however, the information contained in them will generally be found in later progress or topical reports on the subject.

Other U. S. Government agency reports identified in this journal generally are available from CFSTI.

Private-organization reports should be requested from the originator.

United Kingdom Atomic Energy Authority (UKAEA) and Atomic Energy of Canada Limited (AECL) reports are available at USAEC depository libraries. UKAEA reports are sold by Her Majesty's Stationery Office, London; AECL reports are sold by the Scientific Document Distribution Office, Atomic Energy of Canada Limited, Chalk River, Ontario, Canada. UKAEA and AECL reports issued after March 1, 1967, are sold by CFSTI to purchasers in the United States and its territories.

REACTOR MATERIALS

Vol. 12, No. 2 Summer 1969

Contents

Fuel and Fertile Materials (Section I)

Uranium Metal and Alloys . . . 73
Plutonium . . . 74
Thorium and Its Alloys . . . 78
Metal–Ceramic Fuels . . . 78
Uranium and Thorium Oxides . . . 79
Uranium Carbide, Nitride, and Sulfide Fuels . . . 81
Fuel Reactions Following Loss-of-Coolant Accidents . . . 83
Mechanism of Corrosion of Fuel Alloys . . . 83
Basic Studies of Irradiation Effects in Fuel Materials . . . 83
References . . . 85

Moderator and Control Materials (Section II)

Graphite . . . 89
Beryllium Metals and Alloys . . . 89
Beryllium Oxide . . . 92
Solid Hydrides . . . 92
Nuclear Poisons . . . 93
References . . . 94

Cladding and Structural Materials (Section III)

Corrosion by Aqueous and Gaseous Media . . . 95
Corrosion by Nonaqueous Liquids and Vapors . . . 98
Cladding Reactions Following Loss-of-Coolant Accidents . . . 104
Radiation Effects in Structural Materials . . . 106
Metallurgy and Mechanical Properties of Common Cladding and Structural Materials . . . 115
Metallurgy and Mechanical Properties of Refractory Metals . . . 121
Nonfueled Refractories . . . 123
Concrete . . . 130
Ceramic Technology . . . 131
Diffusion Studies . . . 132
References . . . 135

Special Fabrication Techniques (Section IV)

Melting, Casting, and Fabrication of Cast Structures . . . 141
Powder-Metallurgy Materials and Techniques . . . 143
Chemical Plating . . . 145
Explosive Metalworking . . . 147
Welding and Brazing . . . 148
Nondestructive Testing . . . 151
References . . . 152

Superintendent of Documents, U. S. Government Printing Office, Washington, D. C. 20402, $2.50 per year

Reactor Materials

is one of a series of quarterly technical progress reviews broadly covering the field of nuclear science and technology. Under the auspices of the USAEC Division of Technical Information, *Reactor Materials* is prepared by Battelle personnel from worldwide literature. It covers properties, behavior, and fabrication processes of materials applicable to nuclear reactor components and associated equipment.

The reader will recognize that the scope of this Review is too broad to permit detailed coverage of every topic. Rather, the authors and editors attempt to combine the highlights of significant new developments into an information summary of current research for both management and the technical specialist. As a rule, enough of the results are presented to define the research and summarize the findings. For readers desiring more information on any particular topic, a complete set of references is provided at the end of each section.

Each quarter a number of bibliographies, monographs, and books appear on subjects within the scope of *Reactor Materials*. Although the main purpose of this Review is to call attention to findings that are new and significant, such publications are noted in the text because they often represent excellent compilations of available information on important materials topics.

E. M. Simons
D. L. Keller

BATTELLE MEMORIAL INSTITUTE
COLUMBUS LABORATORIES

Issued quarterly by the U. S. Atomic Energy Commission. Use of funds for printing this publication approved by the Director of the Bureau of the Budget on May 12, 1969.

Section

I

Reactor Materials

Fuel and Fertile Materials

Uranium Metal and Alloys

Unalloyed Uranium

The effect of postirradiation annealing on fission-gas bubbles in uranium has been studied by the British[1] with electron-microscope techniques. Irradiation was performed at temperatures of 400 to 715°C to burnups in the range 0.01 to 0.19 at.%. Bubble growth was very slow after annealing for up to 1000 hr at 600°C. Annealing at 800°C resulted in a slow but measurable bubble growth. The application of stress during annealing at 600°C did not affect the coarsening rate of 100-A-diameter bubbles.

The presence of an axial hole in Zircaloy-2-clad uranium rods was found[2] to prevent swelling due to irradiation under power-reactor conditions in the Engineering Test Reactor (ETR), as illustrated in Fig. I-1. As may be seen, 4 vol.% swelling occurs with Zircaloy-2-clad solid uranium rod after a fuel exposure of less than 3000 Mwd/ton, compared with a slight contraction in the hollow-core fuel element at 1 at.% burnup (8700 Mwd/ton). The improvement is attributed to a combination of restraint by the cladding and the presence of the center void, which gradually closes as burnup progresses.

Annealing of nickel-plated and unplated uranium for 3 hr at 550°C under a 10^{-3}-torr vacuum after fabrication was found[3] to improve the room-temperature ductility. This improvement was attributed to a reduction in hydrogen. Integrity of the nickel plate was destroyed during the anneal.

When a U–250 ppm Fe–710 ppm Al–1000 ppm C–50 ppm Si alloy is heated at temperatures in the range 350 to 600°C, UAl_2 phase precipitates from the alpha-phase alloy at a predictable rate.[4] The kinetics of this process are illustrated in Fig. I-2. The time dependence of the precipitation process is consistent with precipitation occurring at subgrain boundaries and on individual dislocations within subgrains.

The alpha-to-beta transition temperature for the U–350 ppm Fe–350 ppm Si–800 ppm Al alloy was shown[5] to be 660 ± 2°C on heating and 627 ± 2°C on cooling at a rate of 2°C/min. Upon prolonged alpha annealing and quenching, this alloy and a U–350 ppm Fe–800 ppm Al alloy were found to be superior to unalloyed uranium in structural properties and stability.[6]

Zircaloy-2-clad U–250 ppm Fe–770 ppm Al–330 ppm Si–600 ppm C alloy fuel elements were heated under steam–water conditions akin to those contemplated in an Italian reactor.[7] The cladding was intentionally defected prior to testing. Lower corrosion rates were observed with fuels that had been beta heat-treated prior to testing than with those tested in the as-coextruded condition. Typical conditions were 282°C water temperature, 71 atm pressure, 400°C fuel temperature, and a thermal gradient up to 120°C across the fuel element. Early detection of leakage in actual reactor operation was considered very important.

French investigators[8,9] have examined grain-refining effects and transformation kinetics of

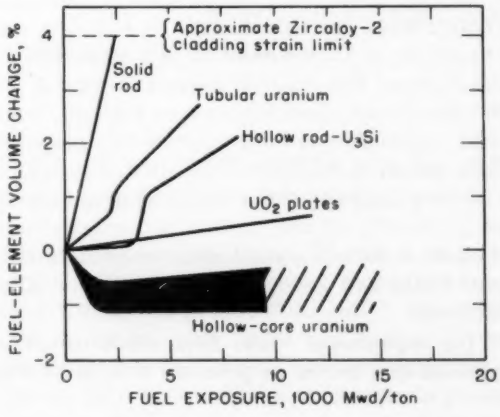

Fig. I-1 Comparison of irradiation behavior of hollow-core uranium fuel element with that of other fuel types.[2]

uranium-base alloys. The alloying agents studied were Cr, Si, Mo, Zr, B, Be, C, and P. A grain-refining effect was noted[10] in U–Cr alloys when a stress was applied in the temperature range where nucleation is slow.

When a gamma-phase U–1.5 Mo* alloy specimen is cooled rapidly, all of the gamma is transformed.[11] Morphological and crystallographic characteristics of the transformation are those of discontinuous precipitation reactions.

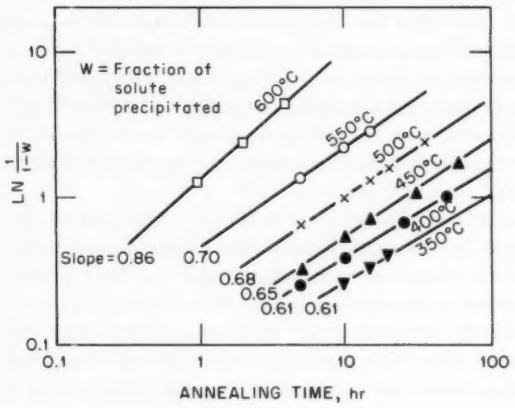

Fig. I-2 Effect of annealing time and temperature on amount of UAl_2 precipitated from U–250 ppm Fe–710 ppm Al–1000 ppm C–50 ppm Si alloy.[4]

Gamma-Phase Uranium Alloys

Heat content of the U–10 Mo alloy has been found[12] to follow the relations

$$H_T{}^\circ\text{C} - H_0{}^\circ\text{C} = 3.217 \times 10^{-2} T + 8.852 \times 10^{-6} T^2 \quad (0 \text{ to } 1000^\circ\text{C})$$

or

$$H_T{}^\circ\text{K} - H_{298}{}^\circ\text{K} = 2.734 \times 10^{-2} T + 8.852 \times 10^{-6} T^2 - 8.932 \quad (298 \text{ to } 1273^\circ\text{K})$$

where H_T is the heat content at the temperature of interest (cal/g) and T is the temperature (°C or °K as indicated).

The experimental values from which the above equations were derived are presented in Table I-1. The relation of specific heat with temperature was obtained by differentiation. This expression is

$$C_p = 2.734 \times 10^{-2} + 1.77 \times 10^{-5} T \quad (298 \text{ to } 1273^\circ\text{K})$$

(J. M. Fackelmann)

Table I-1 Experimental Heat-Content Values for U–10 Mo (Ref. 12)

Temp., °C	Heat content, cal/g
0	0
83	2.79
82	2.78
122	4.09
227	7.76
226	7.74
292	10.23
291	10.28
456	16.46
456	16.46
553	20.45
551	20.36
682	25.88
686	25.76
859	34.13
854	34.95
1001	40.71
401*	14.79
396*	14.32

*Data obtained upon cooling from previous temperature.

Plutonium

Plutonium Metal and Alloys

The temperature and strain-rate dependency of the modes of plastic deformation have been evaluated by Battelle–Northwest investigators[13] for high-purity as-cast alpha plutonium. Grain-boundary sliding and slip were studied by examining structures formed on polished surfaces with 4.5% compressive deformation. Grain-boundary sliding predominated at high temperatures and low strain rates (110°C and 10^{-4} min^{-1}), whereas slip was the primary mode of deformation in alpha plutonium at low temperatures and high strain rates (−10°C and 10^{-1} min^{-1}). Recrystallization occurred concurrently with deformation only after critical strains of approximately 14, 6, and 3% were

*Unless otherwise designated, all compositions are understood to be in weight percent.

reached at 105, 110, and 120°C, respectively, irrespective of the strain rate.

Investigators at Rocky Flats[14] have measured the cerium diffusion in delta-stabilized Pu–Ce alloys by electron-microprobe analysis. Diffusion couples prepared from two compositions (3.74 and 7.17 wt.% cerium) were annealed between 403 and 528°C for periods from 8 to 76 days. A least-squares treatment of the diffusivities yielded an expression of the form

$$D = 1.31 \times 10^{-2} \exp(-29{,}600 \pm 1200/RT) \quad \text{cm}^2/\text{sec}$$

When these findings are compared with similar data for the Pu–Ga system, it is noted that cerium diffuses faster than gallium at the temperatures investigated.

Electron-probe microanalysis was used by Livermore investigators[15] to identify six intermetallic compounds in the Pu–Pb alloy system. In addition to $PuPb_3$ (the existence of which has been previously well established), the investigation revealed the existence of Pu_3Pb, Pu_5Pb_3, $PuPb_2$, Pu_5Pb_4, and, tentatively, Pu_4Pb_5. The Pu_3Pb and Pu_5Pb_3 phases yielded X-ray-diffraction powder patterns that are consistent with these formulas. The $PuPb_2$ and Pu_5Pb_4 yielded single-phase melts, as established by metallography.

The crystal structure of Pu_3Zn_{22} has been identified by researchers at Lawrence Radiation Laboratory[16] from diffractometrically recorded single-crystal intensities. The unit cell is body-centered tetragonal with $a = 8.85$ A and $c = 21.18$ A. The compound has a calculated density of 8.71 g/cm^3. This structure is similar to that of Ce_3Zn_{22} in the Ce–Zn system ($a = 8.930$ A, $c = 21.36$ A).

Investigators at Argonne[17] have studied the ternary Th–U–Pu alloy system by means of metallography, room- and high-temperature X-ray diffraction, dilatometry, electrical-resistivity measurements, and differential thermal analysis. Most of the ternary alloys are alloys in which the phases of the U–Pu system are in equilibrium with alpha thorium. Since the addition of uranium to the (Th,Pu) solid solution greatly lowers the solid solubility of plutonium in thorium, the potentially useful fuel alloys are restricted to a range of compositions with no more than 10 at.% plutonium and up to 25 at.% uranium.

The irradiation behavior of high-burnup U–Pu alloy fuel elements is the subject of a continuing study at Argonne.[18] Alloys selected for this study were U–Pu–Fs (fissium), U–Pu–Zr, and U–Pu–Ti. The most promising alloy tested for fast breeder application was the U–Pu–Zr composition, which contains approximately 15 wt.% plutonium and 10 to 15 wt.% zirconium. Successful irradiations were performed with this alloy at maximum cladding temperatures of 655°C and a burnup of 12.5 at.%. The irradiation studies have been conducted with cylindrical fuel pins sodium-bonded to tubular cladding. Fuel-element design proved to be a significant variable. Improved performance was obtained by allotting sufficient space for annular fuel swelling to accommodate solid fission products and to enable a significant fraction of the fission gas to be released from the fuel alloy.

(D. F. Askey)

Plutonium Compounds

Conversion of PuO_2 to the tetrafluoride by 15-min fluorination was found by Rocky Flats workers[19] to be 93% complete when done at 28°C and 99% at 300°C. The impurities B, Cr, Mo, Si, Ta, and Ti in the PuO_2 were removed in significant quantities by this process. Oak Ridge has reported[20] a one-step process to convert PuF_6 to PuO_2. The conversion was performed at 1000°C in a H_2/H_2O atmosphere. Ohse and Ciani[21a] measured the vapor pressure of hypostoichiometric plutonium oxide as functions of temperature and composition. The results, shown in Fig. I-3, indicate a minimum in the vapor pressure at an O/Pu ratio near 1.87. Microstructural and X-ray diffraction results for the Pu–O and Pu–U–O systems are reported[21b] by Sari, Benedict, and Blank.

Measurements of the physical and thermal properties of the mixed oxides PuO_2–UO_2 are in progress at a number of sites. General Electric reports[22] that the mean thermal conductivity to the melting point of stoichiometric UO_2–20 mole % PuO_2 is 11% lower than that of UO_2, and the thermal conductivity of hypostoichiometric (O/M = 1.98) mixed oxide is 6% less than that of UO_2. The thermal conductivity of stoichiometric UO_2–20 mole % PuO_2 is also reported by Battelle–Northwest.[23] Ogard and Leary[21c] measured the heat content and heat capacities of both hypostoichiometric and stoichiometric UO_2–19.8 mole % PuO_2 up to 2400°K, with the results shown in Fig. I-4. The melting point as a function of stoichiometry for PuO_{2-x} and $U_{0.6}Pu_{0.4}O_{2-x}$ was measured by General Electric,[24] and a maximum melting temperature was reported in the O/Pu region from 1.70 to 1.80 as 2470°C for PuO_{2-x} and 2780°C for the mixed oxide. Rand and Markin[21d] used free-energy data derived from measured oxygen potentials for UO_2–PuO_2 mixtures to calculate the pressure and composition of the vapor above UO_2–15 mole % PuO_2 as a function of time at 2000°K. The change in fuel stoichiometry resulting from the large pressure

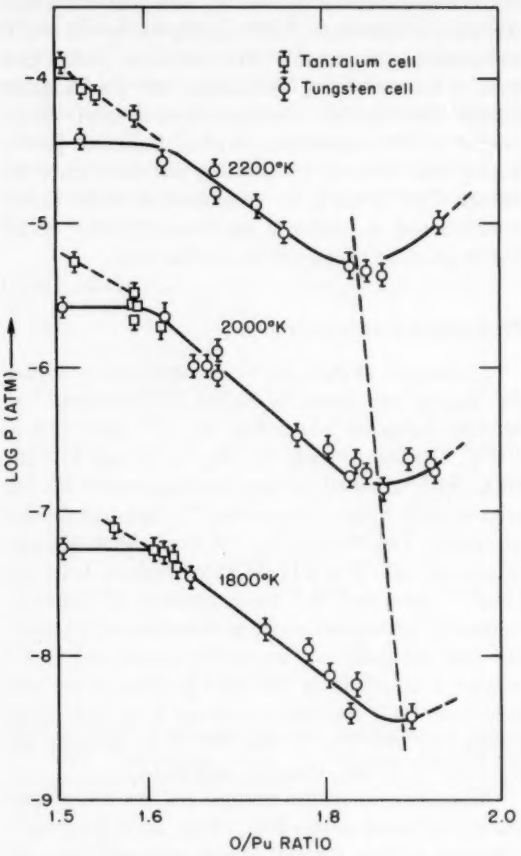

Fig. I-3 Vapor-pressure isotherms of substoichiometric plutonium oxide.[21a]

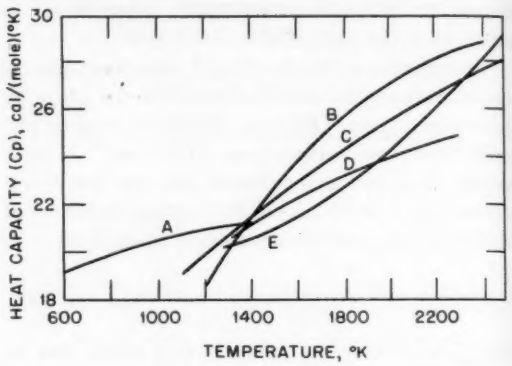

Fig. I-4 High-temperature heat capacities of UO_2 and UO_2–PuO_2 solid solutions.[21c] A, UO_2 (Moore and Kelley); B, $U_{0.802}Pu_{0.198}O_{2.00}$ (Ogard and Leary); C, $U_{0.802}Pu_{0.198}O_{1.98}$ (Ogard and Leary); D, UO_2 (Ogard and Leary); E, UO_2 (Conway and Hein).

gradients during irradiation to 7.03 at.% burnup was considered. Wirtz[25] discussed his studies in Germany on UO_2–PuO_2 fuel at high temperature, using experimental data to confirm the validity of a kinetic model of thermal diffusion.

The sol-gel process has been used for the preparation of PuO_2 and PuO_2–UO_2 fuel particles. Babcock & Wilcox[26] indicate that the gel-addition technique is suitable for thermal-reactor fuels containing 1 to 10 mole % PuO_2, but not for fast reactor fuel material. Emphasis has been shifted to the mixed-sol process. Lloyd and Haire[27] have worked out sol-gel procedures for the preparation of microspheres of PuO_2, PuO_2–ThO_2, and PuO_2–UO_2. Oak Ridge[28a] has utilized the dried-sol technique to produce sinterable-grade UO_2–PuO_2 for both pelletizing and extrusion. Mound reports[29] that the crushing strength of $^{238}PuO_2$ microspheres made by the plasma technique was unaffected by aging for as long as 17 months.

Mound has also reported[30] other studies involving $^{238}PuO_2$ microspheres. An elutriation process is described for the removal of fine particulate oxide ($<47\ \mu$) from microsphere batches. The sol-gel process is under development for the preparation of microspheres; batches up to 58 g of ^{238}Pu have been processed.[31] Helium release from plasma spheres has been determined for the temperature range 600 to 1200°C. After 483 days at 538°C, 13% of the helium was released, whereas 90% was released after 443 days at 1100°C. Because of self-irradiation damage, the lattice parameter increased from 5.4000 ± 0.0003 A to 5.4148 ± 0.0006 A after 4 months at 100°C. Microspheres of $^{238}PuO_2$ were mixed with 10 types of soil and heated to 1000°C for 8 hr (Ref. 32). No reaction was observed, and no significant postexposure differences in the particle crush strength or apparent density were detected.

Irradiation results have been presented for typical thermal-reactor fuel materials. Battelle–Northwest[33] has examined UO_2–2 mole % PuO_2 after a peak burnup of 9700 Mwd/metric ton and a nominal linear power rating of 18 kw/ft. Thirty-eight percent of the xenon and krypton formed was released from the Vipac fuel. The internal fuel-rod pressure was approximately 40 psia lower than the predicted value. The surface dose rate from plutonium which contained 3 at.% or more ^{241}Pu did not increase with time to the degree expected from earlier data. Belgian studies[34,35]

have utilized Vipac fuel rods of both homogeneous and heterogeneous UO_2–PuO_2 fuel. The gas released by the homogeneous fuel, in comparison with gas from the heterogeneous material, was higher in CO_2 and CH_4, lower in hydrogen, and less in overall volume by an order of magnitude. The homogeneous fuel rods swelled 1 to 2%, whereas the heterogeneous rods showed no swelling.

Irradiation results have also been presented for typical fast reactor fuel materials. Argonne[36a] performed an electron-microprobe analysis of UO_2–20 mole % PuO_2 Vipac fuel after 2.7 at.% burnup in Experimental Breeder Reactor II (EBR-II). Fission products that indicated no detectable migration were Zr, La, Ce, Pr, Nd, and Sm. There were no detectable differences in the distribution of fission products stemming from the fast-flux irradiation of the mixed oxide as compared with those found in a thermal-flux-irradiated enriched UO_2 fuel. General Electric[37] reported that significant amounts of ^{137}Cs can be volatilized from a vented fuel element if the temperature of the blanket is sufficiently high. The lattice disruption was more severe in $U_{0.75}Pu_{0.25}O_2$ following burnups to 50,000 Mwd/metric ton in a fast flux than in the same fuel following burnups to 255,000 Mwd/metric ton in a thermal flux. Nuclear Materials & Equipment Corp. (NUMEC)[38] obtained irradiation data for mechanically blended and coprecipitated UO_2–20 mole % PuO_2 after burnups to 49,800, 65,100, and 70,500 Mwd/metric ton at a linear heat rating of 9 kw/ft. Battelle–Northwest[39] has compiled a literature survey of UO_2–PuO_2 irradiation results and problem areas to aid in the conceptual design of fuel for the Fast Flux Test Facility (FFTF).

Irradiation results for pure plutonium oxide have also been reported. Russian[40] data were obtained for PuO_2 pellets irradiated at BR-5 to a burnup of 6.1 at.% over a 5.5-year span. Gaseous swelling of the PuO_2 at 900 to 1400°C was observed. A maximum swelling rate of 2.8%/at.% burnup was measured. The release of gaseous fission products amounted to about 80% of the amount formed. Workers at Battelle–Northwest[2] also conducted irradiations of plutonium oxides. Their burnups were 12.9×10^{21} fissions/cm^3 (55 at.%) in PuO_2 and 9.0×10^{21} fissions/cm^3 in beta Pu_2O_3.

A number of binary and ternary oxide systems involving PuO_2 have been examined. NUMEC[41] carried out a phase study and melting-point determinations for the ternary PuO_2–ZrO_2–UO_2. Irradiation data for the burnup range 5000 to 17,800 Mwd/metric ton are given for compositions containing 6 to 10 vol.% PuO_2. Battelle–Columbus[42] has studied the PuO_2–ThO_2–BeO system and reports on the thermal stability of $(Th,Pu)O_2$ particles prepared by the sol-gel process. Los Alamos[43] reviews the merits of PuO_2–ZrO_2 and PuO_2–ThO_2 solid solutions for application as isotropic heat-source material. Thermal and physical data for a composition containing 40 mole % $^{238}PuO_2$ (1.7 watts/cm^3) are given. Phase studies in the PuO_2–Lu_2O_3 system were performed at Karlsruhe.[44]

Plutonium-bearing carbides and nitrides have received attention. French investigators[45] have reported studies in the Pu–C–N, U–C–N, and (U,Pu)–C–N systems. Potter[21e] has determined the phase relations in the Pu–C–O system and the evaporation from plutonium monoxycarbides as a function of composition. Olson and Mulford[21f] present thermodynamic and vaporization-behavior data for plutonium carbides. Vapor pressure over PuC–Pu_2C_3 mixtures in the temperature range 1375 to 2000°K is shown in Fig. I-5. Cambell, Mullins, and Leary[21g] have measured

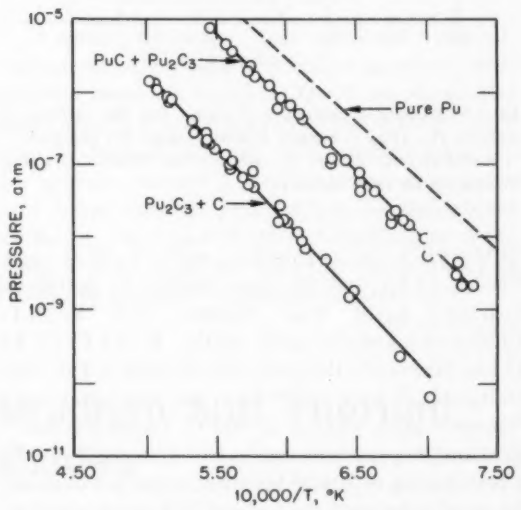

Fig. I-5 Vapor pressures of plutonium over plutonium carbides.[21f]

the free energy of formation of $PuCl_3$, PuN, $PuRu_2$, Pu_2C_3, and PuC by electromotive-force (emf) techniques. Battelle–Northwest[2] presents the melting behavior of PuN, UN–20 mole % PuN, and UN as functions of temperature and nitrogen pressure (Fig. I-6).

Compatibility studies on mixed oxides, carbides, and nitrides with cladding components are continuing. Argonne[46a] reports that UO_2–20 mole % PuO_2

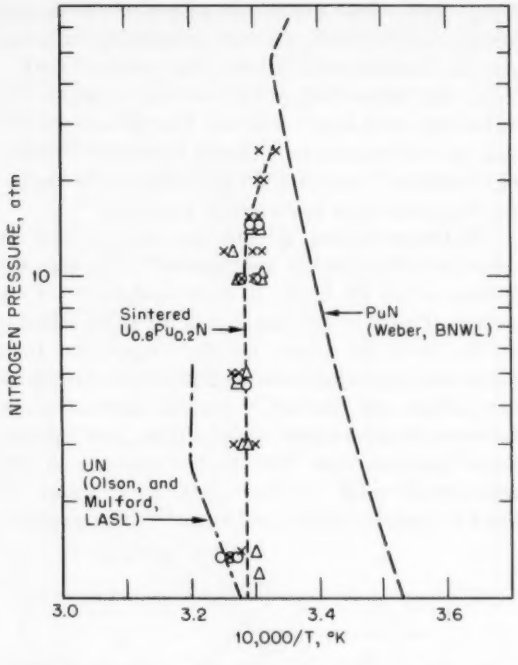

Fig. I-6 Pressure–temperature behavior for the melting of sintered ($U_{0.8}Pu_{0.2}$) nitrides relative to pure UN and PuN.[2] ○, metal-derived nitride; ×, carbothermic nitride; △, carbothermic nitride (high carbon).

(O/M = 1.97) is compatible with V–10 Zr and Vanstar 7,* 8,† and 9‡ after 1000 hr at 800°C. A reaction layer was observed with V–20 Ti (320-μ thickness) and with V–15 Cr–5 Ti (550-μ thickness). However, UC–20 mole % PuC that contained 20 vol.% $(U,Pu)_2C_3$ did not react with Vanstar 9 after 1000 hr at 800°C. United Nuclear[47] irradiated hyperstoichiometric UC–20 mole % PuC to a peak burnup of 30,000 Mwd/metric ton and observed no reaction between the fuel and 316 stainless steel or vanadium. A slight reaction was noted with V–20 Ti. Battelle–Columbus[48] reports that UN–20 mole % PuN is compatible with 304 stainless steel and Nb–1 Zr after 1000 hr at 1000°C. A possible slight reaction was observed between the mixed nitride and vanadium under the same conditions. Battelle–Northwest[2] found that UO_2–25 mole % PuO_2 was compatible with 304 stainless steel after 1000 hr at 1000°C and that UN–20 mole % PuN was compatible with 304 stainless steel after 5000 hr at 1000°C.

*V–9.1 Cr–3.3 Fe–1.3 Zr–0.05 C.
†V–8.5 Cr–9.85 Ta–1.3 Zr–0.05 C.
‡V–6.4 Fe–5.3 Nb–1.3 Zr–0.05 C.

Moser and Kruger[49] determined the thermal conductivity and heat capacity of PuP and PuS. At 650°C the thermal conductivity was 0.019 cal/(sec)(cm)(°C) for PuP and 0.037 for PuS. (M. D. Houston)

Thorium and Its Alloys

A comprehensive summary[50] of most research work on thorium to date has been prepared by Battelle–Northwest. Information pertinent to the use of thorium for heavy-water reactors is given. Effects of irradiation on various thorium-base alloys are described, along with fabrication methods and physical-property data.

The 1000°C isotherm in the Th–U–N ternary system at 50 at.% nitrogen and below was investigated by workers at Oak Ridge.[51] A three-phase equilibrium was found among uranium metal, thorium metal, and the compound $(Th_xU_{1-x})N_y$. The most uranium-rich compound in equilibrium with metallic thorium was found to be $(Th_{0.944}U_{0.056})N_{0.866}$. The 1000°C standard free energy of formation of ThN was estimated to be about −51,100 cal/mole. (R. L. Martin)

Metal–Ceramic Fuels

Dispersions (Less Than 50 Vol.% Ceramic Phase)

Oak Ridge researchers[28b] have studied the swelling behavior of UAl_x–Al and U_3O_8–Al compacts during heat-treatments to prepare the fuel for fabrication into picture-frame fuel elements. Studies of the outgassing at 500°C for 1 hr showed that, in compacts containing up to 35 vol.% fuel, the swelling was a function of the fuel volume but not of the fuel composition. The swelling ranged from 0.5% for approximately 10 vol.% fuel to 2% at 35 vol.% fuel. At 40 vol.% fuel loading, the UAl_x swelled 6 to 9% as a result, in part, of the transformation of UAl_3 to UAl_4, and the U_3O_8 fuel swelled about 2%. The swelling up to about 2% was attributed to evolution of absorbed gases which caused separation at grain boundaries and powder surfaces. The UAl_3 transforms to UAl_4 in discrete layers rather than continuously and generates sufficient stress to cause recrystallization in the aluminum matrix.

The compressive strength of U_3O_8–Al and UAl_3–Al composites was determined at Oak Ridge[28b] over a

fuel-volume range of 0 to 40% at temperatures of 25 to 550°C. The tests were conducted at a crosshead speed of 0.002 in./min with 0.5-in.-diameter by 1.5-in.-long specimens. The compressive strength corresponding to 5% plastic strain in the fuel mixtures is shown in Fig. I-7. For fuel volumes up to about 20%, the strengths of the two mixtures are equivalent at all temperatures studied. As the fuel volume increased, the UAl_3–Al mixtures continued to increase in strength, but the U_3O_8–Al compacts decreased in strength.

(J. T. Smith)

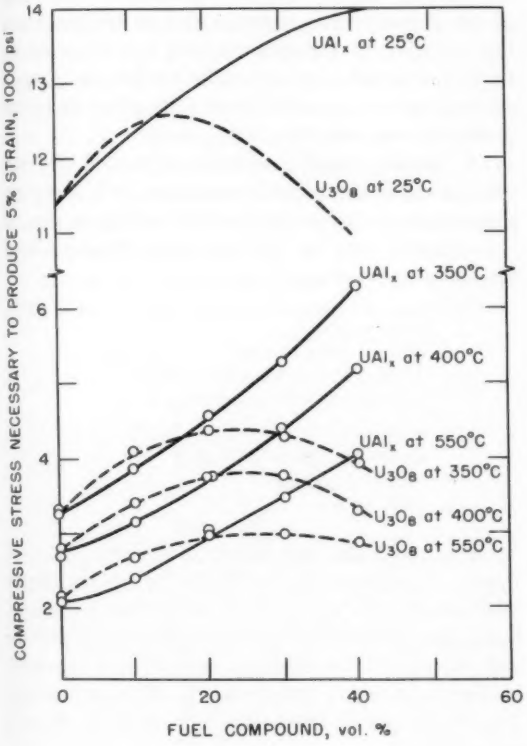

Temp., °C	Corresponding compressive strength of wrought alloys, psi	
	1100	6061
25	10,000	15,400
350	2,000	3,800
400	1,500	2,900
550	900	1,800

Fig. I-7 Compressive yield stress of fuel–aluminum compacts.[28b]

Cermets (Over 50 Vol.% Ceramic Phase)

The thermal conductivity of coated-particle 80 vol.% UO_2–W and 60 vol.% UO_2–W cermets is reported by Grossman.[52] Cermet specimens were fabricated by uniaxial hot pressing to densities greater than 96% of theoretical. Thermal conductivity of the cermets was measured by a radial-heat-flow technique. The experimentally measured conductivities were compared with those predicted by the Bruggeman theory, which applies to dispersed spherical particles in a continuous matrix phase. The following equation was used to predict thermal conductivities:

$$f = \frac{K_D - K}{K_D - K_C} \sqrt[3]{\frac{K_C}{K}}$$

where K = conductivity of cermet
K_D = conductivity of UO_2
K_C = conductivity of tungsten
f = volume fraction of tungsten

It was observed that predicted thermal-conductivity values were in excellent agreement with measured values for 80 vol.% UO_2–W specimens. The model did not fit the measured values for the 60 vol.% UO_2–W specimen, however, since measured values for this specimen showed a positive temperature coefficient rather than the predicted negative temperature coefficient. The measured thermal conductivity of the 80 vol.% UO_2–W cermet was 0.10 watt/(cm)(°C) at 1500°C, or a factor of 5 greater than that of UO_2.

(R. A. Smith)

Uranium and Thorium Oxides

Properties and Behavior

Perron[53] has reported the following conclusions from analysis of existing data on oxygen redistribution in UO_2 during irradiation:

1. Oxygen redistribution does not occur in stoichiometric UO_2 where the axial temperature does not exceed approximately 1650°C unless the fuel also contains significant amounts of oxygen-bearing gases. Without these oxygen-bearing gases, there is no oxygen available for redistribution.

2. In a nonstoichiometric fuel absolutely free of carbon and hydrogen (or moisture), oxygen redistribution is controlled by a uniform oxygen pressure across

the fuel. Thermodynamic equilibrium then requires oxygen depletion of the core of the fuel. This mechanism should apply to carbon-free oxide fuel sheathed with Zircaloy, where hydrogen is gettered by the cladding.

3. For a nonstoichiometric fuel containing carbon or hydrogen, the oxygen redistribution is controlled by a uniform CO_2/CO or H_2O/H_2 ratio across the fuel. The core of a hyperstoichiometric fuel would become enriched in oxygen, whereas the core of a hypostoichiometric fuel would become depleted in oxygen.

Poteat and Morgan[54a] at Oak Ridge have measured thorium self-diffusion in ThO_2. Grain sizes in the sintered material ranged from extremely large to a few microns. The results of these measurements are summarized in Fig. I-8. In the single-crystal ThO_2, thorium self-diffusion followed the relation:

$$D = 2.0 \times 10^{-7} \exp(-74{,}000/RT) \quad cm^2/sec$$

whereas, in the case of the sintered ThO_2, the applicable relation is:

$$D = 2.6 \times 10^{-7} \exp(-69{,}000/RT) \quad cm^2/sec$$

The diffusion rate is increased by decreasing grain size. Grain-size measurements on specimens annealed at 1300°C indicate that the diffusion coefficient is roughly proportional to the grain-boundary or subgrain-boundary size. Also, the results indicate an increase in diffusion coefficient as the measured zone moves deeper into the specimen. This reduced diffusion rate near the surface may be due to the influence of surface forces on atom movement in the grain boundaries. (R. H. Barnes)

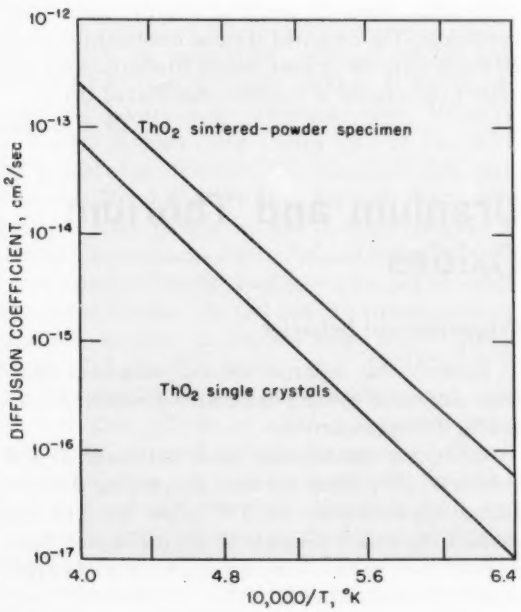

Fig. I-8 Diffusion coefficients of thorium in monocrystalline and polycrystalline thoria.[54a]

Preparation of Fuel Bodies

Japanese investigators[55] have patented a technique for molding uranium dioxide shapes which makes use of the plastic creep properties at high temperatures. For example, an L-shaped molding was prepared by heating a flat slab to 1500 to 2500°C while applying an external force of approximately 3000 psi to deform it plastically into a shaped receiving mold.

A Danish report[56] outlines a process for the manufacture of vibrationally compacted UO_2 fuel pins. Compaction to 83 to 86% of theoretical density is accomplished with an electrodynamic vibrator under the following conditions:

Powder mixture
- 60 wt.% 2000- to 4000-μ UO_2 particles
- 15 wt.% 300- to 500-μ UO_2 particles
- 25 wt.% < 80-μ UO_2 particles

Compaction
- Frequency, 700 to 1000 cps
- Acceleration, 10 *g*'s
- Time, 12 min

A patent[57] has been issued on the preparation of hypostoichiometric UO_2 or ThO_2 by doping. Minor additions (0.1 to 1.0 at.%) of the oxides of yttrium, lanthanum, and niobium are mixed with the fuel oxide and sintered. The dioxides are reduced to a hypostoichiometric state at a temperature in the range 1700 to 2000°C. Oxygen-to-metal ratios of 1.90 to 1.998 have been achieved.

Oak Ridge Gaseous Diffusion Plant[58] has developed techniques for applying thin films of thorium oxide, neptunium oxide, and technetium metal on metal surfaces by electrodeposition. The thorium oxide and technetium films were plated on nickel disks from an ammonium oxalate solution. Thin films of neptunium oxide were applied from an ammonium oxalate or acetate solution, whereas thicker films could be applied only from an ammonium acetate solution. Deposits ranged from 0.001 mg/cm² for technetium to approximately 0.8 mg/cm² for both thorium and neptunium oxides. (T. R. Wright)

Uranium Carbide, Nitride, and Sulfide Fuels

Properties and Behavior

A portion of the U–C–O–N system has been examined and described in detail,[59] as shown in Fig. I-9. An interesting feature of this 1700°C isothermal section is the quasi-binary field between UO_2 and UC_2. The UC_2 is indicated to contain about 7 at.% oxygen at the point K, and the UC, 17 at.% oxygen at the point H. The U_2C_3 dissolves neither oxygen nor nitrogen, and its existence range in the ternary and quaternary fields is very limited—a fact that may help explain why it is difficult to form U_2C_3 in impure samples. The $U_2C_3 + UC_2 + UC$ region on the U–C–N face of Fig. I-9 is shown to contain UC with a composition of about 2 at.% nitrogen at point G. The $UC_2 + C + UC$ region on the U–C–N face of Fig. I-9 is shown to contain UC with a composition of about 20 at.% nitrogen at point E.

According to the British,[60] the Th–C–O system at 1500°C shows quasi-binary ties radiating from ThO_2 to graphite, ThC_2, and Th(C,O), as shown in Fig. I-10. A three-phase equilibrium exists among ThO_2, ThC_2, and $ThC_{0.8}O_{0.2}$.

In the absence of a definitive constitution diagram for the U–C–Al system, any interpretation of the results of a study by Atomics International[61] of the compatibility of UC with aluminum must be regarded as speculative. No reaction was observed between aluminum (SAP) and UC for up to 18,000 hr at 370

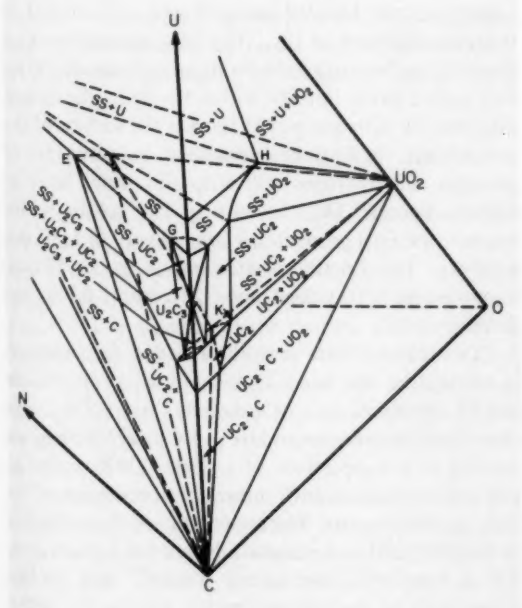

Fig. I-9 Proposed phase diagram of U–C–O–N system at low nitrogen.[59] Isothermal section at 1700°C. Figure is distorted for illustration.

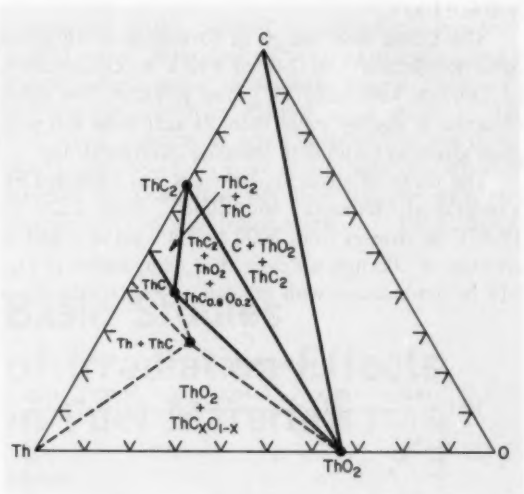

Fig. I-10 Th–C–O system[60] at 1773°K.

and 430°C. Reactions were observed between aluminum and UC at temperatures of 450°C and higher for times over 500 hr. One reaction zone obtained after heating for 8000 hr at 566°C was sampled in two different places. One sample contained aluminum, graphite, and UAl_3, suggesting the possible reaction: $UC + 3Al \rightarrow UAl_3 + C$. However, the other sample contained UC, graphite, UAl_3, and Al_4C_3, suggesting the possible reaction: $3UC + 13Al \rightarrow 3UAl_3 + Al_4C_3$.

The self-diffusion coefficients for carbon in UC, U_2C_3, and the two allotropic forms of UC_2 have been calculated at Los Alamos[62] from chemical diffusion coefficients obtained from layer-growth data. The calculations were based on the concept that chemical diffusion is related to self-diffusion as modified by the presence of a chemical-activity gradient, an effect that can be evaluated from thermodynamic data. The results obtained for self-diffusion of carbon in UC are in excellent agreement with those obtained by the tracer techniques of Lee,[63a] Bentle and Ervin,[63b] and

Chubb,[63c] but not with the results of Linder[63d] and of Villaine.[63d] The success of this calculational technique is a tribute to the state of the art with regard to the understanding of the relation between chemical diffusion and self-diffusion and to the accuracy of the thermodynamic data used in the calculations. An earlier attempt[64] to make this type of calculation by means of a "defect-concentration" concept is noteworthy because the results are apparently correct in spite of the dubious concept and because the data extend our knowledge of diffusion rates over the range 800 to 1100°C.

The Gibbs free energy of formation of UC_2 has been determined[65] at 740 to 890°C by equilibration of bismuth with solid UC_2 and graphite. The value obtained is slightly more than 24 kcal/mole and is in good agreement with data obtained calorimetrically.

The creep of stoichiometric UN was measured by Vandervoort, Barmore, and Cline[66] from 1500 to 1800°C at stresses from 2000 to 5000 psi in a partial pressure of 200 mm nitrogen. The data, shown in Fig. I-11 in combination with the data of Fassler (the three right-hand curves), are stated to be insensitive to grain sizes from 0.03 to 2.00 mm and indicate that the creep resistance of UN increases with oxygen content. Vandervoort's data give an activation energy for creep of 75 ± 10 kcal/mole of UN, and Fassler's data show ~62.0 kcal/mole.

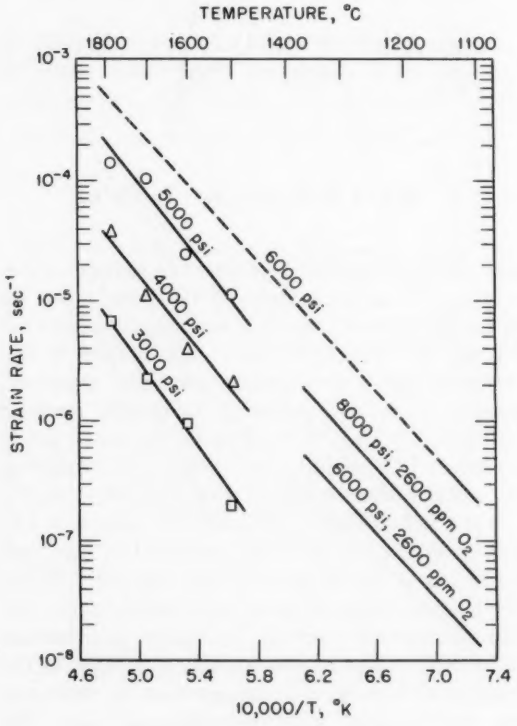

Fig. I-11 Creep data for stoichiometric UN with 400 and 2600 ppm oxygen.[66]

Eight specimens of US have been irradiated by Argonne[46b] at cladding temperatures between 380 and 750°C to burnups between 6.7 and 10.2 at.%. The smear densities of the pellets were 76 to 92%. The Nb–1 Zr cladding on all but the two hottest specimens with the highest burnups failed during the irradiation. It is suggested that the US may be sufficiently weaker and more plastic at 750°C than at lower temperatures to permit the cladding to be strained less at the higher temperatures than at the lower. (W. Chubb)

Synthesis and Fabrication of Uranium Nitrides and Carbides

In continuing work on the synthesis of carbonitrides, Oak Ridge[28c,54b] workers have designed a procedure for converting UO_2 to dense, high-purity U(C,N). The procedure is based on the results to date of studies to convert sol-gel UO_2 and microspheres of UC_2 to U(C,N). Starting with a UO_2 sol, a natural product of aqueous processing, a carbon sol would be added and the blended gel prepared and reacted to form microspheres of UC_2. The UC_2 microspheres are then reacted in nitrogen to form the carbonitride. If no free carbon exists initially within the UC_2, the carbon displaced by nitrogen would form at the surface of the microsphere. A final heat-treatment in a mixture of nitrogen and hydrogen will strip this outer layer of carbon. Because UC_2 has a very low solubility for oxygen, the final product will contain very little of this impurity. The amount of free carbon in the U(C,N) microspheres will depend upon its control during the forming of UC_2.

Two patents were recently awarded for processes involving the synthesis and fabrication of UC. In one,[67] synthesis of UC directly from UF_4 was described. In this process, UF_4, SiO_2, and carbon are reacted at a temperature of at least 400°C under an inert-gas or vacuum environment until evolution of the SiF_4 gas is complete. The temperature is then raised to at least 1300°C and maintained until the formation of UC is complete. The second patent[68] was for the preparation of hypostoichiometric UC by the carbothermic reduction of UO_2 U_3O_8, or UO_3 with an addition of 1 to 5 wt.% of a uranium alloy. The blend of oxide, carbon, and alloy is heated to 1700 to

1750°C, so that the oxide is reduced and the alloy decomposes. The foreign metal is removed as a vapor, and the free uranium combines to produce hypostoichiometric UC. (J. T. Lowder)

Fuel Reactions Following Loss-of-Coolant Accidents

Workers at General Electric[69] studied the steam oxidation of UO_2 between 885 and 1835°C. They found that the reaction obeyed the parabolic rate law according to the following equation:

$$\frac{W^2}{t} = 2.44 \times 10^5 \exp\left[(-52{,}100 \pm 2800)/RT\right]$$

where W = weight gain per unit area, mg/cm^2
t = time, sec
R = gas constant, cal/(mole)(°K)
T = temperature, °K

X-ray analysis and analytical chemistry revealed an oxygen concentration gradient in the UO_2, suggesting that the rate-controlling mechanism is bulk diffusion. The diffusion coefficient for oxygen in UO_{2+x} is given by

$$D = 99 \exp\left[(-56{,}900 \pm 1800)/RT\right] \quad \text{cm}^2/\text{sec}$$

Argonne has begun to study the sodium–fuel reaction by irradiation, in an integral sodium loop in the Transient Reactor Test (TREAT), of an EBR-II driver element that has suffered a sodium-bond loss.[36b] The duration of the run was 8.3 sec, the loop sodium temperature was 435 to 583°C, and the sodium flow rate was 4.3 m/sec. The fuel had melted, but no damage to the exterior of the cladding was evident from visual inspection, and there was no change in the diameter of the tubing.

Researchers in Germany[70] have calculated reaction potentials from thermodynamic free energies for reactions between UO_2 and water or sodium. They have shown that, unlike hyperstoichiometric fuel (see Fig. III-4), stoichiometric UO_2 would not be expected to be reduced by sodium or react with sodium up to 3000°K, confirming existing experimental work in this area. (H. S. Rosenberg)

Mechanism of Corrosion of Fuel Alloys

In-reactor tests in high-temperature water of defected Zircaloy-2-clad U_3Si fuel rods have been conducted at Chalk River.[71] In one test a previously irradiated fuel element (~530 Mwd per ton of uranium) was defected and then exposed to pressurized and boiling water at ~270°C. In a second test an unirradiated fuel element was defected, then waterlogged, and finally exposed to high-temperature pressurized water. Both fuel elements experienced major sheath failures owing to the large volume increase of the corrosion product formed as a result of the fuel–water reaction. It was concluded that the corrosion resistance of U_3Si at 300°C was not seriously affected by irradiation but that the corrosion rate increased rapidly with temperature. (W. E. Berry)

Basic Studies of Irradiation Effects in Fuel Materials

Metals

Studies of the phenomena associated with gas formation during radioactive transformations in solids are of great practical importance because these gases can cause swelling or even disintegration of fuel elements and reactor components. One such study (of the behavior of ^3He in ZrT_2 and zirconium) has been conducted by Vertebnyi et al.[72] The helium was introduced by decay of adsorbed tritium. Tritium has a half-life of 12.262 years and decays through the reaction $^3T \rightarrow {}^3He + \beta^- + \nu$. Since ^3He has a relatively large neutron cross section in the thermal-energy range, the helium concentration can be found relatively easily by transmission, i.e., by determining the specimen's transmissivity for slow neutrons.

Swelling of small samples of uranium alloys under irradiation was studied in France by Lehmann, Paoli, and Azam[73] at controlled temperatures and pressures. Preliminary results were obtained for alloys of U–Si–Cr–Al, U–Mo, and U–Si–Mo–Al. The amount of swelling as determined from density measurements showed a sharply defined maximum between 450 and 550°C, from the beginning of irradiation up to a dose of 500 Mwd/metric ton. A hydrostatic pressure of 40

bars reduced swelling by factors of 2 to 4, depending on the alloy.

The growth and electrical-resistivity changes of uranium brought about by thermal-neutron irradiation at 4.6°K have been investigated by Goller et al.[74] In-pile length measurements of alpha uranium (the specimens were polycrystalline wires with strong [0 1 0] texture in the axis of the wire) at 4.6°K have shown that the growth coefficient G (ratio of fractional change in length to fraction of all nuclei fissioned) varies considerably with burnup. The initial value of G is higher than 250,000. The growth and resistivity changes during irradiation are illustrated in Fig. I-12.

The length changes of uranium single crystals in the [1 0 0], [0 1 0], and [0 0 1] crystallographic directions during thermal-neutron irradiation at temperatures between 5 and 550°K were determined by Loomis and Gerber.[75] The electrical resistivity induced in uranium single crystals during neutron irradiation at temperatures between 4.5 and 20°K was also determined. The recovery of the radiation-induced electrical resistivity and length changes was correlated with the temperature dependence of the radiation-induced length changes. These results are consistent with the hypothesis that elongation of uranium single crystals in the [0 1 0] direction and contraction in the [1 0 0] direction during thermal-neutron irradiation are due to the anisotropic condensation of vacancy and interstitial defects in planar clusters. The substantial decrease in magnitude of the length changes on increasing the irradiation temperature from 20 to 140°K was attributed to the annihilation of interstitials at vacancy defects because of interstitial mobility during irradiation.

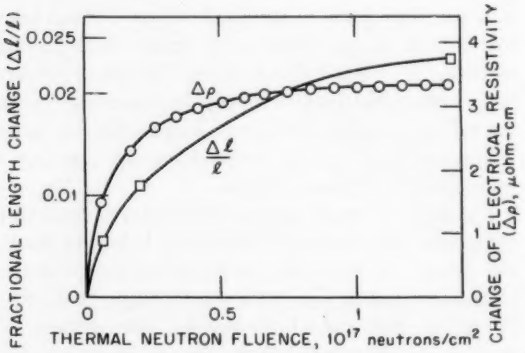

Fig. I-12 Changes in electrical resistivity and length of alpha uranium[74] irradiated at 4.6°K.

The neutron-capture cross section and fission cross section for ^{233}U have been measured simultaneously by Weston et al.[76] in the neutron-energy range 0.4 to 2000 ev. A pulsed and collimated neutron beam was passed through a ^{233}U fission chamber placed at the center of a large liquid scintillator. Capture and fission events in the ^{233}U chamber were detected in the scintillator by means of their prompt gamma rays. Coincident signals from the fission chamber and liquid scintillator distinguished fission from capture events.

The method of fission-track counting has been placed on a precise absolute basis by Gold, Armani, and Roberts.[77] Sources of systematic error were investigated and eliminated or reduced so that precise fission-rate measurements could be made. Solid-state track recorders of preetched mica and polycarbonate resin (Makrofol) were used. Experimental results depended critically on the quality of the fission sources employed. Consequently different methods of fission-source preparation were examined. The efficiency and sensitivity of these methods were determined for both mica and Makrofol. An irradiation assembly providing uniform neutron-flux exposures was used for relative measurements. Absolute calibrations were carried out with ^{244}Cm spontaneous fission sources. A limiting accuracy of close to 1% for absolute uranium-fission-rate measurements was achieved.

Ceramics

The fission-gas escape during fissioning in fuel was interpreted by Iwamoto and Oishi[78] with a newly proposed escape mechanism that comprises the three successive processes of release from trapping sites, diffusion of the released fission-gas nuclides, and desorption from the fuel surface. The expression for the release rate of fission gas was derived from a simple mathematical model postulating a continuous activation-energy spectrum for the release reaction of trapped nuclides. The proposed mechanism satisfactorily explains observed data reported in the literature on the dependence of the escape rate on decay constant, the contribution of the precursor, and the change of escape rate with irradiation time. Diffusion of the released nuclides appears to have only a small effect on the escape rate, which can thus be considered to be controlled mainly by the release reaction from the trapping sites. The present model, based on the release from trapping sites, can also explain qualitatively the influence of differences in irradiation conditions such as time and neutron flux.

The fission-gas release from fissioning UO_2 at temperatures conducive to grain growth is being investigated by Doi et al.[79] The UO_2 specimen is heated by a tungsten heater rod inserted through a hole drilled along the specimen axis and is kept at a temperature of around 2000°C. Fig. I-13 shows how the relative fission-gas release rate tends to become constant with increasing irradiation time. Work is now in progress to evaluate the specific effects of irradiation temperature and specimen grain size.

The re-solution of gas atoms from bubbles back into the irradiated UO_2 matrix has been considered by the British[80] as a particle-collision process. A semi-empirical approach was applied to the problem of the rate of knockout. On this basis, bubble diameters within grains would not be larger than 40 A after irradiation times of $\sim 10^8$ sec and ratings of 20 Mw/metric ton, which is in agreement with observation. The mean time for which fission gases are trapped in bubbles is independent of the bubble size and is ~30 days for a rating of 20 Mw/metric ton. The application of the model to intergranular gas bubbles requires a knowledge of the grain-boundary-diffusion coefficient. This can be obtained by fitting the model to experimental data for the time–temperature dependence of the onset of optically detectable intergranular porosity. It is then possible to predict the conditions of time and temperature at which the grain-boundary bubbles will touch. For irradiation times of $\sim 10^8$ sec, they should do so at ~1150°C. Re-solution will tend to amplify the effect of stress on bubbles by further increasing their radii if the applied stress is tensile, or further decreasing them if stress is compressive. Grain-boundary bubbles greater than 0.7 μ in diameter will be unstable under any tensile stress.

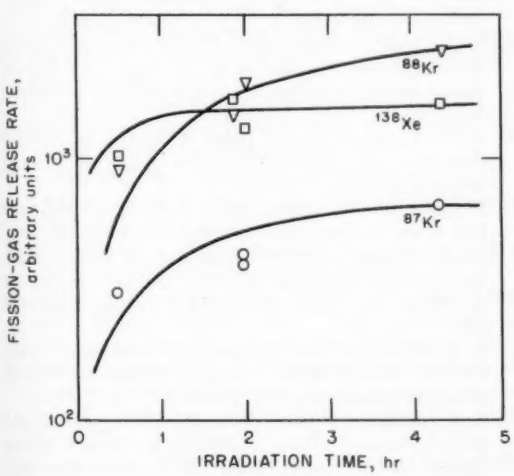

Fig. I-13 Effect of exposure to 10^{12} neutrons/(cm^2)(sec) on fission-gas release rate from UO_2 (Ref. 79).

Experimental data obtained by Gautsch[81] on the fission-induced sorption of krypton in UC surfaces indicated that, as a first step of the sorption mechanism, adsorption of the inert gas occurs. In a second step the adsorbed atoms start to migrate into the bulk of the UC. Experimental data on the thermal release and on the knockout of the sorbed krypton showed that sorption approached a saturation value within 4 days of irradiation at the given experimental conditions.

Samples of UC, UN, and UO_2 were examined[82] for changes in lattice parameter as a function of burnup to 6.4×10^{18} fissions/cm^3 at temperatures below 150°C. A saturation of lattice expansion was noted for UO_2 at 8×10^{16} fissions/cm^3, for UC at 1×10^{17} fissions/cm^3, and for UN at 1×10^{18} fissions/cm^3. This saturation of lattice expansion was associated with pronounced X-ray line broadening, and the two phenomena were therefore attributed to the formation of large interstitial atoms or defect clusters. Thus the above exposures might be called the solubility limits for fission-induced defects and foreign atoms in these fuels at temperatures below 150°C.

Laboratory-scale experiments were carried out by Taketani and Ikawa[83] to obtain information on the sources of CH_3I, reported by various workers to have been detected under reactor accident conditions. Small pieces of slightly irradiated sintered UO_2 and uranium-metal turnings were heated externally up to 1400°C in various carrier gases, and the carrier gases were analyzed for fission-product iodine present in the form of CH_3I. From the data obtained the following conclusions were drawn: In the case of sintered UO_2, some amount of CH_3I appears to be released directly from the fuel below 600°C; whereas, in the case of uranium-metal turnings, direct release apparently does not occur at any temperature. In oxidizing atmospheres, iodine released from either sintered UO_2 or uranium metal is considered to change into CH_3I only to a small extent, probably by gas-phase formation. (A. J. Markworth)

References

1. B. Hudson, Post-Irradiation Annealing Behavior of Fission Gas Bubbles in Various Purities of Uranium, *J. Nucl. Mater.*, **27**: 54-63 (July 1968).

2. J. J. Cadwell, D. R. de Halas, R. E. Nightingale, and D. C. Worlton, Battelle–Northwest, unpublished, August 1968.
3. P. Tilbury, Experiments To Improve the Mechanical Properties of Wrought Uranium, British Report AWRE-O-38/68, June 1968.
4. A. Smith, The Precipitation of Aluminum from Supersaturated Solution in Uranium, *J. Nucl. Mater.*, **27**: 194-200 (August 1968).
5. National Lead Company of Ohio, Inc., Summary Technical Report for the Period July 1–September 30, 1968, USAEC Report NLCO-1025, pp. 3.1-3.4, November 1968.
6. V. Kraus, Thermal Processing and Thermal Resistance of Cast Uranium Alloys with a Low Iron, Aluminum, and Silicon Content, *Jad. Energ.*, **6**: 228-229 (1968).
7. E. Cerrai and A. Scaroni, Some Experiments on High Temperature Aqueous Corrosion of Metallic Uranium Fuel Elements with Defected Cladding, *J. Nucl. Mater.*, **27**: 264-274 (September 1968).
8. M. Callot, J. Lauque, and H. Monti, Study of Transformation Kinetics of Uranium Alloys Under Small Loads, *Mem. Sci. Rev. Met.*, **65**: 317-330 (April 1968).
9. M. Colombie, J. Decours, M. Foure, and P. Magnier, Additional Observations on Grain Refining in Uranium Alloy Castings; Influence of Low Additions, *Mem. Sci. Rev. Met.*, **65**: 401-413 (May 1968).
10. M. Violle, Influence of a Uniaxial Compressive Stress on the Kinetics of the β-α Transformation in Uranium–Chromium Alloys and on Their α Phase Crystallization Condition, *Mem. Sci. Rev. Met.*, **65**: 415-424 (May 1968).
11. F. Giraud-Herand, J. Guillaumin, and R. Sifferler, Continuous and Discontinuous Precipitation Reactions in U–Mo (1.5 Percent) Alloys, *Compt. Rend., Ser. C*, **267**: 40-42 (July 1, 1968).
12. M. Farkas and E. Eldridge, Heat Contents and Specific Heats of Some Uranium-Bearing Fuels, *J. Nucl. Mater.*, **27**: 94-96 (July 1968).
13. R. D. Nelson and S. D. Dahlgren, Deformation of Alpha Plutonium, *Trans. Met. Soc. AIME*, **242**: 1865-1867 (September 1968).
14. M. R. Harvey, A. L. Rafalski, and D. H. Riefenberg, Cerium Diffusion in Delta-Stabilized Pu–Ce Alloys, *Amer. Soc. Metals, Trans. Quart.*, **61**: 629-631 (September 1968).
15. R. F. Nickerson, Electron Probe Microanalysis of the Plutonium–Lead Alloy System, USAEC Report UCRL-50509, University of California Lawrence Radiation Laboratory, Oct. 23, 1968.
16. Q. Johnson, D. H. Wood, and G. S. Smith, The Crystal Structure of Pu_3Zn_{22}, *Acta Crystallogr., Sect. B*, **24**: 480-484 (1968).
17. B. Blumenthal, J. E. Sanecki, and D. E. Busch, Thorium–Uranium–Plutonium Alloys as Potential Fast Power-Reactor Fuels, Part I. Thorium–Uranium–Plutonium Phase Diagram, USAEC Report ANL-7258, Argonne National Laboratory, September 1968.
18. W. N. Beck, R. J. Fousek, and J. H. Kittel, Irradiation Behavior of High-Burnup Uranium–Plutonium Alloy Prototype Fuel Elements, USAEC Report ANL-7388, Argonne National Laboratory, May 1968.
19. J. D. Navratil and R. O. Wing, Impurity Removal by Fluorination of Plutonium Dioxide Between 28 and 300°C, USAEC Report RFP-1052, Dow Chemical Co., Rocky Flats Division, Sept. 5, 1968.
20. W. C. Robinson, Jr., and W. R. Martin, A Feasibility Study of the Conversion of PuF_6 to PuO_2 by Chemical Vapor Deposition, USAEC Report ORNL-TM-2306, Oak Ridge National Laboratory, August 1968.
21. *Thermodynamics of Nuclear Materials, 1967*, International Atomic Energy Agency, Vienna, 1968.
    a. R. W. Ohse and C. Ciani, Evaporation Behavior and High Temperature Thermal Analysis of Substoichiometric Plutonium Oxide for $1.51 < O/Pu < 2.00$, pp. 545-557.
    b. C. Sari, U. Benedict, and H. Blank, Metallographic and X-Ray Investigations in the Pu–O and U–Pu–O Systems, pp. 587-611.
    c. A. E. Ogard and J. A. Leary, High-Temperature Heat Content and Heat Capacity of Uranium Dioxide and Uranium Dioxide–Plutonium Dioxide Solid Solutions, pp. 651-664.
    d. M. H. Rand and T. L. Markin, Some Thermodynamic Aspects of $(U,Pu)O_2$ Solid Solutions and Their Use as Nuclear Fuels, pp. 637-650.
    e. P. E. Potter, The Ternary System Plutonium–Carbon–Oxygen, pp. 337-369.
    f. W. M. Olson and R. N. R. Mulford, Thermodynamics of the Plutonium Carbides, pp. 467-478.
    g. G. M. Cambell, L. J. Mullins, and J. A. Leary, Thermodynamic Properties of Plutonium Compounds by EMF Techniques, pp. 75-88.
22. C. N. Craig and W. E. Baily, In-Pile Comparison of Effective Thermal Conductivity of $(PuO_2–UO_2)$ Mixed Oxides, USAEC Report GEAP-5556, General Electric Company, Advanced Products Operation, November 1967.
23. R. L. Gibby, The Thermal Diffusivity and Thermal Conductivity of Stoichiometric $(U_{0.8}Pu_{0.2})O_2$, USAEC Report BNWL-704, Battelle–Northwest, May 1968.
24. E. A. Aitken and S. K. Evans, A Thermodynamic Data Program Involving Plutonia and Urania at High Temperatures, USAEC Report GEAP-5634, General Electric Company, Vallecitos Nuclear Center, May 1968.
25. K. Wirtz, Thermal Diffusion in Nuclear Reactor Fuels, *J. Amer. Chem. Soc.*, **90**(12): 3098-3099 (June 5, 1968).
26. E. H. Dewell, Gel-Addition Process Chemical Studies, Quarterly Progress Report No. 8, May–July, 1968, USAEC Report BAW-3714-8, The Babcock & Wilcox Co., September 1968.
27. M. H. Lloyd and R. G. Haire, A Sol-Gel Process for Preparing Dense Forms of PuO_2, *Nucl. Appl.*, **5**: 114-122 (September 1968).
28. P. Patriarca, W. O. Harms, and D. J. Rucker (Comps. and Ed.), Fuels and Materials Development Program, Quarterly Progress Report for Period Ending June 30, 1968, USAEC Report ORNL-4330, (*a*) pp. 3-25, (*b*) pp. 316-320, (*c*) pp. 28-29, Oak Ridge National Laboratory, November 1968.
29. W. H. Smith, Effect of Experimental Variables on Crush Strength Determinations, USAEC Report MLM-1540, Mound Laboratory, Sept. 16, 1968.
30. H. A. Woltermann and J. Y. Jarvis, The Separation and Determination of Fines in Plutonium Dioxide Microspheres, USAEC Report MLM-1524, Mound Laboratory, Mar. 5, 1968. (Classified)
31. Mound Laboratory, Isotopic Power Fuels Programs: April–June 1968, USAEC Report MLM-1519, pp. 29-47, Aug. 9, 1968. (Classified)

32. P. E. Teaney and B. R. Kokenge, SNAP-27 Soil–Fuel–Clad Reaction Test, USAEC Report MLM-1505, Mound Laboratory, Apr. 2, 1968. (Classified)
33. Battelle–Northwest, Plutonium Utilization Program, Quarterly Report, June–August 1968, USAEC Report BNWL-907, pp. 2.1-2.22, November 1968.
34. Centre d'Étude de l'Énergie Nucléaire, Thermal Behavior of Ceramic Uranium and Plutonium Oxide Fuels Under Irradiation at High Specific Ratings, USAEC–Euratom Report EURAEC-1999, December 1967.
35. Centre d'Étude de l'Énergie Nucléaire, Use of Plutonium as Nuclear Reactor Fuel, Quarterly Report No. 17, January 1–March 31, 1968, USAEC–Euratom Report EURAEC-2036, April 1968.
36. Argonne National Laboratory, Reactor Development Program Progress Report, July 1968, USAEC Report ANL-7478, (*a*) pp. 100-102, (*b*) pp. 69-71, Aug. 28, 1968.
37. General Electric Company, Advanced Products Operation, Sodium-Cooled Reactors: Fast Ceramic Reactor Development Program, Twenty-Sixth Quarterly Report, February–April 1968, USAEC Report GEAP-5631, June 1968.
38. Nuclear Materials & Equipment Corp., Irradiation Testing of PuO_2–UO_2 Fuels, Quarterly Report No. 15, January–March 1968, USAEC Report NUMEC-3432-44, August 1968.
39. W. J. Bailey, Status and Evaluation of Mixed Oxide Fuel, USAEC Report BNWL-645, Battelle–Northwest, April 1968.
40. O. D. Kazachkovskii, S. N. Votinov, and I. G. Lebedev, Study of the Operation of an Assembly of Fuel Elements Containing Plutonium Dioxide Fuel in the BR-5 Reactor, USAEC Report ANL-tr-609 [translated from *At. Energ. (USSR)*, **24**: 136-143 (February 1968)].
41. Nuclear Materials & Equipment Corp., PuO_2–UO_2–ZrO_2 Fuel Development Program Progress Report, July 1–September 30, 1967, USAEC Report NUMEC-3505-33, June 1968.
42. M. S. Farkas, D. Cheney, M. C. Brockway, and V. W. Storhok, The Development of BeO–ThO_2–PuO_2 Fuels, USAEC Report BMI-X-10242, Battelle–Columbus, Sept. 27, 1968.
43. J. A. Leary, Solid Solution Oxide Fuels for Space Electric Power Heat Systems, USAEC Report LA-DC-9686, Los Alamos Scientific Laboratory, June 4, 1968.
44. U. Sriyotha, Phase Equilibrium in the Systems UO_{2+x}–Lu_2O_3 (Er_2O_3) and Lu_2O_3–UO_2 (NpO_2,PuO_2), German Report KFK-737, April 1968.
45. R. Lorenzelli, Contribution to the Study of the System (U,Pu)C,N, French Report CEA-R-3536, May 1968.
46. Argonne National Laboratory, Reactor Development Program Progress Report, August 1968, USAEC Report ANL-7487, (*a*) pp. 2-3, (*b*) p. 87, Sept. 26, 1968.
47. United Nuclear Corp., Fast Reactor Mixed-Carbide Fuel Element Development Program, Fourth Quarterly Progress Report, April–June, 1968, USAEC Report UNC-5224, pp. 5-7, Sept. 26, 1968.
48. D. L. Keller, Progress Relating to Civilian Applications During July Through September 1968, USAEC Report BMI-1851, p. A9, Battelle–Columbus, Oct. 1, 1968.
49. J. B. Moser and O. L. Kruger, Thermal Conductivity and Heat Capacity of the Monophosphide and Monosulfide of Plutonium, *J. Amer. Ceram. Soc.*, **51**(7): 369-372 (July 1968).
50. R. D. Leggett and R. S. Kemper (Eds.), Status of Thorium Fuel Technology, USAEC Report BNWL-861, Battelle–Northwest, August 1968.
51. J. T. Venard and J. E. Spruiell, Phase Relations in the Th–U–N System at 1000°C, *J. Nucl. Mater.*, **27**: 257-263 (1968).
52. L. N. Grossman, Thermal Conductivity of Coated Particle UO_2–Tungsten Cermets, Report NASA-CR-1154 (N68-32983), General Electric Company, Advanced Products Operation, August 1968.
53. P. O. Perron, Oxygen Redistribution in Uranium Dioxide Fuels, *J. Nucl. Mater.*, **27**: 237 (August 1968).
54. S. Peterson (Comp.), Materials and Ceramics Division Annual Progress Report for Period Ending June 30, 1968, USAEC Report ORNL-4370, (*a*) pp. 30-33, (*b*) pp. 86-88, Oak Ridge National Laboratory, October 1968.
55. T. Nishijima, Method for Shaping Uranium Oxide Moldings, Japanese Patent No. 19,683,712, Feb. 10, 1968.
56. Danish Atomic Energy Commission, RISOE, Research Establishment, Metallurgy Department Annual Progress Report for the Period Ending March 31, 1968, Danish Report RISO-179, pp. 33-34, July 1968.
57. J. E. May and R. L. Stoute, Doped Hypostoichiometric Dioxide Nuclear Fuel Composition and Method of Preparation, U. S. Patent No. 3,374,178, to Atomic Energy of Canada Ltd., Mar. 19, 1968.
58. G. S. Petit, J. D. Griffin, and C. A. Kienberger, Electrodeposition of Thorium, Neptunium, and Technetium, USAEC Report K-1761, Union Carbide Corporation, Oak Ridge Gaseous Diffusion Plant, Oct. 17, 1968.
59. J. L. Henry, R. Blickensderfer, and G. G. Thompson, Quaternary System U–C–O–N at 1700°C: Phase Relations in the Low-Nitrogen Region, *J. Amer. Ceram. Soc.*, **51**: 617-621 (November 1968).
60. P. E. Potter, On the Free Energy of Formation of ThC, *J. Inorg. Nucl. Chem.*
61. A. B. Bremer, Heavy Water Organic Cooled Reactor, Compatibility of Hyperstoichiometric UC and Sintered Aluminum Powder (SAP), USAEC Report AI-CE-77, Atomics International and Combustion Engineering, Inc., May 31, 1968.
62. T. C. Wallace, W. G. Witteman, C. L. Radosevich, and M. G. Bowman, Carbon Diffusion in the Carbides of Uranium, USAEC Report LA-DC-8840, Los Alamos Scientific Laboratory, June 12, 1968.
63. W. Chubb, Carbide and Nitride Fuels: Properties and Behavior, *Reactor Mater.*, (*a*) **9**(4): 212 (Winter 1966–1967); (*b*) **11**(1): 10 (Spring 1968); (*c*) **5**(2): 21 (May 1962); (*d*) **11**(2): 87 (Summer 1968).
64. S. Takeuchi, T. Honma, and T. Satow, The Reaction of Uranium with Graphite at High Temperatures, *Trans. Jap. Inst. Metals* (English ed.), **5**(2): 111-115 (April 1964).
65. J. A. Craig, R. E. Balzhiser, and D. V. Ragone, A Study of the Free Energies of Formation of Uranium Monocarbide and Uranium Dicarbide, *Trans. Met. Soc. AIME*, **242**: 1809-1813 (September 1968).
66. R. R. Vandervoort, W. L. Barmore, and C. F. Cline, Compressive Creep of Polycrystalline Uranium Mononitride in Nitrogen, *Trans. Met. Soc. AIME*, **242**: 1466-1467 (July 1968).

67. Production of Uranium Monocarbide, British Patent No. 1,127,041, Sept. 11, 1968.
68. L. A. Hanson, Preparation of Pure Dense Hypostoichiometric Uranium Carbide, U. S. Patent No. 3,398,098, Aug. 20, 1968.
69. General Electric Company, Missile and Space Division, Interim Summary of Work Applicable to ECC on Physico-Chemical Studies of Clad UO_2 Under Reactor Accident Conditions, USAEC Report GEMP-319, June 1968.
70. N. Henzel, A. Kleine-Tebbe, and H. P. Beck, Study on Chemical Reactions Between Uranium Dioxide, the Most Abundant Fission Products, Water, and Sodium, USAEC Report AEC-tr-6961, Battelle–Frankfurt, Apr. 25, 1968.
71. M. A. Feraday, G. M. Allison, J. F. Ambler, G. H. Chalder, and J. J. Lipsett, In-Reactor Performance of Defected Zircaloy-Clad U_3Si Fuel Elements in Pressurized and Boiling Water Coolants, Canadian Report AECL-3106, May 1968.
72. V. P. Vertebnyi, M. F. Vlasov, A. L. Kirilyuk, R. A. Zatserkovskii, M. V. Pasechnik, and V. A. Stepanenko, The Behavior of ^3He in ZrT_2 and Zirconium, *At. Energ. (USSR)*, **22**(3): 235-237 (March 1967).
73. J. Lehmann, P. Paoli, and N. Azam, Study of Swelling of Uranium Alloys Under Irradiation (in French), *J. Nucl. Mater.*, **27**(3): 285-309 (September 1968).
74. S. Goller, G. Vogl, H. Wenzl, and J. C. Jousset, Growth and Electrical Resistivity Change of Uranium by Thermal Neutron Irradiation at 4.6°K, *Phys. Lett., A*, **27**(7): 408-409 (Aug. 26, 1968).
75. B. A. Loomis and S. B. Gerber, Length and Electrical Resistivity Changes of Neutron Irradiated Uranium, *Phil. Mag.*, **18**(153): 539-553 (September 1968).
76. L. W. Weston, R. Gwin, G. deSaussure, R. R. Fullwood, and R. W. Hockenburg, Measurement of the Neutron Fission and Capture Cross Sections for ^{233}U in the Energy Region 0.4 to 2000 eV, *Nucl. Sci. Eng.*, **34**(1): 1-12 (October 1968).
77. R. Gold, R. J. Armani, and J. H. Roberts, Absolute Fission Rate Measurements with Solid-State Track Recorders, *Nucl. Sci. Eng.*, **34**(1): 13-32 (October 1968).
78. K. Iwamoto and J. Oishi, Analysis of Fission Gas Escape from Reactor Fuel During Isothermal Irradiation, *J. Nucl. Sci. Technol. (Tokyo)*, **5**(8): 387-396 (August 1968).
79. A. Doi, H. Hayashi, Y. Ohsawa, and K. Inoue, Fission-Gas Release from Fissioning UO_2 at Temperatures Conducive to Grain Growth (Around 2000°C), *J. Nucl. Sci. Technol (Tokyo)*, **5**(6): 313-315 (June 1968).
80. A. J. Manley, The Behaviour of Fission Gases in Irradiated UO_2: A Re-Solution Process, British Report TRG-Report-1681, July 5, 1968.
81. O. Gautsch, The Fission Induced Sorption of Krypton in Uranium Carbide, *J. Nucl. Mater.*, **27**(3): 310-315 (September 1968).
82. W. Dienst and D. Brucklacher, Investigation of Irradiation Damage in ZrO_2, ZrC, UO_2, UN, and UC by X-Ray Diffraction, German Report EURFNR-503 (KFK-745), March 1968.
83. K. Taketani and K. Ikawa, Detection of Methyl Iodide upon Heating Irradiated Fuels, *J. Nucl. Sci. Technol. (Tokyo)*, **5**(10): 491-497 (October 1968).

Section

II

Reactor Materials

Moderator and Control Materials

Graphite

The effects of irradiating pyrocarbon disks or spherical coatings on fissile particles to a fast-neutron dose of 4×10^{21} neutrons/cm^2 (equivalent to 2 to 3 years of reactor service) at 650 ± 100°C were studied by the British.[1] The conclusions are as follows:

1. Pyrocarbon coatings with a granular structure can withstand fast-neutron doses of 4×10^{21} neutrons/cm^2 at 650°C without failure. Laminar and featureless coatings crack apart.

2. Granular coatings may have a fairly wide range of properties, Bacon anisotropy factors as high as 2.5, and densities as low as 1.8 g/cm^3, and still withstand irradiation. These parameters imply that the coatings were deposited at high temperatures (>1850°C) and have a large crystallite size (>90 A).

3. Plain pyrocarbon and triplex pyrocarbon/SiC/pyrocarbon coatings perform the same under irradiation.

4. Heat-treating laminar coatings at 2000°C for 2 hr before irradiation improves their radiation behavior but not enough to make them comparable with granular structures.

5. Particle size (300 to 700 μ in diameter) was not a significant variable.

Other observations were made in the study. A featureless pyrocarbon structure was able to creep approximately 6% during irradiation without cracking. All the pyrocarbons except those having initial densities above 2.08 g/cm^3 densified during irradiation.

An Atomics International research program[2] has concluded that growth of high-quality graphite single crystals of substantial size is possible. Crystals were grown by precipitation from carbon-saturated molten iron and nickel. Product crystals included (1) thin platelets, up to 3 cm across and a fraction of a millimeter thick, (2) tabular crystals, measuring several millimeters across, and (3) columnar crystals up to 2 mm long. The latter crystals most nearly approached ideality.

A 1968 volume on physical properties of graphite[3] is authored by W. N. Reynolds, who has contributed greatly to graphite research in recent years. The stated object of the book is to present as succinctly as possible the facts about the physical properties of graphite as they are presently understood in the context of solid-state theory. The major subject areas covered are: structure, mechanical properties, thermal properties, electrical and optical properties, surface and physicochemical properties, point defects, and high-flux neutron damage.

A review of published mechanical-properties data for artificial graphite by Greenstreet[4] may be of special interest to nonspecialists in graphite technology. The intent of the report is to provide a unified description of the complex mechanical behavior of graphite. It also includes historical information and discussions of crystalline structure and manufacturing methods.

(M. C. Brockway)

Beryllium Metal and Alloys

Physical Metallurgy

The effect on grain size of rapidly heating and cooling rolled commercial molybdenum plate was studied by the Japanese.[5] Annealing for short periods at a high temperature was more effective in reducing the grain size than was longtime annealing near the recrystallization temperature. Annealing for about 1 min at 900°C using high-frequency heating resulted in considerable reduction of the grain size.

Defect production due to irradiation by neutrons and electrons and subsequent recovery were studied by means of electrical-resistivity and stored-energy measurements at the Center of Nuclear Studies at Grenoble.[6] Beryllium samples with an impurity content of 0.1 wt.% were irradiated by neutrons at 27 and 77°K and by electrons at 20°K. The defect concentration

was found to increase with increasing flux and energy of the radiation. When the beryllium was annealed at room temperature, more than 95% of the initial radiation-induced resistivity increment was recovered. Three principal recovery ranges were observed: stage I below 80°K, stage II between 95 and 220°K, and stage III between 220 and 300°K.

Mechanical Metallurgy

Three types of thin-wall extruded beryllium tubing and one type of plasma-sprayed and sintered tubing, described in Table II-1, were extensively characterized by Langley Research Center,[7] using metallographic examination, microhardness determinations, X-ray diffraction, dimensional measurements, tensile tests, and compression tests. The room-temperature mechanical properties are summarized in Table II-2.

Powder Metallurgy

Electron micrographs and carbon-extraction replicas of beryllium powder particles, along with transmission-electron and optical micrographs of the consolidated powder, revealed oxides on the surfaces of the beryllium powder particles before compaction, but the oxides were not concentrated at the grain boundaries of the vacuum-hot-pressed compacts.[8] A proposed mechanism of vacuum hot pressing considers it as a two-stage process, involving vacuum sintering during preheating followed by hot working and recrystallization during pressing. The combination of stress

Table II-1 Fabrication History for Beryllium Tubing[7]

Type	Fabrication history
A	Extruded from hot-pressed block. First extrusion at 1750°F (1228°K) at a reduction ratio of 9:1. Second extrusion at 1750°F (1228°K) at a reduction ratio of 13.5:1. Tubes were ground to final dimensions.
B	Hot-pressed billet extruded at 1850°F (1283°K) at a reduction ratio of 28:1. Straightened at 1400°F (1033°K) by using skew-roll techniques. Steel jacket and core removed and tubing machined to length. Tubes chemically etched to final dimensions.
BL	Hot-pressed and machined extrusion billets canned in mild-steel containers by using a core-type mandrel. Billets extruded in the temperature range 1700 to 1900°F (1200 to 1311°K) by employing reduction ratios of greater than 10:1. After extrusion, tubes were cut to length and hot straightened. The steel jacket was then removed, and the tubing was honed and chemically etched to final dimensions.
PS	S-200 grade powder plasma-sprayed on tubular copper mandrel in argon atmosphere. Tubes machined and mandrel leached out. Vacuum sintered at 2.5×10^{-5} torr (3.3 mN/m^2) for 4 hr at 700°F (644°K). Cooled in vacuum to 700°F (644°K). Tubing with bulk density less than 1.80 g/cm^3 resintered for 4 hr at 2150°F (1450°K).

Table II-2 Summary of Room-Temperature Mechanical Properties of Beryllium Tubing[7]

Type	Diameter, in.	Thickness, in.	Ultimate tensile strength, 1000 psi	Tensile yield strength, 1000 psi	Compressive yield strength, 1000 psi	Young's modulus in tension, 10^6 psi	Young's modulus in compression, 10^6 psi	Elongation in 2 in., %
A	0.50	0.020	67.5	64.5	65.3	40.7	40.2	<1
B	0.50	0.020	57.3	42.4	41.6	41.0	39.0	<1
BL	0.25	0.020	89.4	53.1	43.8	40.0	39.1	5
	0.25	0.040	84.7	46.0	44.5	40.2	40.2	5
	0.50	0.020	85.8	42.4	42.6	41.1	39.6	7
	0.50	0.040	83.3	40.7	38.3	40.8	39.4	9
	0.75	0.020	78.1	43.8	41.7	41.0	39.2	5
	0.75	0.020	85.0	42.3	39.6	40.1	39.4	7
PS	0.54	0.020	46.4		56.6	39.4	40.6	<1
	0.58	0.040	72.8		79.0	40.5	40.1	<1

and temperature during pressing is thought to be analogous to conventional hot working, producing extensive recrystallization.

Corrosion Protection

Bare beryllium was not attacked[9] when exposed to 95% relative-humidity environments at 100°F (38°C). However, unprotected beryllium exposed to aqueous sodium chloride at 100°F was severely pitted as a result of electrochemical attack at local anodic sites. Commercially pure beryllium was not found to be susceptible to stress-corrosion cracking in the presence of aqueous-salt environments. When exposed alternately to an aqueous salt and elevated temperature, bare beryllium exhibits a maximum corrosion resistance at 600°F (315°C) owing to the formation of a protective oxide film at this temperature. Below 600°F, beryllium is pitted by exposure to aqueous salt, and above 600°F, catastrophic oxidation is encountered.

Both anodized and aluminized coatings on beryllium offer good corrosion protection at elevated temperature. Black anodized coatings provided corrosion protection for beryllium exposed alternately to an aqueous salt and elevated temperatures to 600°F. The anodized coating appeared to dissolve when exposed to these conditions at 800°F (425°C). Aluminized coatings 1 to 2 mils in thickness were found to offer greater protection, being capable of service at the highest test temperature of 800°F as compared with the 600°F maximum for the anodized coating.

Joining

Partial-penetration electron-beam welds were made[10] on ¼-in.-thick vacuum-hot-pressed beryllium which had a preplaced aluminum shim as the brazing material. The beryllium specimens contained varying quantities of beryllium oxide from 0.7 to 2.5 wt.%. Other variables studied were weld-travel speed and the number of welding passes. Increasing the beryllium oxide content resulted in increased weld porosity and decreased weld tensile strength (Fig. II-1). As the number of weld passes increased from one to five, the amount of weld porosity was reduced, resulting in improved tensile strength (Fig. II-2). Varying the weld-travel speed from 10 to 30 in./min had no significant effect on the porosity or strength of the weld.

It was found by Lockheed[11] that many of the problems of joining beryllium by brazing could be alleviated by interposing a barrier layer of electrodeposited copper with or without an overplate of nickel on the beryllium surface. The plating of the beryllium permitted brazing in vacuum, inert gas, or in air with commercial fluxes. Beryllium could be joined in this manner to itself, steel, stainless steel, or any other brazeable metal. Joint strengths were consistently in excess of 20 ksi in shear, with all failures occurring in the parent material. In the barrier-layer approach to brazing beryllium, the barrier metal must be well suited to brazing. Nickel and copper are useful in this respect, but nickel requires a copper undercoat. Silver was found unsatisfactory owing to the occurrence of blistering during brazing. (F. T. Zurey)

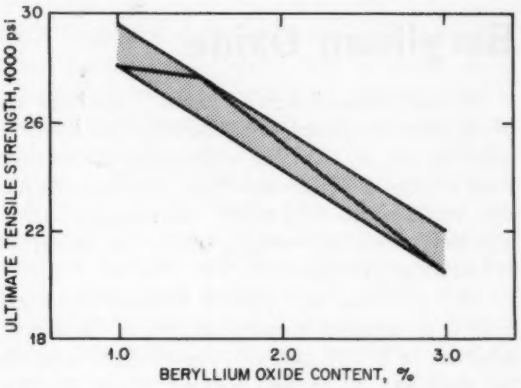

Fig. II-1 Effect of oxide content on strength of beryllium welds.[10]

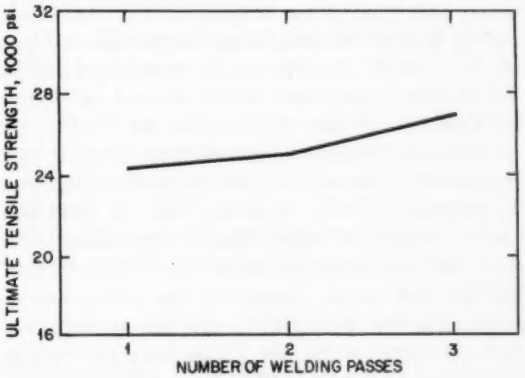

Fig. II-2 Effect of multiple weld passes on strength of beryllium welds.[10]

Beryllium Oxide

A Gulf General Atomic report[12] discusses the physical integrity, dimensional stability, and ability to retain Xe, Kr, Sr, and Cs of a hot-pressed BeO-matrix, 5 vol.% UO_2 dispersion-type fuel. The ½-in.-OD fuel was irradiated to 1.24×10^{21} neutrons/cm^2 ($E >$ 0.18 Mev) with an energy density in excess of 125 watts/cm of length.

The fuel was hot pressed between 1525 and 1700°C to densities in excess of 99% of theoretical. Additives of C, SiC, and SiO_2 were used to maintain the grain size of the BeO between 3 and 5 μ. The irradiations were conducted between 800 and 1600°C to burnups in excess of 30% of the fissile atoms, with equal amounts of fissions from ^{238}U and ^{239}Pu. Measurements during irradiation showed that the ratio of the rate of release to the rate of production of xenon and krypton was between 10^{-6} at 800°C and 10^{-5} at 1600°C. Postirradiation analyses showed that the retention of strontium was between 87 and 98% of the total atoms produced, but for cesium it was 67% at 1400 and 1600°C, and ~100% at 800 and 1100°C.

The data appear to confirm that BeO creep at high temperature is important in preventing fracturing since no microcracks were observed. Even at 1400 and 1600°C, where the volume changes approached 10%, there were no microcracks observed at the interfaces of the fuel and matrix. Apparently the matrix was of sufficiently low permeability that gas pressure was built up enough within the fuel to cause the swelling observed at 1400 and 1600°C. These data, contrary to earlier studies by other investigators, indicate that this type of fuel might be useful in the temperature range of 800 to 1600°C. (M. C. Brockway)

Solid Hydrides

Zirconium Hydride

The phase boundary between the alpha-plus-delta and delta regions of the Zr–H phase diagram has been more completely defined in work done at Atomics International.[13] Although this study was carried out on SNAP fuel containing 4 at.% uranium, it has been demonstrated by various investigators in past years that this amount of uranium acts as an inert constituent as far as the hydrogen is concerned, and the results may be considered typical of the Zr–H system. Four experimental techniques were employed in obtaining the data points needed to define the boundary: optical hot-stage microscopy, room-temperature metallography, dilatometry, and X-ray diffraction. The phase boundary was found to exist between 1.33 H/Zr atom ratio at 1020°F (550°C) and 1.60 H/Zr at 75°F (24°C). A metastable phase, gamma prime, coexisting with the delta and alpha phases was found to transform to delta phase at about 560°F (295°C) between H/Zr values of 1.20 and 1.50, which is the boundary value at that temperature.

Further definition of the boundaries of the delta and epsilon regions of the phase diagram has also been provided by Atomics International.[14] The two-phase delta-plus-epsilon region exists between H/Zr atom ratios of 1.64 and 1.74 at room temperature. This region narrows as the temperature increases and closes at 850°F (455°C) at the composition $ZrH_{1.70}$. At higher temperatures and compositions of hydrogen, the delta–epsilon transition occurs without an intervening two-phase region. Extrapolation of the boundary from about 1300°F (705°C) at $ZrH_{1.81}$ to the composition ZrH_2 gives a value of 1700°F (925°C), which is in agreement with extrapolations by other investigators. The high-hydrogen portion of the Zr–H phase diagram, which is of particular interest in nuclear reactor technology, is shown in detail in Fig. II-3. The latest

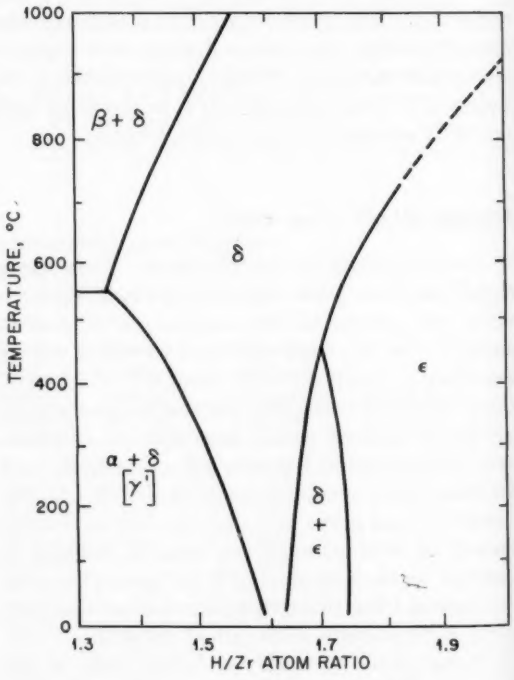

Fig. II-3 High-hydrogen portion of Zr–H phase diagram.[14]

and most complete version of the entire phase diagram is presented in Fig. II-4.

Investigators at the Kurchatov Institute of Atomic Energy, USSR, have reported[15] an experimental study of the neutron-thermalization process in zirconium hydride. Nonstationary neutron spectra were measured at room temperature as a function of slowing-down time, using a large zirconium hydride prism. The spectra were found to fall in a range of slowing-down times greater than 30 μsec, with a mean neutron energy less than 0.13 ev. The energy exchange between the neutron gas and the medium in this range is caused mainly by the excitation of acoustic lattice vibrations. Thermalization proceeds relatively slowly, and the time required to establish an equilibrium neutron spectrum is of the order of 400 μsec.

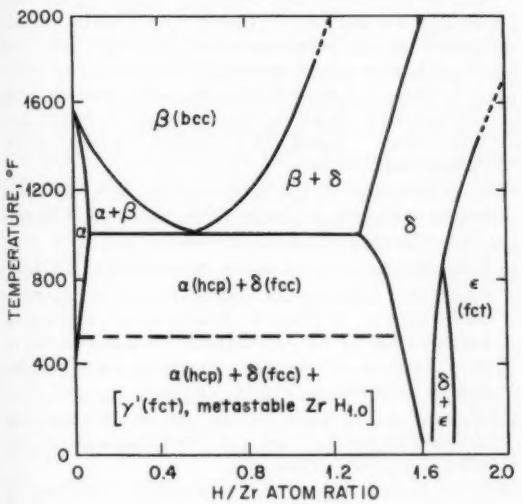

Fig. II-4 Phase diagram of the Zr–H system.[13]

Niobium and Tantalum Hydrides

In order to resolve some of the discrepancies that have been found in studies of niobium and tantalum hydrides, Amato and Negro of the Institute of General and Applied Chemistry, Turin, Italy, started with fully hydrided powders and dehydrided them.[16] They found that, on heat-treatment at 500°C for 1 hr under a dynamic vacuum, both hydrides were largely transformed into the metallic alpha phase. When the temperature was reduced to 450°C, the dehydriding process did not go to completion, and the lattice was that of a distended metallic phase. Heat-treatment at 400°C resulted in the simultaneous appearance of the cubic metallic phase, alpha, and a second phase designated alpha prime which has a cubic structure in the case of niobium and a tetragonal structure in the case of tantalum. Heat-treatment of the niobium hydride at 350°C resulted in the simultaneous formation of the metallic alpha phase, the hydride beta phase, and the intermediate alpha-prime phase. For tantalum hydride, only the alpha-prime phase was found under these conditions. At 300°C, only the alpha-prime phase occurred, and the compositions were $NbH_{0.7}$ and $TaH_{0.7}$ under these conditions. When the temperature was dropped to 200°C, no dehydriding occurred in the niobium compound, and traces of the alpha-prime phase appeared for the tantalum compound.

Barium Hydride

The diffusion coefficient for hydrogen in barium metal was found by workers at Ames[17] to be 4.0×10^{-3} over the temperature range 200 to 620°C, with a ΔH of 4.5 kcal. The solubility of BaH_2 in barium metal, determined by the surface concentrations at the temperatures studied, ranged from 35 at.% hydrogen at 620°C down to 2.5 at.% hydrogen at 200°C. The heat of solution of the BaH_2 in barium metal was determined to be 5980 ± 450 cal/mole.

(H. H. Krause)

Nuclear Poisons

Boron and Boron Compounds

Scientists at the University of Surrey[18] have investigated the oxidation behavior of TiB_2 and ZrB_2. Their work consisted of heating powder compacts of the compounds in oxygen at pressures of 200 to 760 torrs. The TiB_2-O_2 reaction rate was found to be parabolic except near 950°C where it is cubic. The activation energy is 45 kcal/mole below 950°C and 31 kcal/mole above 950°C. The ZrB_2-O_2 reaction rate was found to be parabolic throughout the range of 700 to 1050°C, and the activation energy is 28 kcal/mole. A minimum rate of reaction was found at a pressure of 600 torrs for both TiB_2 and ZrB_2.

Radiation-induced swelling behavior of uncoated and pyrolytic carbon (PyC)-coated B_4C microspheres was investigated at Gulf General Atomic.[19] Boron carbide microspheres approximately 200 μ in diameter, both uncoated and coated with 100 μ of PyC, were

subjected to neutron irradiation at 500°C in inert gas to a ^{10}B burnup of 78% in the Engineering Test Reactor (ETR). The specimens were irradiated for 2300 hr to a fluence of 2.7×10^{21} neutrons/cm^2 ($E > 0.18$ Mev). The uncoated B_4C expanded an average of 9% in diameter. The PyC-coated B_4C spheres were restrained from swelling. The overall coated-particle diameter actually decreased 4% in diameter as a result of shrinkage of the coating. The maximum radial pressure exerted by the PyC was estimated to be about 40,000 psi. These results are believed to demonstrate the range of radiation-induced dimensional changes in B_4C particles under extreme conditions of high or low restraint by a matrix.

Rare Earths and Others

The phase diagram of the ZrO_2–HfO_2 system was studied[20] under the sponsorship of the office of Aerospace Research. The system was investigated between 600°C and the liquidus temperatures using metallographic, X-ray diffraction, and electron-probe analyses. The results show complete solid solubility. The monoclinic tetragonal inversion was investigated by differential thermal and high-temperature X-ray analyses and was found to exhibit a continuous increase as the composition moves from ZrO_2 to HfO_2.

(D. E. Lozier)

References

1. D. J. Clough, K. S. B. Rose, and J. B. Sayers, An Irradiation Damage Study of Pyrolytically Deposited Carbon Coatings, British Report AERE-R-5797, July 1968.
2. S. B. Austerman, J. W. Wagner, and S. M. Myron, Graphite Crystal Growth, USAEC Report NAA-SR-12486, Atomics International, Aug. 15, 1968.
3. W. N. Reynolds, *Physical Properties of Graphite*, American Elsevier Publishing Company, Inc., Amsterdam and New York, 1968.
4. W. L. Greenstreet, Mechanical Properties of Artificial Graphites. A Survey Report, USAEC Report ORNL-4327, Oak Ridge National Laboratory, December 1968.
5. M. Goto and K. Tuya, Reducing of Grain Sizes of Rolled Beryllium Metal (in Japanese), *Kinzoku Zairyo Gijutsu Kenkyusho Kenkyu Hokoku*, **10**: 429-433 (November 1967).
6. J. G. Nicond, J. Deloplace, H. Hillacret, D. Schumacher, and Y. Adda, Study of Defects Produced in Beryllium by Irradiation at Low Temperature, *J. Nucl. Mater.*, **27**: 147-165 (Jan. 8, 1968).
7. D. R. Rummler, H. B. Dexter, G. H. Harth, and R. A. Buchanan, Mechanical Properties and Column Behavior of Thin Wall Beryllium Tubing, Report NASA-TN-D-4833, National Aeronautics and Space Administration, Langley Research Center, October 1968.
8. J. W. Butcher, H. M. Lindsay, J. N. Lowe, and V. D. Scott, A Mechanism for the Pressure-Sintering of Beryllium, *Powder Met.*, **11**(21): 188-202 (Spring 1968).
9. T. L. Mackay and C. B. Gilpin, Corrosion and Protection of Beryllium in Turbine Engine Applications, *Electrochem. Technol.*, **6**(7-8): 235-240 (July–August 1968).
10. G. K. Hicken, Effects of Beryllium Oxide on the Braze Weldability of Beryllium, *Weld. J. (N. Y.)*, **47**: 364s-370s (August 1968).
11. L. Missel and R. K. Titus, Plating of Beryllium for Brazing, *Metal Finish.*, **65**: 59-61 (October 1967).
12. R. A. Meyer, F. H. Loftus, and R. C. Weed, Irradiation Effects on Hot Pressed Beryllium Oxide Matrix Fuel Between 800 and 1600°C, USAEC Report GA-8559, Gulf General Atomic Incorporated, May 15, 1968; submitted for publication in *Nucl. Sci. Eng.*
13. K. E. Moore and M. M. Nakata, Phase Relationships in the (Alpha + Delta) Region of the Zirconium–Hydrogen System, USAEC Report AI-AEC-12703, Atomics International, Sept. 30, 1968.
14. K. E. Moore and W. A. Young, Phase Studies of the Zr–H System at High Hydrogen Concentrations, *J. Nucl. Mater.*, **27**(3): 316-324 (September 1968).
15. S. N. Ishmaev, V. I. Mostovoi, I. P. Sadikov, and A. A. Chernyshov, Experimental Study of the Neutron Thermalisation Process in Time in Hydrogeneous Moderators, British Report AERE-Trans-1088 (translated from pp. 643-655 of *Pulsed Neutron Research*, Vol. I, Symposium held at Karlsruhe, May 10–14, 1965).
16. I. Amato and A. Negro, On the Niobium–Hydrogen and Tantalum–Hydrogen Systems, *J. Less-Common Metals*, **16**: 468-471 (December 1968).
17. D. T. Peterson and C. C. Hammerberg, Diffusion of Hydrogen in Barium Metal, *J. Less-Common Metals*, **16**: 457-460 (December 1968).
18. R. J. Irving and I. G. Worsley, Oxidation of Titanium Diboride and Zirconium Diboride at High Temperatures, *J. Less-Common Metals*, **16**: 103-112 (October 1968).
19. O. M. Stansfield, Irradiation-Induced Dimensional Change in Boron Carbide, USAEC Report GA-8884, Gulf General Atomic Incorporated, Sept. 17, 1968; submitted for publication in *J. Nucl. Mater.*
20. R. Ruh and H. J. Garrett, Determination of Zirconia-Hafnia Phase Diagrams, *Res. Rev.*, **7**(5): 7-8 (May 1968).

Section

III

Reactor Materials

Cladding and Structural Materials

Corrosion by Aqueous and Gaseous Media

Comparative Resistance of Various Materials

Cavitation-damage studies on 316 stainless steel, Nickel 270, and 6061-T6 aluminum have been described by NASA–Lewis[1] as part of an ASTM round-robin test program. A magnetostrictive transducer was used to vibrate specimens at a frequency of 25,000 cps with a total displacement amplitude of 1.75 mils in distilled water at 75°F and 1 atm pressure. The relative resistance of the materials to cavitation was 316 stainless steel > Nickel 270 > 6061-T6 aluminum. The volume loss and mean depth of penetration of the 6061-T6 aluminum alloy was 45 times that of the 316 stainless steel after 160-min exposure.

The corrosion behavior of a variety of materials in iodine-absorbing sprays is being investigated at Oak Ridge.[2] Initial results of a 168-hr test in a spray containing 0.15*M* NaOH and 0.28*M* H_3BO_3 at *p*H 9.3 and 100°C revealed negligible corrosion on 304 and 316 stainless steel, Inconels 600 and 718, 90-10 and 70-30 cupronickel, Monel 400, and Zircaloy-2. Carbon steel developed occasional rust spots and slight weight gains. Unalloyed copper experienced moderate weight losses, which extrapolated to a penetration of 3 to 4 mils/year. Aluminum alloys 1100, 3003, 5052, and 6061 had high weight losses and extrapolated corrosion rates of several inches per year. Attack was greater on specimens exposed to the spray than on those submerged in the liquid.

The corrosion behavior of metals in Freon-11 at 300°C and 60 atm has been studied by Russian scientists.[3] Weight-loss results after 50 hr of exposure are shown in the tabulation at the top of the next column. The copper and brass were disintegrating; the rates of attack on the aluminum and titanium were increasing with time.

Material	Weight loss, mg/cm^2
Steel	2.00 to 3.00
13 Cr steel (0.4 C)	1.40
17 Cr–2 Ni steel	0.33
Titanium	30.70
Aluminum	11.70
Copper	856.0
Brass	877.0

Corrosion of Zirconium Alloys

Pickling

Bettis has determined the maximum oxide thickness on Zircaloy that can be uniformly removed by acid pickling.[4] Specimens were exposed to air for varying periods of time at several temperatures and were then pickled at 100°F for 3 min in 2.5 vol.% concentrated HF–39 vol.% concentrated HNO_3–balance H_2O. As shown in Fig. III-1, pickling effectiveness decreased with increasing temperature and time of oxidation. At temperature–time combinations above the curve, the Zircaloy was pitted or the oxide could not be removed. As a practical guideline it was observed that the gold-colored temper film represented the limiting thickness that could be uniformly removed

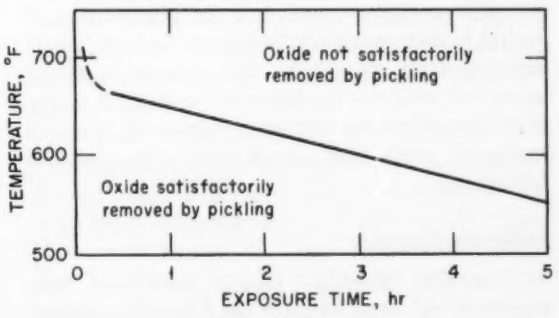

Fig. III-1 Pickling behavior of Zircaloy exposed to air atmosphere for various temperature–time combinations.[4]

by pickling. Multicolored oxides either could not be removed or led to pitting.

Studies at Chalk River[5] have revealed two types and sizes of intermetallic particles on the surface of Zircaloy-2. The larger particles contained equal concentrations of iron and nickel but little or no chromium. During pickling, the matrix around these particles was selectively attacked and some particles were dislodged. The smaller particles contained little or no nickel and twice as much chromium as iron. These particles and the surrounding matrix were not attacked selectively during pickling.

Oxidation

A literature review of the kinetics and phenomena associated with the oxidation of "pure" zirconium metal by oxygen gas has been prepared by Denver Research Institute.[6] The review discusses the parabolic kinetics of oxidation of alpha and beta zirconium and their relation with the lattice diffusion of oxygen in the metal, as well as the diffusion coefficients of oxygen in alpha zirconium. Little is known and/or established about the initial stages of oxidation, the transport of oxygen across the zirconium oxide film, or the contribution of oxygen transport in the oxide due to diffusion along dislocations, crystallite boundaries, or cracks.

Hydrides

Bettis has proposed a model of diffusion and concomitant precipitation to explain the distribution of hydride precipitates during the isothermal aqueous corrosion of Zircaloy.[7] A model was also proposed for the redistribution of the hydride phase in specimens with surface hydride layers during thermal cycling. The models assume that the alpha phase of the Zircaloy can supersaturate with hydrogen, that this supersaturation is metastable and precipitation occurs internally under favorable conditions, and that the precipitation of surface hydride layers is inhibited by the local stresses resulting from the 10 to 20% volume expansion associated with the formation of the hydride. Equations derived for the thermal-cycling model predicted hydrogen values that agreed well with published information.

In-Reactor Corrosion

Two NPD Zircaloy-2 pressure tubes have been examined by Chalk River[8] after 1420 equivalent full-power days of operation (~1450 days in D_2O between 200 and 277°C). Maximum weight gains (as determined from oxide thickness) on the D_2O side ranged from 135 mg/dm^2 at the inlet and outlet to 360 mg/dm^2 at the flux-centerline position. This amount of corrosion was equivalent to out-of-flux exposure at 345°C for the same period of time. Deuterium (hydrogen) pickup ranged from 6 to 20 ppm (1.7 to 5.7 mg/dm^2) and, like the corrosion attack, was greatest at the flux center line.

Zircaloy-2-clad UO_2 fuel elements have been examined by General Electric–San Jose[9] after 1200 days in the Dresden reactor. Average burnups ran 7 to 8×10^{20} fissions/cm^3 (23,000 to 30,000 Mwd/ton of uranium). Measurements of ZrO_2 thickness indicated weight gains ranging from 218 to 529 mg/dm^2, with a mean value of 338 mg/dm^2 for the 1200 days of exposure. Hydrogen content of the Zircaloy-2 cladding was estimated to be less than 100 ppm. Crud thickness (oxides of iron, nickel, and chromium) on the cladding surfaces ranged from 8 to 10 μ.

Corrosion of Iron-Base Alloys

The corrosion behavior of carbon steel in boiling water at 250°C containing 0.1 ppm oxygen was studied in Norway.[10] The corrosion rate was 25 mg/(dm^2)(month) after 3000 hr of exposure and decreased to 10 mg/(dm^2)(month) after 9000 hr of exposure. High oxygen conditions at startup produced less corrosion during initial exposure but had little effect on the corrosion rate at long exposures. The rates of release of corrosion products to the water at 3000 to 9000 hr of exposure were ~15 mg/(dm^2)(month) and 5 mg/(dm^2)(month), respectively. Experiments with activated iron indicated that about 50% of the iron oxide produced by corrosion remained on the metal and part of the remaining 50% that went into solution deposited back on the metal surface. The corrosion rate in the steam phase above the boiling water was unusually high at 40 mg/(dm^2)(month). The high rate might have been related to the abnormally low oxygen content in the steam (0.6 ppm oxygen).

The effect of high-velocity steam on tube bends in once-through steam generators has been examined in a unit operated for 10 years by Babcock and Wilcox.[11] The steam generator was constructed of $\frac{3}{4}$-in.-OD, $\frac{5}{16}$-in.-ID C–Mo-steel (SA209) tubing. It had been operated for approximately 8500 hr at pressures from 500 to 6000 psi and temperatures from 450 to 950°F (230 to 510°C). On the basis of the results of visual and low-powered magnification plus thickness measurements of tube samples, it was concluded that there was no evidence of internal erosion by the steam.

The corrosion-fatigue behavior of 1015 steel in gases, water, and 3% NaCl solution has been studied at the Massachusetts Institute of Technology.[12] The fatigue life was decreased in aqueous environments in the presence of dissolved oxygen (air or oxygen gas), but the normal fatigue limit was regained in deaerated water or deaerated 3% NaCl. Moisture in gaseous oxygen increased the fatigue life but had the opposite effect in argon. Cathodic protection in aerated 3% NaCl regained the normal fatigue limit. The critical potential for optimum life was approximately that required to cathodically protect steel from rusting in soil and water, and this fact indicated that the iron atoms at the crack nuclei were not in a higher energy or activated state.

Corrosion of Nickel- and Cobalt-Base Alloys

The effects of stress, thermal cycling, and isothermal exposure on the oxidation and mechanical properties of nickel-base alloys have been reported by Bendix.[13] Exposure times ranged up to 600 hr at temperatures of 1400, 1600, 1800, and 2000°F (760, 870, 980, and 1095°C). TD-nickel–chromium (2.5 ThO_2–20 Cr) had superior no-load oxidation resistance but was sensitive to stress, and it oxidized internally at temperatures above 1600°F. DH-242 (19 Cr–1.2 Nb + Ta) had good oxidation resistance and ductility retention but was limited to small loads because of excessive elongation at temperatures above 1600°F. Hastelloy X (22 Cr–18.5 Fe–9 Mo) had fair oxidation resistance and ductility retention, despite a comparatively high spall rate. Cyclic oxidation was substantially more severe than steady-state isothermal oxidation for all materials studied.

NASA–Lewis has studied the oxidation behavior of L-605 superalloy (Co–20 Cr–10 Ni–15 W–2 Fe)* in the 1000 to 1200°C temperature range.[14] Both oxidation resistance and ductility were optimized by limiting the silicon and manganese contents of the alloy to the range of 0.1 to 0.4 and 1.4 to 1.65 wt.%, respectively. Alloys within this composition range exhibited parabolic reaction rates and formed scales containing chromium oxide and a spinel phase.

The oxidation behavior of Co–25 Cr and Co–35 Cr alloys has been reported by Battelle–Columbus.[15] Reaction rates were parabolic in the temperature range 900 to 1300°C. For the Co–25 Cr alloy, the parabolic rates at high oxygen pressure (>100 torrs) were about two orders of magnitude higher than those at low oxygen pressure (<10 torrs). The oxidation rates of the Co–35 Cr alloy were independent of oxygen pressure over the range 0.2 to 760 torrs and were comparable to those obtained on the Co–25 Cr alloy at low oxygen pressures. The oxide scale on the Co–25 Cr alloy at high oxygen pressures consisted of an outer layer of CoO and an inner layer of $CoCr_2O_4$ and some CoO. The oxide scale on the Co–25 Cr alloy at low oxygen pressures and on the Co–35 Cr alloy at all pressures was mainly a single layer of $CoCr_2O_4$ with some Cr_2O_3. It was postulated that the initial oxidation rate was controlled by cobalt-cation diffusion through CoO. The diffusion of cobalt and chromium through the spinel then controlled the oxidation when the spinel grew to appreciable thickness. (W. E. Berry)

Corrosion of Refractory Metals

The oxidation of niobium has been studied in the temperature range 450 to 720°C at oxygen pressures of 1 to 760 torrs.[16] Particular emphasis was placed on correlating the morphology of the reaction products with the oxidation kinetics. During the initial, approximately parabolic oxidation period, the scale appeared compact. At the transition from parabolic to linear kinetics, the scale blistered and cracked. The scale that formed during linear oxidation grew in a series of crude layers. From the relations determined between the oxidation rate and oxide-layer thickness, it was deduced that oxidation was controlled by the diffusion properties of the oxide layer in contact with the metal phase. The sensitivity of the oxidation rate to oxygen pressure was ascribed to the pressure sensitivity of the parabolic rate constant for the formation of Nb_2O_5, and to a lesser extent to changes in the width of oxide layers and the rate of their formation. The inversion in the temperature coefficient on lowering the temperature from 625 to 600°C was associated with the disappearance of NbO and NbO_2 layers from the reaction zone and the appearance of a metastable platelet phase.

The state of knowledge of the interaction of Nb, Ta, Mo, W, and their alloys with active gases in vacuum and inert-gas environments has been documented[17] by Oak Ridge. At temperatures of 600 to 2000°C and pressures of 10^{-3} to 10^{-10} torr, contamination, degassing, decarburization, and sublimation reactions occur between the metal and absorbed gases. The extent and kinetics of these reactions are governed by the deviation of the interstitial concentration from the equi-

*Unless otherwise designated, all compositions are understood to be by weight percent.

librium concentration dictated by the temperature and pressure of the active gas. The reaction rates in inert gases are equivalent to vacua approximating 10^{-5} to 10^{-7} torr.

Grumman Aircraft[18] has studied the effect of Li_2O on the air oxidation of Nb, Ta, Mo, W, Ta–10 W, and Cb-752 from 400 to 1100°C. Oxidation was retarded more for niobium and tantalum than for molybdenum and tungsten. The protective mechanism appeared to be the substitution of OH^--ion chemisorption for oxygen chemisorption.

The Bureau of Mines found[19] the chemical and galvanic corrosion behavior of TZM molybdenum and Mo–30 W to be generally equal or superior to that of unalloyed molybdenum in many aqueous solutions of acids, bases, and salts. Notable exceptions occurred in 1*N* HNO_3, where both alloys corroded appreciably faster than molybdenum. In $HgCl_2$ solutions, TZM was susceptible to a type of crevice corrosion that was not due to differential aeration. The alloys were usually not affected adversely by contact with dissimilar metals in galvanic couple experiments, but the dissimilar metals sometimes corroded galvanically. Both alloys were resistant to substitute ocean-water spray at 60°C.

The oxidation of molybdenum, tungsten, and rhenium powders at 20°C in air of various humidities was investigated in Germany.[20] In air saturated with H_2O, the formation of hydrous molybdenum oxides followed a linear rate law. In the case of tungsten, oxidation was initially logarithmic and then linear. The oxide formed by tungsten corresponds to $WO_3 \cdot 2H_2O$. After exposure of specimens to dry air for 70 days, the amount of oxygen on the surfaces of the three metals corresponded to 1 to 3 monatomic layers.

Oxygen adsorption and thermal stability of the (1 1 1) molybdenum surface has been investigated by NASA–Lewis[21] using low-energy electron diffraction. The interaction of oxygen with polycrystalline tungsten ribbon has been studied by National Bureau of Standards[22] using electron-stimulated desorption.

(B. C. Allen)

Corrosion by Nonaqueous Liquids and Vapors

Steels in Sodium or NaK

General Electric is in the 10th year of an experimental program designed to provide reliable predictions of the ability of candidate structural materials to withstand corrosion by flowing sodium. Hopefully, by delineating the effects of operating variables on corrosion and mechanical properties, the program will permit the establishment of sodium-purity requirements and other materials specifications for large liquid-metal-cooled fast breeder reactor (LMFBR) plants.

To date the following have been established concerning the rate of corrosion of austenitic stainless steels by 1300°F (700°C) peak-temperature sodium:[23]

1. In an isothermal zone the rate decreases with increasing distance downstream, as shown in Fig. III-2.

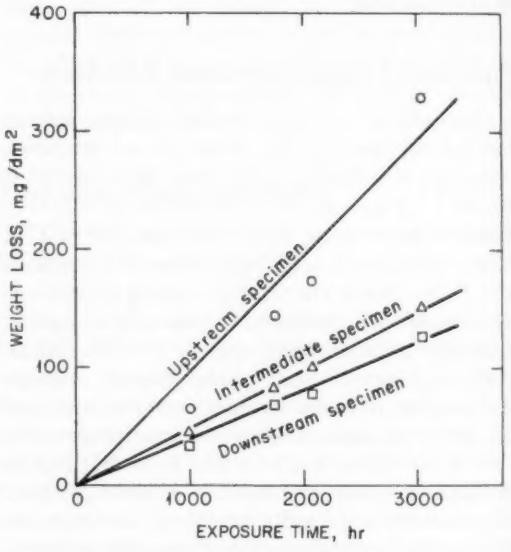

Fig. III-2 Influence of location in loop on corrosion rate[23] of annealed 316 stainless steel in 1300°F (700°C) sodium (<10 ppm oxygen, ~9 ft/sec).

2. The rate increases with increasing velocity.

3. Corrosion proceeds by (1) selective leaching of chromium, nickel, and manganese and (2) stoichiometric dissolution of the resulting surface-alloy composition with diffusion of chromium, nickel, and manganese in the iron-rich surface layer.

4. In a monometallic austenitic loop, the steel is decarburized in the 1200 to 1300°F (650 to 700°C) sodium temperature range and carburized in lower temperature regions.

5. Type 316 stainless steel is corroded in 1200 to 1300°F sodium more rapidly under heat-transfer conditions than under isothermal conditions.

6. The corrosion rate of 316 stainless steel is linear with time and is lower than that of 304 or 347 stainless steel. Incoloy 800 corrodes much faster in 1300°F sodium than do the austenitic steels. These effects are apparent in Fig. III-3.

Mass transfer by sodium in stainless-steel systems has been studied extensively. However, there is no reliable way to estimate the amount and location of corrosion products deposited from flowing sodium as functions of temperature, flow rate, sodium purity, and system geometry. In addition to being undesirable from the standpoints of fouling of passages and weakening of structures, mass transfer could cause the buildup of such concentrations of long-lived radioactive deposits in out-of-core LMFBR piping as to interfere drastically with maintenance and inspection procedures.

By observing the migration of radioactive species carried by flowing sodium from irradiated source tabs inserted in loops, workers at Battelle–Northwest[24a] are learning some interesting facts about radioisotope transport and deposition in sodium systems. For instance, ^{51}Cr moves downstream from the source by random isotopic exchange, the rate being governed by the frequency with which ^{51}Cr atoms collide with the pipe walls. This mechanism explains the relatively slow observed migration of ^{51}Cr, as well as the increased deposition in turbulent regions. On the other hand, the transport of ^{54}Mn depends on other factors besides isotopic exchange, although the latter is still important.

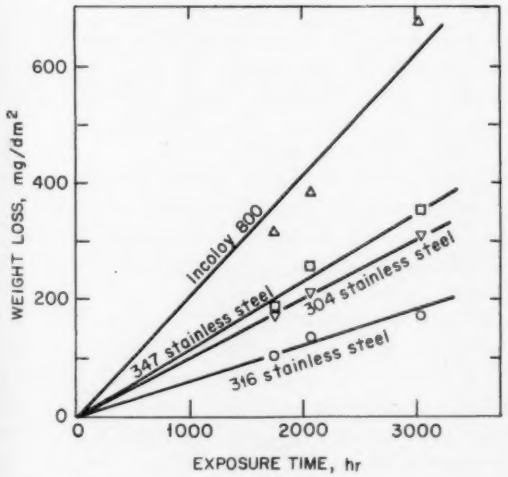

Fig. III-3 Corrosion rates[23] of annealed materials in 1300°F (700°C) flowing sodium (<10 ppm oxygen, 17 ft/sec).

The presence of ^{54}Mn activity on the downstream side of the heat exchanger and in higher concentrations in the cold trap suggests a solution-precipitation process. In the cold trap the manganese retention may be assisted by the reaction:

$$Mn\ (\text{in Na}) + 4Na_2O\ (\text{on trap surfaces}) = NaMnO_4\ (\text{on trap surfaces}) + 7Na\ (\text{liquid})$$

Regions of increased sodium velocity seem to have higher surface concentrations of ^{54}Mn, indicating that the thinner boundary layers facilitate deposition. Comparison of the amounts and mobility of ^{51}Cr and ^{54}Mn in the different experiments indicates that manganese is more preferentially leached from stainless steel by sodium than is chromium.

Examinations were conducted on several 316 stainless-steel components of a circulating NaK loop which had run over 24,000 hr between 600 and 760°C at the Idaho Chemical Processing Plant.[25] About 1 mil of decarburization was found on the inside walls in the hot region, and about 5 mils of carburization was noted on the electromagnetic pump cell, which was in the colder region of the loop. Hardness and tensile-strength values of the exposed pipe were not significantly different from values for unexposed pipe. However, the room-temperature elongation decreased about 43%, and the elongation at 760°C decreased about 63%. The exposed pipe cracked badly during an ASTM A-376 flattening test, whereas unexposed pipe passed the test. The Izod V-notch impact resistance of exposed pipe was 65% less than that of unexposed pipe. The ASTM A-262 boiling nitric acid tests indicated that the exposed piping was sensitized.

The general conclusion is that 316 stainless steel is a suitable material of construction for polythermal NaK loops at 600 to 760°C, if proper attention is paid to keeping the oxygen level in the NaK and the stresses in the parts sufficiently low. This is based on the fact that extensive cracking and brittle fracture were found only in stressed fittings, following progressive sigma formation, grain-boundary precipitation of carbides, and accompanying embrittlement.

Although mass transfer of carbon in flowing-sodium systems has been studied extensively, the phenomenon is not well understood. When ferritic and austenitic steels are present in one loop, the former may be decarburized and the latter carburized. On the other hand, it has been noted by the Soviets that sodium containing some oxygen impurity can decarburize plain-carbon steels to form CO in the absence of any other carbon sink. Still other work suggests that

the decarburization is tied in with a surface reaction. Borgstedt, for example, noted[26] that carbon was transferred isothermally by 700°C sodium from an unstabilized austenitic steel (18 Cr–9 Ni) to a stabilized austenitic steel (16 Cr–13 Ni–Mo–V–Nb), causing the latter to be embrittled to a depth of 0.1 mm in 1000 hr.

For more information, British investigators examined metallographically some specially tailored carbon steels that had been exposed for 260 hr to 600°C sodium containing ~30 ppm oxide.[27] The compositions and observations are summarized in Table III-1. These results suggest the following:

1. Contact with sodium enhances graphitization and decarburization of carbon steel.
2. Chromium in the steel prevents or retards graphitization by sodium.
3. Neither manganese nor silicon affects graphitization of carbon steel in the presence of sodium.
4. Decarburization by sodium is effectively inhibited by chromium or manganese in the steel, whereas the presence of silicon in the steel or the presence of stainless steel in the system does not seem to affect the depth of decarburization.

The mechanism is obscure by which sodium accelerates graphitization and causes decarburization and surface deposits. One theory suggests that graphitization is the result of sodium electrons passing into the steel and being taken up by the carbon "ions," and decarburization and surface deposits stem from the carbon ions moving out of the steel to the sodium electrons. This is consistent with the inhibiting effect of chromium, which is an avid electron acceptor that leaves none of the sodium electrons available to promote either graphitization or decarburization. Silicon, on the other hand, is an electron donor and should have the opposite effect, but this was not observed.

Table III-1 Carbon Migration Observed in Steels After 260-hr Capsule Exposures to 600°C Sodium[27]

Test alloy (balance iron), wt.%	Graphitization, %*	Depth of decarburization, mm	Graphite deposit?
1.2 C†	40	0.23	No
1.2 C‡	2	0	No
0.3 C§		0.27	Yes
0.8 C–0.9 Cr§	0	0	No
0.7 C–0.9 Mn§	35	0	No
0.7 C–0.9 Si§	25	0.25	Yes

*Estimated percentage of total possible graphitization.
†Nickel capsule with one end cap made of test alloy and the other of stainless steel.
‡Nickel capsule with bottom made of test alloy, heat-treated in vacuo as a control.
§Capsule and both end caps made of test alloy.

Work at Argonne[28] has shown that disodium acetylide, Na_2C_2, is an important species in carbon transport. This compound is the most likely precursor of the acetylene found in the off-gas following hydrolysis and acidification of sodium that had been heated in contact with ^{14}C-labeled Fe–C alloy at ~650°C, either with or without a carbon sink present. Studies are continuing to see how the concentration of Na_2C_2 in sodium is affected by various parameters.

Ceramic Fuels in Sodium

Workers at General Electric[29] have combined published values of the partial molar free energy of oxygen, $\Delta\bar{G}_{O_2}$, for U–Pu oxides with those for the Na–O system into a composite graph, Fig. III-4. This can be used to estimate under what conditions it is thermodynamically possible for sodium to reduce the oxide fuels (i.e., when the $\Delta\bar{G}_{O_2}$ for the fuel is more positive than the $\Delta\bar{G}_{O_2}$ for the sodium). Note that the hyperstoichiometric fuel, UO_{2+x}, is easily reduced by sodium under virtually all practical conditions, whereas reduction of the hypostoichiometric fuels is much more sensitive to operating conditions. For instance, sodium containing 10 ppm oxygen will reduce $(U_{0.8}Pu_{0.2})O_{1.98}$ at 700°C, whereas sodium containing 100 ppm oxygen will not.

In preparation for compatibility tests of sodium-bonded (U,Pu)C fuel pellets with 316 stainless-steel cladding, workers at Los Alamos[30] made a study to determine which method of removing the sodium bond has the least effect on the fuel surfaces. Bonds were removed by dissolution in various solvents and by distillation (5×10^{-6} torr at 485°C), after which the sintered (U,Pu)C structures were examined metallographically and porosities determined by a two-dimensional point-count method (Table III-2). The results showed conclusively that low-temperature distillation has markedly less effect on the pore size and shape than do the dissolution methods. The ethyl alcohol–5 vol.% water caused the severest attack. Butyl and ethyl alcohols produced rounded pore edges, probably because the dissolution did not remove all of the sodium prior to metallography. However, the sharp pore edges of the original sample were still present in the vacuum-distillation specimens.

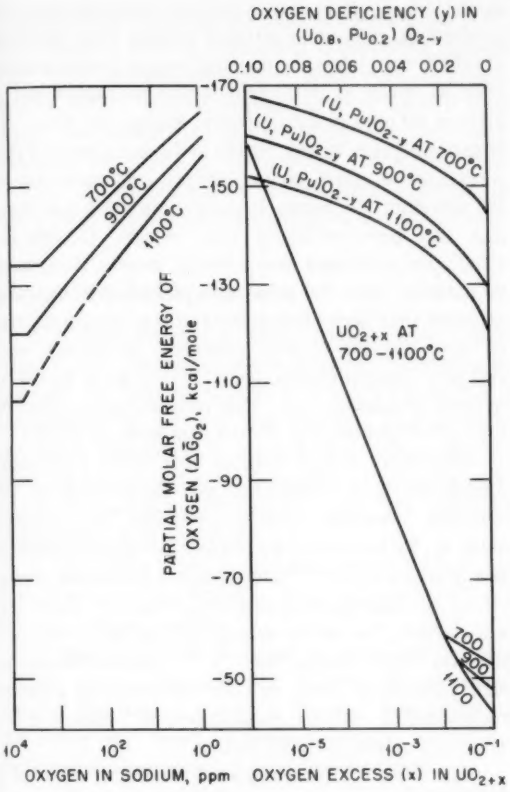

Fig. III-4 Effect of oxygen content on chemical potential of oxygen in sodium and in oxide fuels.[29]

Table III-2 Effect of Sodium-Removal Techniques on Porosity of (U,Pu)C Pellets[30]

Technique	Porosity, % Av.	Porosity, % Max.	Max. pore size, μ
As-received (unbonded)	10.0	11.0	16.6
Dissolution			
Ethanol	12.5	13.0	21.8
Butanol	11.7	12.2	16.2
Ethanol + 5 vol.% H_2O	19.7	23.3	33.3
Distillation	8.5	10.0	12.9

Solubilities in Sodium

There is a wide variation in the values for the solubility of oxygen (or of Na_2O) in sodium reported by different investigators. Since this solubility is a key factor in the behavior of sodium in practical heat-transfer systems, Eichelberger at Atomics International[31] reviewed all the published data and derived the following solubility expression from 107 of the most valid determinations from five laboratories:

$$\log S(\text{wppm oxygen}) = 6.239 - 2447/T(^\circ\text{K})$$

from the melting point of sodium up to about 550°C. The low-temperature portion of the curve is shown in Fig. III-5.

South African scientists[32] used radiotracers to measure the solubilities of silver, zinc, and cerium in molten sodium. The resulting equations for the mole fraction, X_i, of solute dissolved as a function of the absolute temperature, T, are:

For silver,

$$\log X_i = 0.899 - \frac{1.642 \times 10^3}{T(^\circ\text{K})} \quad (100 \text{ to } 270^\circ\text{C})$$

For zinc,

$$\log X_i = 0.998 - \frac{2.562 \times 10^3}{T(^\circ\text{K})} \quad (190 \text{ to } 550^\circ\text{C})$$

For cerium,

$$\log X_i = -9.467 + \frac{0.659 \times 10^3}{T(^\circ\text{K})} \quad (120 \text{ to } 460^\circ\text{C})$$

The oxygen content of the sodium used was 11 ppm (by vacuum distillation), which is several times the concentration of the observed cerium solubility. The decreasing solubility of cerium with increasing temperature (and consequent apparent negative heat of solution) is not very likely thermodynamically. Thus, as the authors suggest, it appears plausible that Ce_2O_3 and not cerium was the reference solute in this system and that metallic cerium is substantially less soluble than Ce_2O_3 in sodium.

Corrosion by Potassium

Alloys of niobium that contain strong oxide formers like zirconium or yttrium have shown excellent resistance to boiling potassium at temperatures up to 1300°C for times as long as 5000 hr. Subsequent comparable studies[33a] revealed that, without such oxide formers, niobium is heavily attacked by 1200°C refluxing potassium and that the severity of the attack increases with increasing oxygen content of the potas-

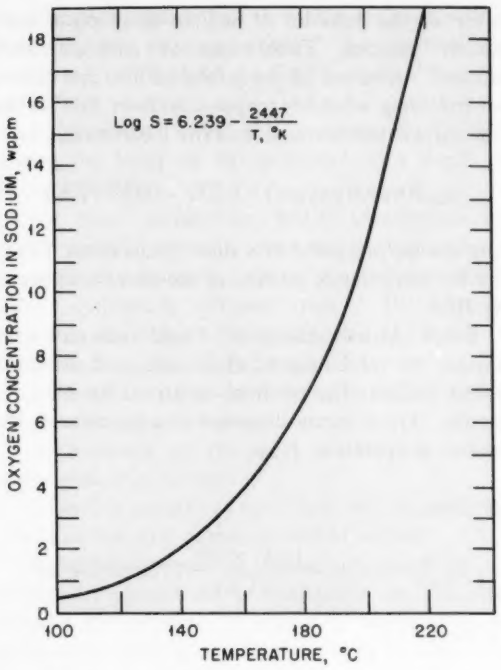

Fig. III-5 The solubility[31] of oxygen in liquid sodium to 220°C.

sium. This sensitivity to the oxygen content of the potassium is much more pronounced in boiling-refluxing systems than in nonboiling potassium systems. For example, additions of up to 2400 ppm oxygen to the potassium in an all-liquid (nonboiling) system caused only slight increases in attack of the niobium. The Oak Ridge researchers hypothesize that the difference stems from increased local concentrations of oxygen as a result of distillation effects in the boiling process. Although niobium does not normally getter oxygen from potassium, these local enrichment effects are believed to drive the oxygen into the niobium and cause gross attack.

The usual behavior in the Nb–O–K system is for oxygen to migrate from the niobium to the potassium at a rate governed by the diffusivity of oxygen in niobium. As shown in Table III-3, diffusion coefficients calculated on the assumption that the final oxygen concentration measured in Oak Ridge capsule experiments at 600 to 1250°C had been maintained at the niobium surface throughout the exposures were in good agreement with those found in the literature.

Experiments at Oak Ridge[33d] indicate that the role of oxygen in the Ta–O–K system is similar to that in the Nb–O–K system. Contrary to thermodynamic predictions, potassium gettered oxygen from tantalum at 600°C even when the starting oxygen concentrations were as much as 3400 ppm in the potassium and as little as 40 ppm in the tantalum. Adding oxygen to the potassium prior to the 500-hr refluxing capsule exposures had no effect on the posttest microstructure of the tantalum specimens. However, tantalum specimens that had been predoped with oxygen (to 600 and 1300 ppm) exhibited heavy attack, mostly along grain boundaries. Also, the potassium picked up tantalum in amounts that depended on the starting oxygen content of the potassium. For example, potassium with 100 ppm oxygen picked up 0.2 to 0.3 wt.% tantalum, whereas potassium with 3400 ppm oxygen contained 1.2 wt.% tantalum after 500-hr exposures at 600°C.

The above results indicate that some potassium-soluble Ta–O–K compound may be involved in the tantalum corrosion process—perhaps the complex oxide K_3TaO_4 isolated by NASA–Lewis and discussed in a previous review.[34] This complex oxide and several others in analogous systems ($K_4Nb_6O_{17}$, K_3NbO_4, and $NaNbO_3$) were the subjects of crystal-growth and property studies during 1968.[35,36] Characterization of such compounds may well be important to a better understanding of the mechanisms of corrosion of refractory metals by alkali metals.

Oak Ridge[37] has completed a 3000-hr test of a Nb–1 Zr boiling-potassium forced-circulation loop containing three stages of nozzles and simulated turbine blades subjected to 97 to 83% quality potassium vapor at 1015 to 680°C. The only surface change found in the entire loop was a roughening of the leading edge of the second-stage blade specimen to a depth of 1 mil where it had been impinged upon by 3080 ft/sec vapor of 83% quality. The Nb–1 Zr alloy had gettered oxygen from the potassium—particularly in the hotter loop regions. A chromium-rich layer found on the second-stage blade was attributed to

Table III-3 Diffusion of Oxygen in Niobium[33c]

Temp., °C	Diffusion coefficient, cm^2/sec, obtained by indicated method		
	ORNL exposures (R. L. Klueh)	Internal friction (C. Y. Ang)	Hardness traverses (R. I. Jaffee et al.)
600	3.50×10^{-9}	1.81×10^{-9}	2.24×10^{-9}
815	2.23×10^{-8}	4.23×10^{-8}	4.07×10^{-8}
1000	4.35×10^{-7}	2.68×10^{-7}	2.19×10^{-7}
1250	1.64×10^{-6}	1.62×10^{-6}	1.10×10^{-6}

chromium leached from the stainless-steel pump cell. This suggests that stainless-steel components should have been avoided altogether since even this very limited surface area of low-temperature stainless steel caused noticeable chromium transport. The creep resistance of Nb–1 Zr is marginal for service near 1100°C, as evidenced by a significant increase in diameter of the tubing at the dryer section of the loop.

Corrosion by Lithium

A Cornell University dissertation has been published[38] on the penetration of grain boundaries of niobium by lithium at 800 to 1050°C, including a quantitative model for the process. The niobium specimens consisted of oriented bicrystals, each containing a simple tilt grain boundary at an angle of 6, 16, or 33° and 0 to 2400 ppm oxygen. The following observations were reported:

1. Specimens without oxygen showed no reaction with lithium; the reaction rate increased with increasing oxygen content.

2. Specimens of all three orientations suffered surface attack, but only the 16 and 33° specimens showed preferential attack in the grain boundaries. In the latter the depth of grain-boundary penetration increased as the square root of exposure time.

3. The rate constant k for grain-boundary attack, according to X (depth of penetration) $= kt^{1/2}$, had an activation energy of ~70 kcal/mole.

4. Penetration was anisotropic, the rate parallel to the common ⟨1 1 0⟩ being larger than the rate perpendicular to it.

5. The corrosion process appeared to be controlled by solid-state grain-boundary diffusion.

The effect of oxygen contamination of T-111 (Ta–8 W–2 Hf) and T-222 (Ta–10 W–2.5 Hf) TIG-welded specimens on their corrosion resistance to lithium was determined by Oak Ridge workers[33b] in 100-hr exposures at 750 and 1200°C. No attack of the weld or heat-affected zones was observed in samples containing up to 540 ppm oxygen. However, the base metal was attacked to a depth of 10 mils unless it had been heat-treated for 2 hr at 1300°C after welding. This was explained by the fact that the weld heat was sufficient to homogenize the oxygen concentration and cause precipitation of HfO_2 in the weld and in the heat-affected zone but not in the base metal. Unless the base metal was annealed, the large concentration of oxygen near the surface rendered it susceptible to heavy attack.

Workers at the Lawrence Radiation Laboratory[39] have devised a pumped-capsule apparatus for dynamic corrosion testing of materials by high-temperature molten metals. They demonstrated its feasibility by circulating liquid lithium at about 1500°C (hot end) and 1250°C (cold end) at about 1 ft/sec for close to 700 hr and found little corrosion damage to the W–30 at.% Mo–30 at.% Re capsule parts. The pumped capsule consists of a closed tube containing a splitter plate that separates the bore into two semicircular channels. The two channels join at both ends of the tube to form a complete loop. The molten metal is circulated by a d-c electromagnetic Faraday conduction pump. Heating one end of the tube and cooling the other simulates a polythermal coolant loop.

Corrosion by Cesium

In connection with thermionic cell development, workers at Gulf General Atomic[40] subjected 11 ceramic-to-metal seals to 1200°C cesium vapor for 1950 hr. Specimens included niobium-to-Lucalox joints prepared by metallizing the ceramic and brazing with 60 V–40 Nb, graded seals, and a sandwich insulator prepared by vapor depositing niobium on both sides of an alumina wafer. Posttest visual appearance, peel strength, microstructure, and microprobe analyses of these specimens showed no significant differences from corresponding features of comparable thermal-stability test specimens, indicating that the cesium caused no observable deterioration.

Corrosion by Diphenyl

The Soviets conducted studies[41] of the interactions of various nuclear fuel and cladding materials with diphenyl by exposing samples in diphenyl-filled stainless-steel capsules under argon at 320 to 450°C for periods up to 540 hr. Pyrolytic decomposition of the diphenyl was not significant below about 400°C but increased rapidly with increasing temperature and test time. Powdered specimens of UO_2, ZrO_2, TiO_2, Ta_2O_5, Nb_2O_5, Cr_2O_3, Fe, UC, ZrH, and Al were stable in diphenyl under all test conditions. Powdered U_3O_8 was reduced to UO_2, and powdered SAP containing aluminum hydroxide was reduced to pure aluminum. Other powders yielded carbides or hydrides, as shown in Table III-4. Also, oxides could be formed from metals (e.g., U, Mg, Zr, Fe) when the diphenyl contained water or oxygen as impurities.

Water additions (above about 0.1 wt.%) to diphenyl were found to accelerate the 500-hr corrosion

Table III-4 Changes in Powdered Materials Exposed to Diphenyl[41]

Starting material	Test conditions °C	Test conditions Hr	Final product
MoO_3	410	540	$MoC + MoO_3$
Ti	450	240	TiC
Ti	410	540	Ti + TiC
Ti	370	500	Ti + TiC
U	420	200	$UC + UH_3$
U	370	500	UH_3
Zr	450	240	ZrH
Zr	410	540	ZrH
Zr	370	500	ZrH
Nb	450	240	NbH
Nb	410	540	NbH
Nb	370	500	NbH
Ta	450	240	TaH
Ta	410	540	TaH
Ta	370	500	TaH

of both aluminum and SAP at 410°C, the aluminum being more sensitive. Sulfur additions up to 3 wt.% had no noticeable effect on the 250°C interaction of diphenyl with either SAP or aluminum.

Another phase of this study involved the kinetics of the corrosion of uranium and U–Mo alloys by diphenyl. Diphenyl attacks unalloyed uranium by progressive formation of the hydride or hydride plus carbide (depending on temperature) at grain boundaries. Uranium tabs 20 mils thick were found to be completely converted to powder after 400 hr in 450°C diphenyl. The addition of enough molybdenum to uranium to produce a stable gamma structure (6 to 10 wt.% molybdenum) gives the alloy excellent stability in diphenyl. For instance the U–9 Mo alloy showed no evidence of surface alteration after 400 hr at 450°C. The effects of temperature and molybdenum content are apparent in Fig. III-6. (E. M. Simons)

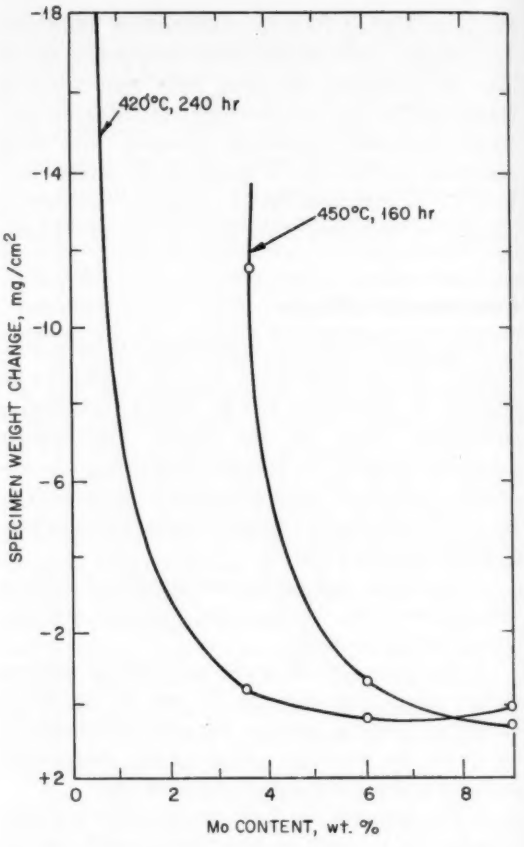

Fig. III-6 Influence of molybdenum alloying additions on resistance of uranium to attack by diphenyl.[41]

Cladding Reactions Following Loss-of-Coolant Accidents

Argonne has published a computer program[42] for determining the extent of core heating and metal–steam reaction following a hypothetical loss-of-coolant (LOC) accident in a water-cooled power reactor. The program carries the calculations from the end of blowdown, through core heating, chemical reaction, failure, and collapse of the core onto the bottom of the supporting structure. Material properties and metal–water reaction rates among other parameters are required for program input. The program output includes fuel, cladding, and gas temperatures throughout the core, thickness of cladding reacted, fraction of steam or hydrogen in the gas, and several other parameters, all as functions of time.

At Argonne, simulated fuel rods consisting of UO_2 pellets encased in Zircaloy tubing were heated inductively in a flowing steam atmosphere and water quenched to simulate emergency core cooling following an LOC accident to assess the extent of damage to the fuel rods.[43] The results of these experiments are

Table III-5 Results of Out-of-Pile Loss-of-Coolant Experiments Using Inductively Heated Simulated Fuel Rods[43]

(Fuel Was Zircaloy-2-Clad, UO_2-Pellet Core; Steam Flow Rate Was 2 g/min; Flow Rate of Cooling Water Was 190 g/min)

Heating rate, °C/sec	Quench temp., °C	Bottom or top quench?	Power on or off during quench?	Hydrogen collected,* mole	ZrO_2 produced,† mole %		Apparent dissolved O_2 in unoxidized metal, mole %	Equivalent average reaction,‡ mole %	Rod failed or intact?
					Av.	Max.			
9.0	1064	Top	On	0.0	1.6	3.2			Intact
4.8	1462	Bottom	Off	0.025	3.5	6.8	3.45	6.87	Intact
6.0	1488	Bottom	On	0.026	3.7	6.1	3.6	7.14	Intact
~50§	1182	Top	On	0.024	3.8	5.4	2.9	6.59	Intact
6.4	1548	Top	Off	0.025	4.0	8.0	3.0	6.87	Intact
3.1	1534	Bottom	On	0.029	4.8	3.0	3.34	7.97	Intact
5.2	1498	Top	On (3.55)¶	0.042	7.0	12.0	4.88	11.54	Intact
5.0	1663	Bottom	Off	0.062	12.3	21.1	5.0	17.03	Intact
4.8	1798	Bottom	Off	0.067	14.0	22.0	4.5	18.40	Failed
4.6	1569	Top	On (3)¶	0.068	14.3	22.3	4.5	18.68	Failed
5.7	1849	Top	Off	0.081	16.0	22.1	7.3	22.25	Failed
4.7	1646	Bottom	On	0.093	13.0	25.0		25.55	Failed
4.5	1650	Top	Off	0.080	17.6	29.0	5.18	21.98	Failed
5.7	1864	Bottom	Off	0.081	17.4	34.5	5.6	22.25	Failed
5.1	1663	Top	On (4.18)¶	0.102	20.5	34.0	9.3	28.02	Failed
6.5	2052	Top	On (2.75)¶	0.14	30.0	41.0	12.0	38.46	Failed
6.3	2110	Top	On	>0.1		~100			Failed
5.2	1868	Top	On	>0.1		~100			Failed

*Oxygen produced was taken to be one-half this amount.
†From metallurgical examination of 3-in. heated length of cladding.
‡Equivalent average reaction of 3-in. heated length of cladding based on total oxygen produced.
§This run followed a predetermined temperature–time curve simulating a particular ECC (emergency core cooling) situation.
¶Power turned off at this time (min) after initiation of quench.

shown in Table III-5. The rods with equivalent average reactions (see table) of 18.4 mole % or greater failed, whereas those with equivalent average reactions of about 17 mole % or less remained intact. The failure pattern of the claddings in these experiments is shown in Table III-6. The lowest quenching temperature at which cladding failure was observed (1534°C) occurred in the experiments in which the power remained on after a quench was initiated at the top. The estimated maximum temperature for fuel rods subjected to an actual emergency core-cooling situation following an LOC accident in a water-cooled power reactor is in the range 1000 to 1200°C. However, it is difficult to convert the measured critical quenching temperature to the same basis because of vast differences in geometry, restraint, oxidation effects, and radiation effects between the test setup and an actual fuel assembly.

(H. S. Rosenberg)

Table III-6 Failure Pattern of Out-of-Pile Loss-of-Coolant Experiments Using Single, Inductively Heated, Simulated Fuel Rods[43]

Quench temp., °C	Power on after quench initiated		Power off after quench initiated	
	Top quench	Bottom quench	Top quench	Bottom quench
1064	I*			
1182	I			
1462 to 1498	I	I		I
1534 to 1569	F†	I	I	
1646 to 1663	F	F	F	I
1798				F
1849 to 1868	F		F	F
2050 to 2110	F			

*I indicates that test rod remained intact.
†F indicates that test rod failed.

Radiation Effects in Structural Materials

Stainless Steels and Nickel Alloys

In a study of the effect of cold work on the postirradiation elongation of stainless steels at elevated temperatures,[44] specimens of annealed [1800°F (980°C), air cooled] and of 25% cold-rolled 304 and 348 stainless steels were irradiated in the EBR-II at 590 ± 80°C to a total fluence of 1.7×10^{22} neutrons/cm^2. The annealed specimens showed large yield-strength increases, but the cold-worked specimens did not. Irradiation at 590°C in EBR-II actually improved the ductility of cold-worked specimens when they were tested at 500°C or lower, whereas at higher testing temperatures their ductility was less than it was before irradiation. For equal testing temperatures and heat-treatments, there was little difference in elongation behavior between 304 and 348 stainless steels. Both steels showed greater postirradiation elongation in the annealed condition than in the cold-worked condition, the difference increasing with increasing testing temperature.

Longitudinal and transverse specimens of cold-rolled and recrystallized 16/13 CrNi stainless steel were irradiated by the Germans[45] to a fluence of 3×10^{20} neutrons/cm^2 and tested in tension at 500 to 800°C. The specimens pulled parallel to the rolling direction showed significantly less radiation-induced embrittlement than did those pulled perpendicular to the rolling direction. To study the relative effects of recrystallization (2 hr at 900°C) before and after irradiation and annealing without recrystallization (170 hr at 700°C), the investigators irradiated specimens of the same steel in the FR-2 reactor to a thermal fluence of 3×10^{20} neutrons/cm^2 and tested them in tension at 750°C at a strain rate of 0.1 min^{-1}. The results of the experiments are summarized as follows:

1. Annealing at 700°C before irradiation led to a remarkable reduction in the high-temperature embrittlement. This effect may be attributed, in part, to an increasing dispersion of carbide particles.

2. Specimens that had been recrystallized at 900°C prior to irradiation showed more embrittlement after irradiation than did specimens that had been annealed at 700°C before irradiation.

3. Cold-worked specimens that were recrystallized after irradiation showed a higher ductility than did specimens that had been recrystallized before irradiation. This effect decreased with an increasing amount of cold work.

Table III-7 shows tensile properties of 304 stainless-steel sheet that was irradiated[46] in contact with flowing sodium in the EBR-II. These results show the typical trend of decreasing ductility and increasing strength with increasing fast fluence. The irradiation temperature appears to be important, with more hardening resulting from irradiation at 370°C than from the same fluence at 480°C.

Stress-rupture tests on irradiated 304 stainless steel at elevated temperatures indicated[24b] that the rupture life was reduced about fourfold by irradiation in EBR-II at 480°C to fluences ranging from 0.5 to 2.0×10^{22} neutrons/cm^2 in a helium atmosphere. The data are shown in Table III-8.

Thin-walled tubes of Inconel 625, Incoloy 800, 16/13 CrNi stainless steel, and 20/25 CrNi stainless steel were stress-rupture tested at 600 and 700°C in the Belgian material test reactor (BR-2), where the maximum neutron flux above 0.1 Mev was 4×10^{14} neutrons/(cm^2)(sec).[47] All the alloys underwent radiation-induced reductions in rupture life, the greatest reductions taking place in Inconel 625 and 16/13 CrNi stainless steel. The results are typified by Fig. III-7, which shows the stress-rupture plots for the 16/13 CrNi steel.

Irradiation of 316 stainless steel to 3×10^{18} neutrons/cm^2 ($E > 1$ Mev) at 70°C was found[48] to reduce its fatigue life by a factor of about three at 650°C under cyclic strains of 1 to 2% at a strain rate of 4×10^{-5} sec^{-1}.

Short-time burst tests and longtime creep tests have been performed on irradiated tubing to evaluate its postirradiation ductility for fuel-pin applications. However, this approach provides a test that only simulates the fission-gas pressure in the fuel element. Swelling of the nuclear fuel superimposes a progressive strain on the cladding that may alter its behavior. A ring ductility test has been developed by workers at General Electric[49] to simulate the swelling of the fuel in a fuel element during irradiation. The ring test utilizes an expanding cylindrical mandrel inside a ring section of the tubing to be tested. Rings of 347 stainless-steel tubing that had been irradiated in the EBR-II to a fast fluence of 2×10^{20} neutrons/cm^2 at 540°C were tested at 705°C, with the results shown in Table III-9. The irradiated tubes exhibit ductilities that are much higher than the ductility that results from a burst test on irradiated tubing. At comparable temperatures the burst-test ductility ($\Delta D/D_0$) of an unirradiated tube is

Table III-7 True Stress–True Strain Properties of Irradiated 304 Stainless Steel[46]

Test temp., °C	Fluence, 10^{22} neutrons/cm^2	Irradiation temp., °C	Yield stress, 1000 psi	Ultimate stress, 1000 psi	Fractional uniform strain	Fractional total strain
450	0.4	460	36.0	75.0	0.169	0.176
450	2.0	480	64.6	77.9	0.056	0.072
450	2.0	480	64.6	80.2	0.072	0.080
450	2.0	371	75.0	78.3	0.025	0.036
450	2.0	371	85.1	91.5	0.027	0.039
450	4.8	420	95.6	100.3	0.020	0.027
550	<0.1	460	21.0	57.7	0.182	0.190
550	<0.1	460	25.7	66.0	0.180	0.189
550	0.6	480	41.8	62.8	0.122	0.132
550	0.6	480	41.9	64.8	0.125	0.139
550	2.0	371	69.6	72.3	0.020	0.031
550	3.6	460	70.5	75.6	0.021	0.025
650	0.4	460	25.4	40.4	0.086	0.095
650	1.4	480	33.0	39.3	0.048	0.065
650	1.4	480	34.9	42.7	0.045	0.069
650	2.6	480	37.7	42.6	0.029	0.034
650	2.6	480	35.9	40.4	0.025	0.038
750	<0.3	460	15.1	19.0	0.055	0.092
750	1.0	480	15.5	19.4	0.054	0.092
750	1.0	480	15.5	21.1	0.065	0.088
750	2.6	480	20.2	21.5	0.018	0.038
750	2.6	480	20.6	23.0	0.020	0.033

generally less than 20% and that of an irradiated tube is generally less than a few percent. The large ductility values for the irradiated tubes in ring ductility tests are attributed to surface shear loads, which originate from the friction between the mandrel and the test ring and suppress necking. This resistance to necking allows uniform strain to proceed almost to fracture.

Workers at Atomics International[50] measured the elevated-temperature tensile properties of samples of Incoloy 800 and 405 stainless steel that were helium impregnated by cyclotron bombardment to a helium atom fraction of 4×10^{-5}. They found that the ultimate and yield strengths of Incoloy 800 were not affected by helium over the 500 to 800°C range of testing temperatures. However, at 700 and 800°C, helium reduced uniform elongation by about 30% and the total elongation by a factor of about 3. The presence of fine precipitates produced by 50% cold work and annealing (100 hr at 760°C) did not alter the behavior of the helium-impregnated Incoloy 800, except that the elongation at 700 and 800°C was reduced even more. The ductility of the ferritic 405 stainless steel at 750°C was less affected by helium than the ductility of either Incoloy 800 or austenitic stainlesss steels.

Table III-8 Postirradiation Creep Rupture of 304 Stainless Steel[24b]

Test temp., °C	Stress, 1000 psi	Rupture life, hr*
704	20	5.9 (25)
677	20	21.9 (83)
538	45	25.3 (88)
538	40	57.1 (215)

*Values in parentheses are for as-fabricated control specimens.

Considerable effort has been directed toward investigating the radiation-induced volume change of stainless steel in a fast reactor environment.[24b,51] This volume change is attributed to vacancy condensation, with the voids possibly stabilized with helium or hydrogen atoms. Figure III-8 summarizes the latest data on volume change as a function of fluence. This curve indicates a higher volume increase at lower fluences than at intermediate fluences. It is suggested that the volume increase at lower fluences is caused by a different mechanism than void formation by vacancy condensation. A suggested possibility is that the

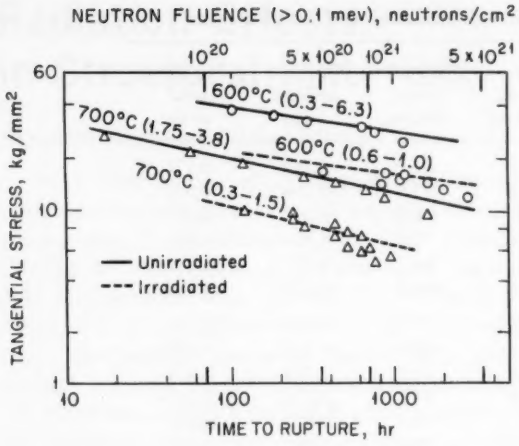

Fig. III-7 Multiaxial stress-rupture properties[47] of unirradiated and irradiated 16/13 CrNi stainless-steel tubes at 600 and 700°C. Numbers in parentheses are tangential strains.

second-phase distribution might be different in the low-fluence specimens.

Density changes of various alloys that were irradiated by General Electric[52] in the EBR-II at elevated temperatures are shown in Table III-10. The largest density changes occurred in Incoloy 800, and stabilized 321 and 347 stainless steels underwent the least changes. Elevated-temperature mechanical properties of these alloys did not show comparable differences.

Irradiation of 304 stainless steel in the Engineering Test Reactor (ETR) at 290°C to a fast fluence of 6×10^{21} neutrons/cm^2 was found to result in cavities, as observed by transmission electron microscopy (TEM).[53,54] The average size of the cavities was 110 A, and, on the basis of the density of the cavities, it was found that 300 ppm helium would balance the surface tension (1500 ergs/cm^2) of these cavities. However, it was calculated that only 12 ppm of helium was produced by neutrons from the boron impurity and from other elements in the stainless steel. It was further found that annealing of the irradiated stainless steel resulted in increased cavity size, with the anneal at 1090°C resulting in a cavity size of 500 A. These findings are analogous to previous TEM observations on stainless-steel specimens that had been irradiated in predominantly fast reactors. However, in the latter specimens, the observed cavities disappeared as a result of annealing at 900°C. The stability of cavities at high temperatures is generally attributed to the presence of helium in the cavities. It is suggested by the authors that hydrogen produced by (n,p) reactions or introduced from the ETR cooling water may account for the higher-than-calculated gas content. Another possible explanation may be the fact that cross sections for (n,α) reactions, especially in nickel,[55] are considerably higher than originally reported.

An attempt has been made by workers at Argonne[28b] to predict the swelling of stainless steel

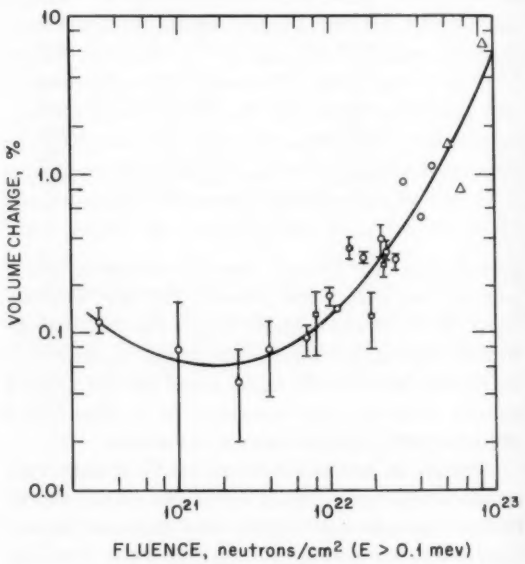

Fig. III-8 Fast-reactor-induced volume changes in austenitic stainless steels.[24b] ○, control-rod thimble (304L); □, experimental capsule (304L); △, Dounreay data (316).

Table III-9 Circumferential Ductility of Irradiated* 347 Stainless-Steel Tubing[49] at 705°C

Average strain rate, min^{-1}	1.1	0.3	0.05	0.004	0.0005
$\Delta D/D_0$, %	>65†	>63‡	48 to 54	22 to 36	35 to 44‡

*Irradiated in EBR-II to 2×10^{20} neutrons/cm^2 at 540°C.
†These specimens did not fracture.
‡Only an upper limit could be determined due to multiple fracture.

Table III-10 Density Changes in Irradiated LMFBR Cladding Alloys[52]

Material	Irradiation temp., °C	Total fluence, 10^{22} neutrons/cm^2	Density, g/cm^3	$\Delta\rho/\rho_0$
304	Control		7.907	
304	>660	1.8 to 2.7	7.811	0.0121
316L	Control		7.949	
316L	>660	1.8 to 2.7	7.850	0.0125
321	Control		7.884	
321	>660	1.8 to 2.7	7.873	0.0014
347	Control		7.904	
347	>660	1.8 to 2.7	7.861	0.0054
I-800	Control		7.969	
I-800	>660	1.8 to 2.7	7.772	0.0247
304	Control		7.902	
304	405	1.3 to 2.6	7.866	0.0046
304	480	1.3 to 2.6	7.847	0.0070

during irradiation in EBR-II. The model is based on the theory of classical nucleation and growth in conjunction with the Johnson–Mehl equation, which relates second-phase volume fraction to the total time of precipitation. This model takes into account both the irradiation temperature and the instantaneous neutron flux and has yielded swelling predictions for a 304 stainless-steel control-rod thimble irradiated in EBR-II which are in excellent agreement with measured density changes.

Zirconium and Aluminum Alloys

Strain aging in Zircaloy-2 at 300°C is generally attributed to the presence of oxygen atoms as impurities. Irradiation of Zircaloy-2 specimens to a fast fluence of 3.4×10^{19} neutrons/cm^2 was found[56] to decrease the rate of strain aging to about one-third at 300°C. Postirradiation annealing at 650°C for 1 hr eliminated the radiation-induced decrease in strain aging. It is suggested that some oxygen atoms are tied up by the radiation-induced point defects and are not available for strain aging when a specimen is tested in the as-irradiated condition. Then, as the defects are removed by postirradiation annealing, the oxygen atoms are released and cause strain aging.

The in-reactor creep data for Zircaloy-2 and Zr–2.5 Nb at 300°C are compared with ex-pile data[57] in Figs. III-9 and III-10. The Zircaloy-2 was cold worked 16% and annealed for 72 hr at 400°C before irradiation, and the Zr–2.5 Nb alloy was quenched from 870°C and aged at 500°C. It is seen that whereas the creep of Zircaloy-2 is increased by irradiation, the creep of Zr–2.5 Nb is decreased by irradiation. The increase in creep resistance of Zr–2.5 Nb is attributed to the formation of defects, by irradiation, that are stable at 300°C and thus impede dislocation motion.

Irradiation of 1100 aluminum at 60°C was found to result in decreased density,[58a] as illustrated in Fig. III-11. Examination of highly irradiated X8001 aluminum specimens by transmission electron microscopy revealed the presence of voids that are similar in appearance to those found in irradiated stainless steel. These voids measured about 100 to 600 A in diameter, and there was a 1000-A denuded zone next to the grain boundaries. A 1-hr anneal at 120°C did not affect the voids, but resulted in a precipitate that is believed to be silicon that had been transmuted from aluminum by

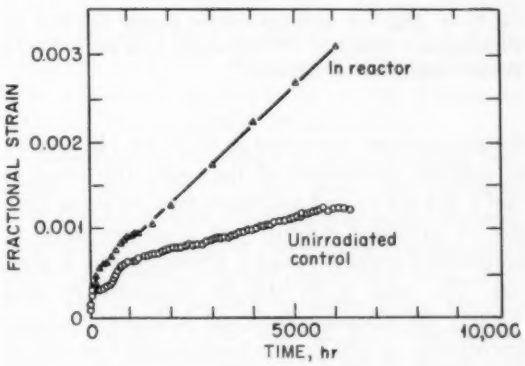

Fig. III-9 Comparison of in-pile and out-of-pile creep[57] of Zircaloy-2 at 300°C under a stress of 16,500 psi.

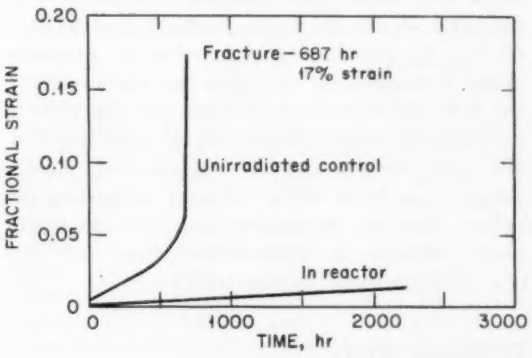

Fig. III-10 Comparison of in-pile and out-of-pile creep[57] of Zr–2.5 Nb alloy at 300°C under a stress of 83,000 psi.

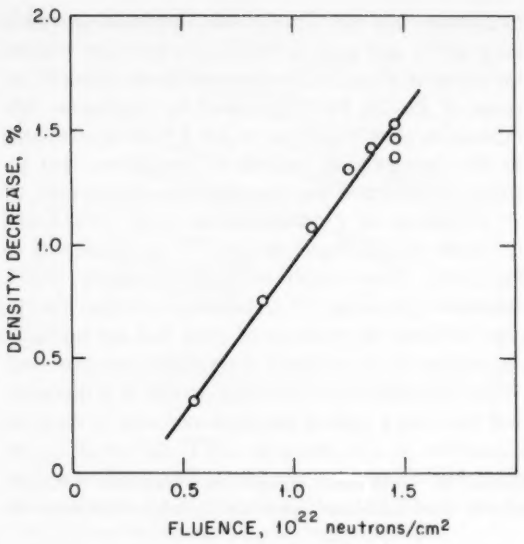

Fig. III-11 Effect of total fast-neutron fluence (>1 Mev) on the immersion density of 1100 aluminum from the N_f tray of the Oak Ridge Research Reactor.[58]

thermal neutrons. An anneal at 260°C for 1 hr resulted in complete elimination of the voids. The anneal at 260°C did not cause a significant increase in the grain size of irradiated material, but a similar anneal of unirradiated material caused a 10-fold increase in grain size. The voids could also be eliminated by cold working the irradiated aluminum 65% at either room temperature or 120°C. The loads required to deform irradiated specimens were more than twice those required to deform unirradiated specimens.

Specimens of X8001, 6061-0, and 1100-0 alloys and of SAP containing 7.5 wt.% Al_2O_3 were impregnated with helium by cyclotron bombardment to determine whether the helium produced from the (n,α) reaction in aluminum is responsible for embrittlement.[58a] The amount of helium that was introduced was 5×10^{-6} atom fraction, which was equivalent to the expected helium production by (n,α) reactions. The yield strength, ultimate strength, and uniform elongation at 20 to 425°C were not affected by the helium. However, the necking elongation was significantly reduced at temperatures above 0.5 T_m. (T_m = absolute melting temperature.)

Refractory Alloys

Previous tube-burst tests had indicated that specimens of V–15 Ti–7.5 Cr irradiated in the EBR-II at about 600°C underwent only about half as much diametral strain as did unirradiated specimens. To see whether the large scatter in experimental data had been influenced by the large stored energy of the pressurized gas, the tests were repeated[28b] with most of the volume inside the tubes occupied by solid rods. Results of the new tests, shown in Fig. III-12, do indicate somewhat less severe effects.

Irradiation of commercially pure vanadium to a fluence of 3×10^{22} neutrons/cm² at 650°C produced polyhedral cavities[43b] as observed by transmission electron microscopy. These cavities were about 200 A in diameter and were randomly distributed. As discussed earlier, similar cavities have been observed in austenitic stainless steel. No such cavities were found in a V–20 Ti alloy irradiated at 550°C to 2×10^{22} neutrons/cm².

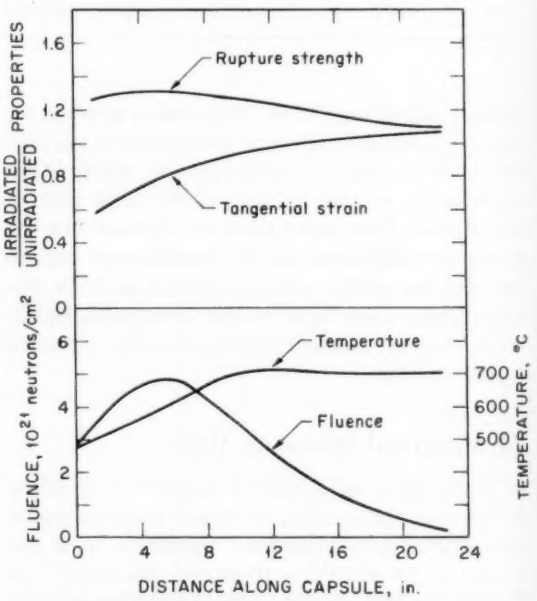

Fig. III-12 Effect of irradiation on the tube-burst properties of V–15 Ti–7.5 Cr alloy.[28b]

As shown in Fig. III-13, most of the fast-neutron radiation damage in tantalum can be removed by annealing for 1 hr at 1000°C. However, some residual hardening remained even after annealing at 1400°C. Postirradiation annealing affected[48] the room-temperature hardness of irradiated Ta–10 W in a similar manner. Irradiation of Cr–0.7 Y at 70°C to a fast fluence of 2.3×10^{20} neutrons/cm² caused its

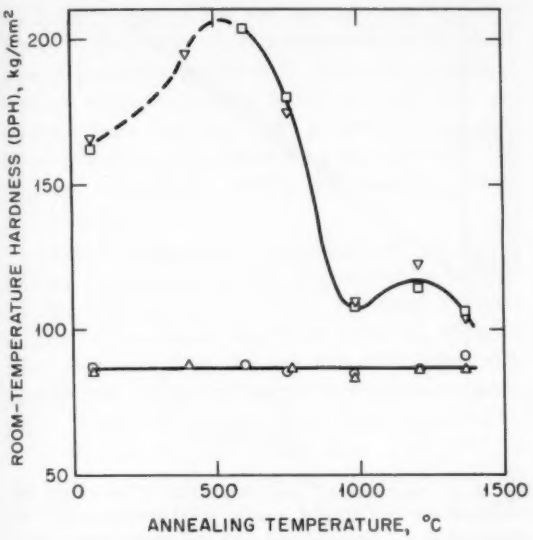

Fig. III-13 Effect of annealing temperature (1-hr anneals) on room-temperature hardness of irradiated and unirradiated polycrystalline tantalum.[48] Irradiated to 1.2×10^{20} neutrons/cm² ($E > 1$ Mev) at 700°C: □, 500-g load; ▽, 100-g load—normalized data. Unirradiated: ○, 500-g load; △, 100-g load—normalized data.

ductile-to-brittle transition temperature to increase from 130°C to 400°C.

Polycrystalline, recrystallized tungsten specimens irradiated to a fast fluence of 1×10^{20} neutrons/cm² at less than 100°C suffered[59] large reductions in both fracture strength and ductility, particularly at the higher testing temperatures (to about 700°C). Also, the brittle-to-ductile transition temperature increased by about 165°C as a result of the irradiation.

Pressure-Vessel Steels

Studies were performed at the Naval Research Laboratory[60] to determine the effects of nickel and copper contents on the radiation-induced ductile-to-brittle transition-temperature shift in weld metal. Charpy V-notch specimens were taken from an 8-in.-wide A543 base plate, two commercial weldments, and four experimental weldments—all having different copper and nickel compositions, as shown in Table III-11. These specimens were irradiated at 550°F (290°C) to a fast fluence of 3.5×10^{19} neutrons/cm². The table shows that the smallest shift in transition temperature occurred in the weld that was low in both copper and nickel (experimental weld 1936), whereas the highest shift occurred in the weldment that was high in copper (Linde 100). The investigators consider copper to be the main cause for the radiation-induced transition-temperature shifts, although the nickel content also appears to play a secondary role. For example, experimental weldments 1934 and 1938 contain the same amount of copper, but 1938 has more than twice the nickel content and also undergoes a larger increase in transition temperature (200°F vs. 95°F).

The relative response of temper-embrittled and nonembrittled (brine quenched from tempering) Ni–Cr–Mo steel to irradiation has also been studied.[60] It was found that, although the 30 ft-lb transition temperature of a nonembrittled material is much lower in the unirradiated condition (−220 vs. 90°F), irradiation increases the transition temperature of the nonembrittled material at a faster rate. Consequently there is essentially no difference in the transition temperatures of nonembrittled and temper-embrittled Ni–Cr–Mo steel after irradiation at 650°F to a fast fluence of 2.5×10^{19} neutrons/cm² (90 vs. 75°F) or after irradiation at 280°F to a fast fluence of 1.1×10^{20} neutrons/cm² (290 vs. 315°F).

Evaluation of the PM-2A pressure vessel has been almost completed.[60,61] This vessel was fabricated from two 2.4-in.-thick ring forgings of A350-LF3 steel. Because of its small size, the reactor pressure vessel reached its allowable design fluence in a rather short time, and it was decided to destructively test the pressure vessel. Greater stresses were required to fracture the pressure vessel than would be encountered

Table III-11 Nickel and Copper Contents and the Transition-Temperature Shift of Irradiated Weldments[60]

Material identification	Wt.%*		Transition-temperature shift† [T_{30} (irrad.) − T_{30} (unirrad.)], °F
	Copper	Nickel	
A543 plate	0.06	3.45	105
Linde M1-88	0.24	1.42	415
Linde 100	0.42	2.30	530
1934	0.10	0.78	95
1936	0.02	0.75	45
1938	0.11	1.78	200
1948	0.05	1.61	110

*Averaged values.

†T_{30} = impact test temperature to produce a Charpy V-notch energy of 30 ft-lb.

in service. Even with the high imposed stress, a very large flaw was also required to cause fracture. Charpy V-notch specimens cut from sections throughout the vessel showed irradiation-induced changes in transition temperature that correlated reasonably well with those of other specimens irradiated to similar fluences at identical temperatures. The conditions for failure of the PM-2A reactor vessel are in agreement with the generalized fracture-analysis diagram, although better results were obtained by using the irradiation-condition yield stress (which is higher) as the reference in place of the unirradiated-condition yield stress.

Basic Mechanisms of Radiation Damage

Irradiation has been shown to cause a decrease in the work-hardening coefficient of a metal compared with the work-hardening coefficient of unirradiated metal at equivalent strain. However, the work-hardening portions of the tensile curves (on a true stress vs. true strain plot) for irradiated and unirradiated iron can be superimposed by shifting the irradiated curves to the right, along the strain axis.[62] This implies that irradiation does not affect the strain-hardening coefficients of iron but produces the same type of behavior as prestraining does. The value of prestrain (ϵ_0)—the amount that the curve has to be shifted to the right—was found to be a function of (fluence)$^{\frac{1}{6}}$. The "effective-prestrain" concept of irradiation hardening also allows one to predict the onset of plastic instability (necking). In most materials the true strain (ϵ) at which necking starts is equivalent to the work-hardening coefficient (n). Therefore the true strain at which necking starts would be given by $\epsilon = n - \epsilon_0$. Since n is independent of fluence and ϵ_0 increases with fluence, the start of necking is expected to increase with fluence. The good agreement of the superimposed true stress–true strain curves for unirradiated and irradiated specimens is illustrated in Fig. III-14.

The effect of irradiation on the tempering of quenched plain-carbon steel has been studied by the Australians.[63] Plain-carbon-steel specimens containing 0.67 and 1.0 wt.% carbon were annealed at 1050°C for 3 hr and then quenched in water. The quenched martensite was then irradiated to fast fluences ranging from 10^{17} to 5×10^{19} neutrons/cm^2 at irradiation temperatures of 105°C or less. The postirradiation tempering behavior was studied by electrical-resistivity measurements, hardness measurements, X-ray measurements, and transmission-electron-microscopy observations. Figure III-15 shows that the irradiated martensite tempered considerably faster than did the unirradiated martensite, provided the tempering temperature was below 300°C. At higher tempering temperatures there was essentially no difference in tempering behavior between the unirradiated and irradiated martensite. It can also be seen from Fig. III-15 that the tempering behavior was altered

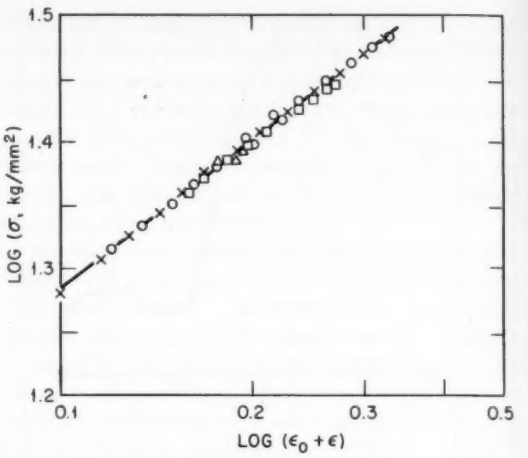

Fig. III-14 Superimposed true stress–true strain curves for irradiated and unirradiated iron at room temperature.[62] x, unirradiated; ○, fluence = 1.2×10^{16} neutrons/cm^2 ($E >$ 1 Mev) – $\epsilon_0 = 0.039$; □, fluence = 2.5×10^{17} neutrons/cm^2 ($E > 1$ Mev) – $\epsilon_0 = 0.067$; Δ, fluence = 2.5×10^{18} neutrons/cm^2 ($E > 1$ Mev) – $\epsilon_0 = 0.10$.

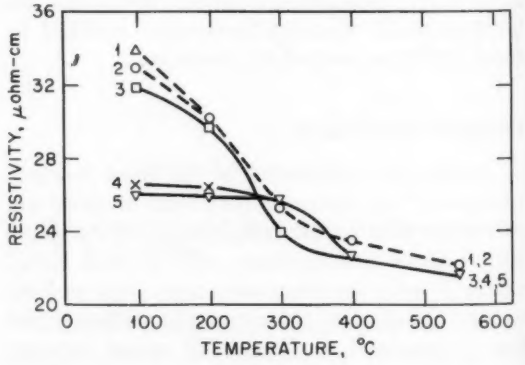

Fig. III-15 Effect[64] of fast-neutron irradiation on the change in electrical resistivity during isochronal (1 hr) tempering of a quenched 1% carbon steel: (1) 70°C control specimen; (2) 100°C control specimen; (3) irradiated to 2×10^{18} neutrons/cm^2; (4) irradiated to 1.5×10^{19} neutrons/cm^2; (5) irradiated to 5×10^{19} neutrons/cm^2.

significantly only if the fast fluence were well over 2×10^{18} neutrons/cm^2. It is suggested that the point defects generated in the iron lattice by irradiation interact with the carbon atoms so that they are removed from interstitial sites to substitutional positions. Migration then occurs by a radiation-enhanced vacancy mechanism, leading to speedier carbide precipitation.

Neutron irradiation of supersaturated solutions is believed to affect the process of precipitation in either of two different ways: (1) by providing a higher vacancy concentration and thus increasing diffusion coefficients or (2) by forming imperfect high-energy regions that can act as sites for heterogeneous nucleation. Aluminum–copper alloys were irradiated at 40°C to fast fluences ranging from 1.8×10^{14} to 1.2×10^{17} neutrons/cm^2 and annealed at higher temperatures after irradiation.[64] This sequence of events was chosen to allow the study of the second possibility. It was found that annealing at 110 and 130°C resulted in accelerated precipitation in the irradiated alloys. However, when the annealing was done at 235°C, there was no difference in the precipitation behavior of unirradiated and irradiated alloys. It was concluded that the regions of disorder promote heterogeneous nucleation at the lower annealing temperatures but that these centers themselves are removed by annealing at the higher temperatures, and consequently there is no accelerated precipitation in the irradiated alloy at the higher temperatures.

Length and lattice-parameter measurements of single crystals of rhenium irradiated with fast neutrons at 60°C showed[65] that the hexagonal lattice increased in the *a* direction and decreased in the *c* direction. These changes were a function of fluence, as illustrated in Fig. III-16. This behavior is explained in terms of easier migration of interstitials to form defect clusters, whereas the less mobile vacancies remain in solution. The observed decrease in unit cell volume is then a result of the relaxation about the vacant lattice site.

To study the effect of high pressure on recovery, workers at Battelle–Northwest[66] irradiated high-purity molybdenum to a fast fluence of 6.2×10^{18} neutrons/cm^2 at 40°C. The electrical resistance of irradiated molybdenum has been found to recover in three distinct stages: 0.15 T_m, 0.24 T_m, and 0.29 T_m (T_m = absolute melting temperature). Application of 20 kbars of hydrostatic pressure was found to shift the original 0.15 T_m stage downward by 60°C and the 0.29 T_m stage downward by 200°C. The temperature at which complete recovery of lattice-parameter increase (0.022%) in irradiated molybdenum occurs was reduced from 750°C to 350°C by the application of 20 kbars.[67] The average cluster diameter in the irradiated molybdenum is 25 to 35 A. Postirradiation annealing at 1 bar or less causes the cluster density to decrease at 150°C, increase at 400°C, and decrease to zero during final recovery at 750°C. The application of 20 kbars of hydrostatic pressure during isochronal recovery lowers the first cluster-density-decrease temperature[68] from 150°C to 90°C and the final one from 750°C to 450°C.

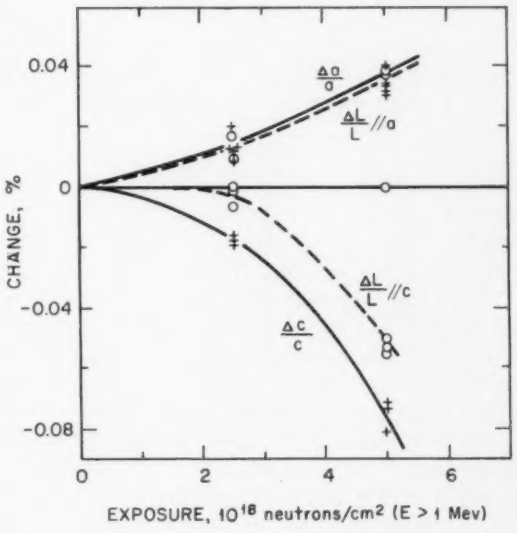

Fig. III-16 Length and lattice-parameter changes due to irradiation of rhenium single crystals.[65] ○, length changes; +, lattice-parameter changes.

Irradiation of high-purity molybdenum at ~40°C to 6.2×10^{18} neutrons/cm^2 ($E > 1$ Mev) induces a 19% increase in the Vickers hardness of the metal.[69] High-pressure (20 kbar) anneals of this material in the 80 to 400°C range do not significantly change its hardness, whereas anneals in the 400 to 500°C range produce rapid recovery. The recovery of radiation-induced hardness appears to be related, in a very complex manner, to the recovery of observable defect clusters. The recovery of hardness as a function of temperature for two different pressures is illustrated in Fig. III-17.

Transmission electron microscopy (TEM) has become a powerful tool for studying the microstructure of irradiated materials. With the advent of more

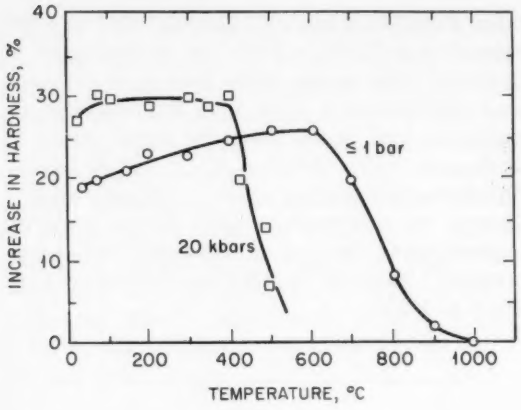

Fig. III-17 Effect of hydrostatic pressure on the isochronal annealing of radiation-induced hardness in molybdenum.[69]

powerful transmission electron microscopes, it becomes necessary to consider the possible changes in structure that may result from the electron beam during examination.[70] For changes in microstructure to occur, both the electron energy and defect supersaturation must exceed critical values. It has been shown that, when the voltage is greater than 600 kv and the beam current is high (0.1 amp in a 5-μ spot), defect clusters are formed in unirradiated copper during examination at 20°C, the density and size of loops varying with examination time. The structure of irradiated copper can also be significantly changed by the use of an electron microscope. These findings indicate that some studies concerned with defect formation in irradiated materials and utilizing TEM may be suspect, in that the observed structure may have been formed during examination rather than during irradiation. The greatest changes would be expected during "in-microscope" stressing or annealing experiments.

The defect structures caused by neutron irradiation in copper at 80°C were compared with those in nickel.[71] The defect size in nickel is generally only about one-half that in copper for a comparable fast fluence. The difference is attributed to the larger stacking-fault energy of nickel.

Transmission electron microscopy on specimens of pure nickel (99.997%) that had been irradiated[72] at 400 to 450°C to a fast fluence of 5×10^{19} neutrons/cm^2 revealed the presence of voids that measured 50 to 150 A. A zone of about 1000 A next to twin and grain boundaries was denuded of the cavities. Annealing at 600 and 700°C resulted in a decrease in cavity density but an increase in cavity size. An anneal at 800°C caused the complete disappearance of all the cavities. These cavities are believed to be due to vacancies, since about 700 ppm helium would be required to produce these cavities as calculated from surface-energy considerations. However, only 0.1 ppm helium was produced by (n,a) reactions, according to calculations.

Table III-12 illustrates the size and distribution of defect clusters observed by TEM in irradiated pure vanadium as a function of annealing temperature.[48,73] In another study,[74] commercial vanadium was irradiated at 80°C to a fast fluence of 7.4×10^{19} neutrons/cm^2. This irradiation resulted in a high density of clusters about 70 A in diameter, which were believed to be interstitial in nature. A 0.1-μ-wide denuded zone near the grain boundary is believed to be due to migration of the interstitials to the grain boundary. Annealing in the 400 to 600°C range resulted in large vacancy loops. The diameter of these loops depended on annealing temperature, being 92 A after annealing at 400°C and 229 A after annealing at 600°C. Annealing at 700°C resulted in complete annihilation of the loops. Comparison of these experimental results with those in Table III-12 suggests that the radiation-induced defect structure in pure vanadium is more stable than the defect structure in commercial vanadium.

Table III-12 Defect-Cluster Sizes and Densities in Irradiated* and Annealed Vanadium[48]

Annealing temperature, °C	T/T_m	Average cluster size, A	Average cluster density, No./cm^3
As irradiated, 70°C	0.16	25 to 50†	10^{16} to 10^{17}
330	0.28	75	1.24×10^{16}
510	0.36	125	4.59×10^{15}
650	0.42	175	9.70×10^{14}
815	0.50	400	2.07×10^{14}
1175	0.67	500	1.12×10^{14}

*Irradiated at reactor ambient temperature (~70°C) to an estimated fluence of 5×10^{19} neutrons/cm^2 ($E > 1$ Mev).
†Estimated values.

The degree[75] of irradiation hardening in iron single crystals containing 8 and 20 ppm carbon increased with increasing carbon content. The iron containing 8 ppm carbon reached a saturation in the radiation-induced strength increase slightly sooner (3×10^{17} neutrons/cm^2) than the iron containing 20 ppm

carbon. However, the difference was not great. This behavior is explained by the fact that the lower the carbon content, the sooner all the carbon is utilized for the formation of carbon-stabilized defect clusters. The radiation hardening was removed by annealing at 230°C.

An attempt has been made[76] to calculate the expected relative defect production in iron irradiated in different reactors to provide a basis for the correlation of the results of mechanical-property tests on materials irradiated in different reactors. The stable-defect density as a function of fluence in four different reactors is plotted in Fig. III-18. The fluences expected to be required to produce a 1% change in density in specimens in the different reactors are:

Reactor	Fluence, 10^{20} neutrons/cm^2 ($E > 362$ ev)
Experimental Breeder Reactor (EBR-II)	1.3
Dounreay Fast Reactor (DFR)	1.4
Anticipated Fast Test Reactor (FTR)	1.8
Engineering Test Reactor (ETR)	4.6

Since these results were calculated for absolute zero temperature, one would expect defect migration to sinks at higher temperatures to reduce the defect density. However, it is felt that the figures provide a useful guide for relative defect production in the various reactors, even at elevated temperatures.

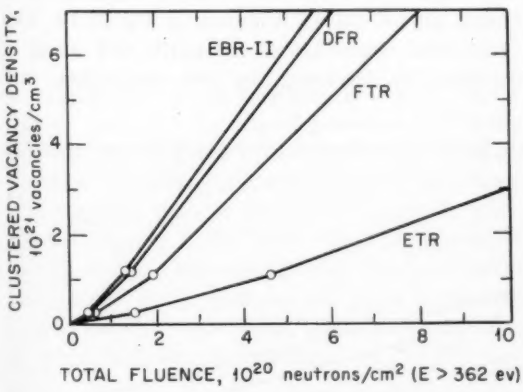

Fig. III-18 Stable-vacancy-cluster production in different nuclear reactors.[76]

(M. Kangilaski)

Metallurgy and Mechanical Properties of Common Cladding and Structural Materials

Aluminum and Magnesium Alloys

Dispersion aluminum alloys with better properties than ordinary SAP alloys have been developed by workers at Oak Ridge.[58b] Embedment of the dispersant in the new alloys is accomplished by grinding in a hermetically sealed drum of a high-energy ball mill. Table III-13 shows that the experimental alloys provide higher strength, especially considering the lower dispersion content, at most testing temperatures and strain rates. In an Italian study[77] it was established that the hot hardness of SAP alloys in the 20 to 600°C range can be correlated with tensile properties. The creep behavior of SAP alloys can also be predicted from indentation creep tests.

Elevated-temperature creep and tensile tests were performed in Italy[78] on SAP, PUROXAL, and PUROXAL-M alloys. (PUROXAL is simply SAP produced from extra-pure aluminum powder, whereas PUROXAL-M is produced from extra-pure powdered Al–2 to 2.5 wt.% Mg alloy.) The test results led to the following observations:

1. The high mechanical strength at elevated temperature of the composites examined is attributed mainly to their very fine grain size, which, owing to the presence of the dispersed phase, does not grow excessively at high temperature.

2. The mechanical strength of SAP material is comparable to that of PUROXAL material with different oxide content, so long as the two have the same grain size.

3. At low strain rates the strength of the grain boundaries is reduced in comparison with the strength of the grains. Consequently creep tests show lower elongations at fracture than do short-time tensile tests.

4. Microcracks present in the structure of these composites can grow in number and dimensions at elevated temperature under tensile creep stresses and also lead to rupture with very reduced elongations.

5. In PUROXAL-M, transformation of the dispersed phase from Al_2O_3 to a mixed oxide ($MgO + MgOAl_2O_3$) results in good creep ductility for the first 500 hr or so under stress. In normal SAP materials,

Table III-13 Comparison of Tensile Properties of Two Experimental Aluminum Alloys with Conventional SAP-Type Materials[58b]

Alloy	Strain rate, min^{-1}	Test temperature, °C	Yield strength, (0.2% offset), psi	Ultimate tensile strength, psi	Total elongation, %
XAP-001*	0.02	25 to 29	32,000	38,270	11.5
(with 6 wt.%	0.02	450	10,280	11,280	2.7
Al_2O_3)	0.002	450	9,690	10,400	1.8
	0.0002	450	8,650	9,170	1.3
SAP 895*	0.2	25 to 29	33,310	40,220	9.9
(with 11 wt.%	0.02	450	13,490	14,650	2.0
Al_2O_3)	0.002	450	12,410	12,900	1.4
	0.0002	450	10,720	11,390	1.1
Experimental	0.02	25 to 29	60,820	76,300	6.6
Al–11 Ce	0.02	450	18,838	19,411	0.59
splat with	0.002	450	16,162	16,818	0.37
4 wt.% SiO_2†	0.0002	450	14,720	15,120	0.93
Experimental	0.02	25 to 29	53,640	61,830	6.12
Al–5.5 Mg	0.02	450	11,440	11,770	5.45
filings with	0.002	450	9,810	10,300	3.60
4 wt.% AlOOH‡	0.0002	450	8,800	9,290	2.26

*Commercial alloy in which the oxide was formed in aluminum powder by reaction with air during open ball milling with a proprietary grinding liquid. Powder consolidated and extruded at 25 : 1 reduction.

†Oxide dispersant formed by chemical reaction from 140-A SiO_2 additive milled for 1 day into the Al–11 Ce powder. Mixture was annealed at 450°C, cold pressed, and extruded at 500°C at 20 : 1 reduction.

‡Oxide dispersant formed by chemical reaction from fibrillar AlOOH (50 A in diameter by 1000 A long) milled for 1 day into the Al–5.5 Mg powder. Mixture was annealed at 500°C, cold pressed, and extruded at 500°C at 20 : 1 reduction.

ductility persists for only 1 hr or less. From a practical point of view then, this characteristic of PUROXAL-M can prevent failure when the material has to withstand a brief, limited overstress—a likely occurrence during the life of a fuel cladding.

In a study[79] of the cyclic-strain fatigue behavior of three SAP alloys (SAP 930, XAP 005, and SAP 865) in air, the longest fatigue lives were exhibited by SAP 865. No strain-rate effect was observed in tests at 80°F (27°C), but at 500 and 800°F (260 and 425°C) slower strain rates resulted in lower fatigue lives. A typical set of curves is shown in Fig. III-19. The cyclic-strain fatigue life of the brittle SAP alloys is decreased by increasing the test temperature; the

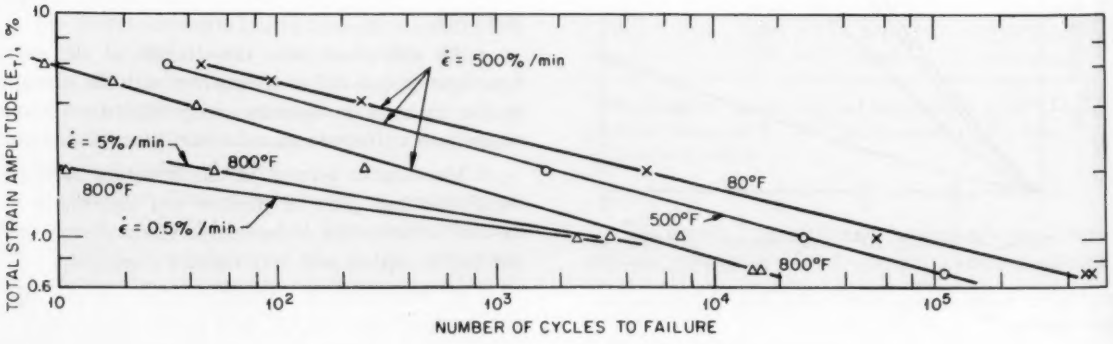

Fig. III-19 Cyclic-strain fatigue behavior[79] of SAP 865.

opposite is true for ductile aluminum. This decreased fatigue life of SAP alloys at higher temperatures and lower strain rates is consistent with their low ductility in high-temperature, low-strain-rate tensile tests, along with their inability to recover easily.

The results of rotating cyclic-stress fatigue tests[80] on 2024-T3 aluminum alloy (Al–4.4 Cu–0.5 Fe–0.5 Si–0.6 Mn–1.5 Mg) both in air and in 10^{-10} torr vacuum at room temperature are shown in Fig. III-20. The presence of air reduces the fatigue life considerably at stresses significantly above the endurance limit. The endurance limit itself is not changed by changing the atmosphere from air to vacuum. Water vapor in the air is believed to be responsible for the reduced fatigue life in air.

Tensile tests with controlled strain rate were undertaken[81] on Magnox Al80 with various grain sizes

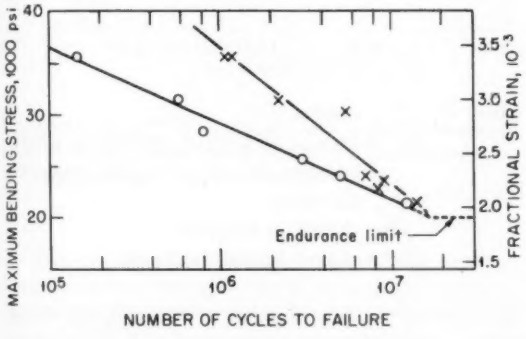

Fig. III-20 Influence of atmosphere on the room-temperature fatigue life of 2024-T3 aluminum.[80] ×, ultrahigh vacuum; ○, air.

to establish the role of grain-boundary sliding on the fracture mode. As the rate of grain-boundary sliding increased, the tendency toward intergranular fracture increased, particularly in the larger-grained specimens. It is suggested that the critical sliding rate for intergranular fracture is that above which the growth of voids by sliding is faster than the rate of propagation of transgranular cracks. However, this is not expected to hold at low test temperatures, where crack nucleation is more difficult than crack propagation.

The density of Magnox Al80 decreased[82] with increasing strain during creep testing at elevated temperatures. This density decrease, illustrated in Fig. III-21, is attributed to the formation and growth of cavities at the grain boundaries.

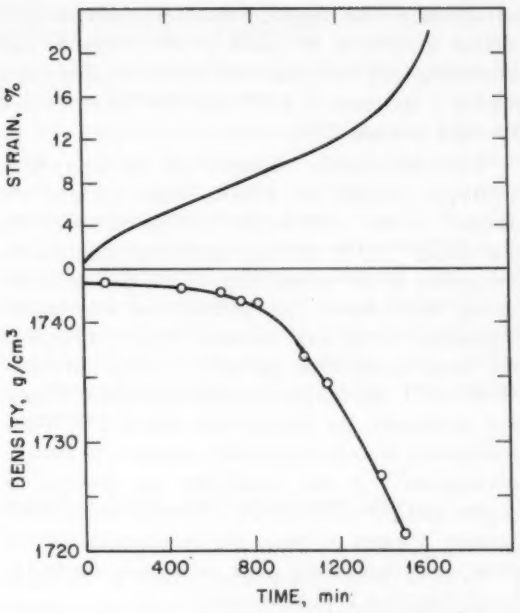

Fig. III-21 Relation[82] between density and strain of Magnox Al80 during creep at 275°C under a stress of 2300 psi.

Zirconium Alloys

A national symposium titled "Applications Related Phenomena in Zirconium and Hafnium and Their Alloys" was sponsored by the American Society for Testing and Materials (ASTM) in Philadelphia on Nov. 5–7, 1968. Papers presented covered properties, fabrication, mechanical properties, corrosion, and testing practices. The proceedings of this symposium will be published as an ASTM special technical publication.

The deformation behavior of both zirconium and Zircaloys has been thoroughly reviewed.[83] It was concluded that the mechanism of deformation was the overcoming of interstitial impurity-atom barriers by thermally activated dislocations moving on the first-order prism planes. However, the flow stress was directly proportional to the interstitial content, rather than to the square root of interstitial content as is the case in other metals. This difference is attributed to the fact that nearly symmetrical lattice distortions are produced in zirconium by interstitials, whereas asymmetrical distortions are produced in other metals.

The activation volume and energy for the deformation of zirconium increase rapidly to about 300°C, above which the thermal component of the flow stress reaches zero. At higher temperatures the activation energy for deformation is approximately that for

self-diffusion. This suggests that either nonconservative motion of jogs or the climb of dislocations is rate controlling. The strain-rate sensitivity of the flow stress reaches a maximum at 130°C and then decreases to a low value at about 300°C.

The deformation behavior of Zr–O (130 to 1200 ppm oxygen by weight) single crystals was studied[84] in the −196 to 680°C range. It was found that below 290°C the rate-controlling deformation mechanism is the overcoming of oxygen atoms by moving dislocations. This phenomenon is evidently responsible for the large increases in yield strength at low temperatures with increases in oxygen content. Above 290°C the oxygen atoms do not hinder dislocation movement. At temperatures above 530°C the deformation process is thermally activated. In another investigation[85] it was found that the presence of oxygen does not influence the amount of deformation twinning. Oxygen promotes slip on nonprismatic slip planes, and consequently more cross slip is observed in Zr–O alloys than in pure zirconium.

The flow stress of zirconium at low temperatures (<500°C) is also very sensitive to nitrogen content,[86] as illustrated in Fig. III-22. This is believed to be due to the effective obstruction of dislocation motion by nitrogen atoms. At higher temperatures (~500°C) the flow stress becomes insensitive to nitrogen content.

Electrical-resistivity measurements have been used[87] to study the solubility and precipitation of hydrogen in unalloyed zirconium. The terminal solid solubility of hydrogen thus measured agrees with that reported by previous investigators. The activation energy for hydrogen precipitation (7.6 ± 0.7 kcal/mole) was found to be identical to the activation energy for hydrogen diffusion in alpha zirconium. It was found that no hydrogen could be held in solution when annealed zirconium containing 100 ppm hydrogen was quenched in ice water from 300°C. However, some hydrogen remained in solution when annealed zirconium containing only 20 ppm hydrogen was given an identical quench. The rate of hydrogen precipitation in zirconium during quenching was increased significantly by cold working.

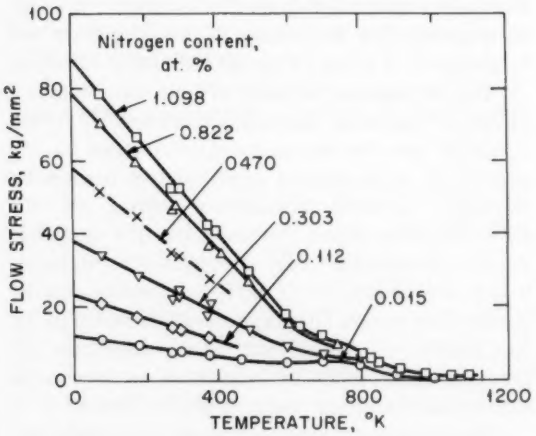

Fig. III-22 Variation of flow stress at a strain rate of 10^{-4} sec^{-1} with temperature for a series of Zr–N alloys.[86] $T_{\alpha-\beta}$ is the temperature of transformation from hcp (low-T phase) to bcc.

The orientation of hydride platelets in Zircaloy-2 has been previously shown to depend on both the reduction of tubing diameter and wall thickness during fabrication. A new relation, defined as "directional strain parameter," has been developed by workers at Savannah River.[88] This relation is given as

$$f_{48} = C_1 - C_2\,(\Delta D - 0.475\,\Delta W)$$

where C_1, C_2 = constants
f_{48} = fraction of hydride platelets oriented between 48° and 90° to the reference direction
ΔD = change in diameter
ΔW = change in wall thickness

and shows that the reduction in diameter has about twice as much effect as reduction of wall thickness on the orientation of hydrides. The above relation was found to hold for Zircaloy-2 tubing containing 60 ppm hydrogen and fabricated by tube reduction, mandrel drawing, and rotary swaging. It was also found that variation of grain size from 0.005 to 0.029 mm was only marginally significant in influencing the platelet orientations. Also, the fraction of platelets that precipitated within the grains (58 to 89%) had no significant effect on platelet orientation.

The effect of hydrogen (30 to 1000 ppm) on tensile properties of Zr–1 Nb alloy[89] is illustrated in Fig. III-23. Strength of the alloy is increased and the ductility is decreased by increasing hydrogen content. The reduced ductility with increasing hydrogen content is believed to be due to stress-induced precipitation of hydride platelets, particularly above 300°C. Varying the strain rate from 0.1 to 3.1 min^{-1} did not affect the tensile properties significantly at testing temperatures below 450°C. Above 450°C the higher strain rate resulted in lower ductilities.

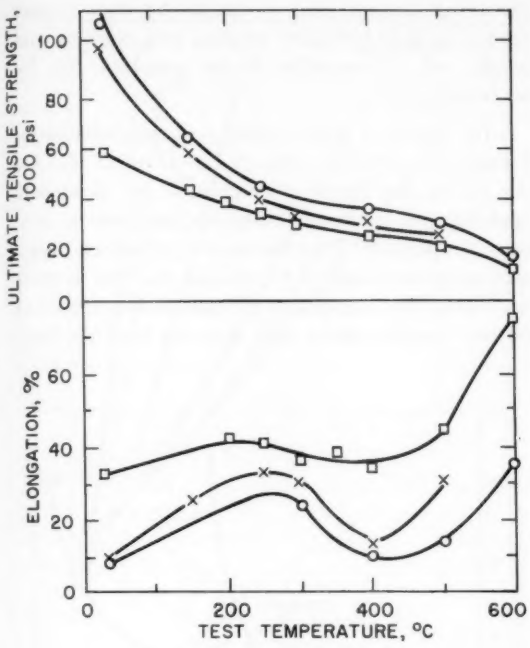

Fig. III-23 Effect[89] of hydrogen on the mechanical properties of Zr–1 Nb for a strain rate of 0.1 min^{-1}. □, 0.003% hydrogen; ×, 0.05% hydrogen; ○, 0.10% hydrogen.

Pronounced acoustic signals have been received from Zircaloy-2 during testing in tension and fatigue at room temperature.[90] The peak in acoustic emission was obtained just before the 0.2% offset yield strength was reached. It is believed that the noise is caused by initiation of dislocation movement. During fatigue testing the majority of signals were received just prior to failure and are believed to be caused by twinning, initiation of dislocation movement in the plastic zone ahead of the crack tip, and possibly physical slapping together of the crack walls with each load cycle.

A French patent[91] has been issued for a zirconium-alloy fuel cladding that utilizes two different metallic layers. The outer layer is especially corrosion resistant and consists of Zr–2.5 Nb–0.5 Cu or Zr–0.5 Mo–0.5 Cu. The inner layer is especially designed for mechanical strength and consists of Zr–1.25 Al–1.0 Sn–1.0 Mo. An intermediate layer of ZrO_2 is placed between the two layers of zirconium alloys to minimize diffusion of hydrogen.

The $\beta \rightarrow \alpha$ transformation temperature of Zr–2 at.% Cr–0.16 at.% Fe appears[92] to be sensitive to the cooling rate. For cooling rates below 1700°C/sec, the transformation occurs at 760°C, whereas for higher cooling rates the transformation occurs at 705°C. Cooling rates below 1700°C/sec resulted in a non-martensitic structure, but higher cooling rates caused an acicular martensitic structure.

The production of zirconium containing dispersed Y_2O_3 particles was attempted[93] by internal oxidation of Zr–1 Y. However, it was not possible to obtain a dispersion-strengthened alloy because the Y_2O_3 particles were too large and hence were ineffective in impeding dislocation movement. Because of its very high energy of formation, yttria would be expected to form into small particles. Since it did not, it is unlikely that any other alloying elements will permit dispersion-strengthening of zirconium by internal oxidation.

Stainless Steels and Nickel-Base Alloys

The American Society of Mechanical Engineers has published a timely monograph titled *Behavior of Superheater Alloys in High Temperature, High Pressure Steam.*[94] This monograph discusses the effect of longtime exposure (up to 36 months) in 2000-psi steam at 1100 to 1500°F (595 to 815°C) on the mechanical properties, metallographic structure, heat-transfer characteristics, and scale formation of various alloys. The alloys covered are austenitic stainless steels, high-nickel alloys, and alloy steels. Generally, the yield and ultimate strengths of the austenitic alloys were not significantly affected by the longtime heat-treatments. The greatest losses in both ductility and impact strength were exhibited by 310 and 316 stainless steels, 16-25-6, and 15-15N. These losses in properties are attributed to the formation of sigma phase in these alloys. The least changes in properties were shown by the stabilized 321 and 347 stainless steels, Inconel 600, and IN-102.

The growth of $M_{23}C_6$ particles at the grain boundaries of austenitic stainless steel has been studied[95] using specimens that were solution annealed at 1150°C, water quenched, and then annealed for various times at 750°C. The grain-boundary precipitates are believed to form by a process involving grain-boundary migration. The $M_{23}C_6$ particles at the boundary are in parallel orientation with one of the grains constituting the boundary. Distribution and morphology of the particles appear to be sensitive to grain-boundary misorientation.

The solubility of nitrogen in 304 stainless steel in the temperature range 540 to 980°C has been determined[96] by equilibrating the stainless-steel speci-

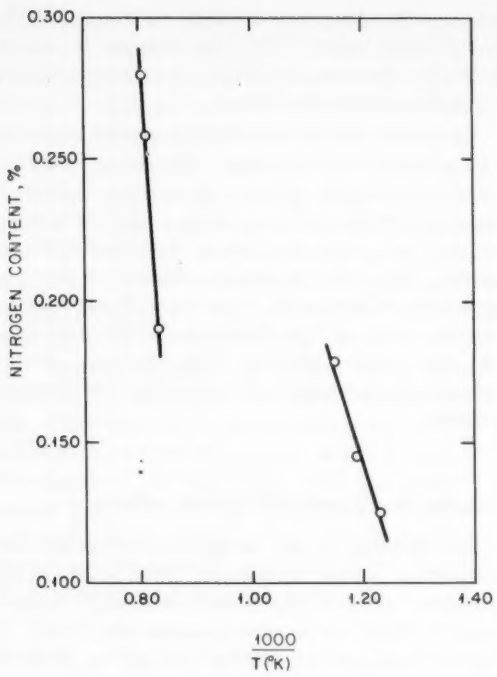

Fig. III-24 Solid solubility of nitrogen in 304 stainless steel.[96]

mens with various nitrogen-containing gases and then examining them metallographically. Results are shown in Fig. III-24. It was not possible to determine the solubility of nitrogen in the temperature range 600 to 900°C, owing to the precipitation of carbides in that range. The nitrogen that is not in solution is precipitated as chromium nitrides.

It was found[97] that austenitic stainless steels in which strain-induced martensite is formed are embrittled by hydrogen at room temperature. Type 304L stainless steel was embrittled, whereas the stabler 310 stainless steel in which no martensite is formed during straining was not. The presence of hydrogen causes embrittlement at the martensitic structure and changes the fracture mode from ductile to quasi-cleavage. This embrittlement phenomenon was noted only in notched specimens, not in unnotched specimens.

Figure III-25 shows that the rupture life of Nimonic 105 (Ni–20 Co–15 Cr–5 Mo–4.7 Al–1.2 Ti) can be improved considerably by giving the alloy a heat-treatment in the middle of a creep-rupture test. It is suggested[98] that the heat-treatment brings about a healing of grain-boundary voids (induced by low stress) by causing grain-boundary migrations. However, the creep damage that is caused by high stresses results in grain-boundary shearing and cracking and would not be expected to be annealed out by reheat-treatment.

The effect of stress cycling on creep behavior of Udimet 700 at 955°C (Ni–20 Co–15 Cr–5 Mo–4.4 Al–3.4 Ti) has been investigated[99] by alternately applying and removing stresses on specimens at constant temperature. The time spent at zero stress during each cycle was usually 4 hr, whereas the time at stress was varied from a minimum of 9 min to a maximum of 60 min. Constant-stress tests were run to obtain base-

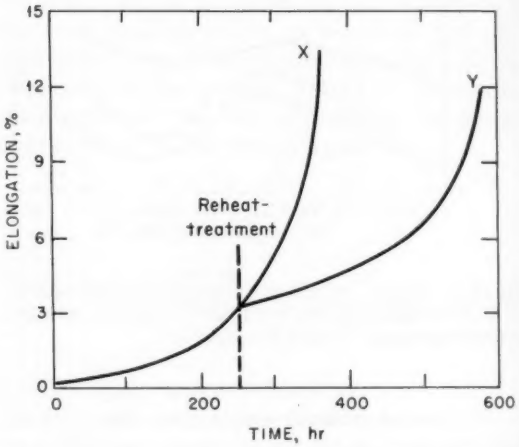

Fig. III-25 The effect of reheat-treatment[98] on the creep of Nimonic 105. Test conditions: 22,000 psi, 870°C. Heat-treatment: 4 hr 1150°C, air cooled, + 16 hr 1050°C, air cooled, + 16 hr 850°C, air cooled. *X* = creep curve, no reheat-treatment; *Y* = creep curve, reheat-treated after 250 hr.

line data. From the results summarized in Fig. III-26, it is apparent that stress cycling induces greatly accelerated creep during periods of load application. In fact, the briefer the period of load application in relation to the "load-off" time, the faster the creep rate during the "load-on" time. This phenomenon is attributed to removal of the creep-retarding dislocation network during holding of the specimen at 955°C without stress.

Pressure-Vessel Steels

Tubes of several Cr–Mo alloy steels[94] were exposed to 2000-psi steam at 1100 and 1200°F (595 and 650°C) for 21,600 hr. No failures occurred in any of

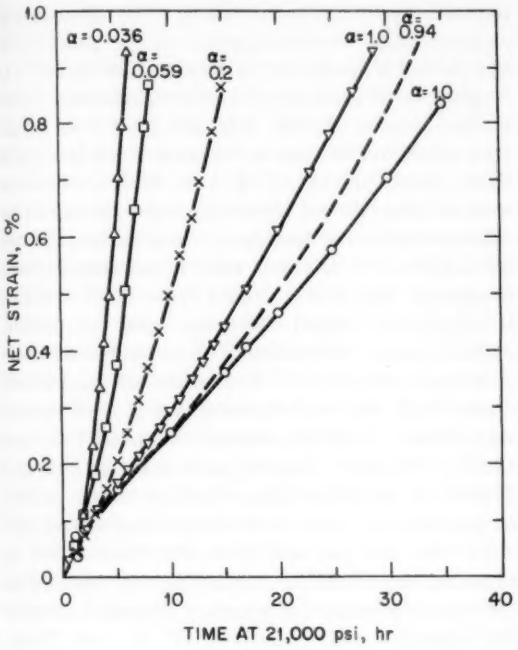

Fig. III-26 Effect of proportion, α, of time spent at stress on creep[99] of Udimet 700 at 955°C and 21,000 psi. Time at zero stress = 1 min/cycle for dashed curve; others were 4 hr/cycle.

the tubes at 1100°F, but the titanium- and silicon-modified 5 Cr–0.5 Mo steel ruptured at 1200°F after comparatively short times. The room-temperature and elevated-temperature tensile properties of the Cr–Mo–V and unmodified Cr–Mo steels were not significantly changed by the heat-treatments.

Varying[100] the vanadium content of 0.5 Mo–B steels from 0 to 0.33 wt.% increased the yield strength but decreased the toughness. The higher vanadium contents resulted in larger carbide particles. Large carbide particles fracture easily and thus provide longer Griffith's cracks that, in turn, reduce the toughness and increase the brittle-to-ductile transition temperature.

An investigation was undertaken to study the influence of nitrogen, titanium, and zirconium on the boron hardenability effect in low-carbon structural steel. It was found[101] that the nitrogen reacted with the boron, and only the unreacted boron contributed to the hardenability of steel. Additions of titanium and zirconium increased the effectiveness of boron because they reacted preferentially with nitrogen. Maximum hardenability was obtained with 10 ppm unreacted boron. (M. Kangilaski)

Metallurgy and Mechanical Properties of Refractory Metals

Data produced in an Oak Ridge study[58c] of the effect of fabrication variables on the creep rupture of molybdenum alloys are shown in Fig. III-27. Of the three alloys investigated, Nb–TZM (Mo–0.5 Ti–0.08 Zr–0.02 C–1.5 Nb) showed the best high-temperature properties. Additional tests performed on Nb–TZM(6) at 1500°C showed a significant drop in stress-rupture strength between 1300 and 1500°C.

Of nine different niobium-base alloys studied, SU-16 (Nb–11 W–3 Mo–2 Hf–0.08 C) in the recrystallized and aged condition (1600°C for 1 hr

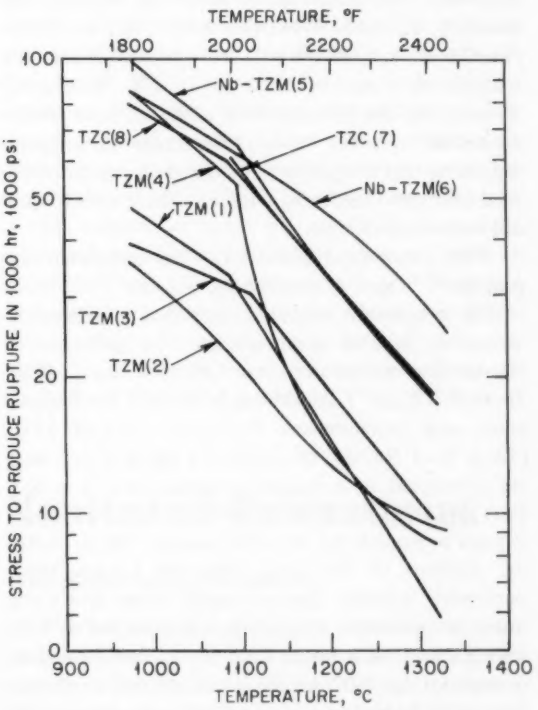

Fig. III-27 The 1000-hr stress-rupture data for selected molybdenum-base alloys.[58c] TZM (1): stress relieved at 1230°C; TZM (2): recrystallized at 1540°C; TZM (3): 1540°C warm worked at 1040°C and stress relieved at 1230°C; TZM(4): annealed 2095°C, reextruded, and warm worked at 1315°C; Nb–TZM (5): annealed 2095°C, reextruded, and warm worked at 1315°C; Nb–TZM (6): annealed 1927°C and warm worked at 1370°C; TZC (7): same as Nb–TZM (5); TZC (8): same as Nb–TZM (6).

followed by 3 hr at 1200°C) showed the highest 1000-hr rupture strength. In the stress-relieved condition (1200°C for 1 hr), its strength was comparable to that of D-43 (Nb–10 W–1 Zr–0.1 C) and FS-85 (Nb–27 Ta–10 W–1 Zr) in similar metallurgical states.

Other studies conducted at Oak Ridge[102] include the effect of heat-treatment on the creep-rupture properties of the niobium-base alloys D-43, FS-85, and Cb-752 (Nb–10 W–2.5 Zr) and the comparative mechanical behavior of some tantalum-base alloys. The creep-rupture properties of D-43, heat-treated according to the revised commercial fabrication schedule, which involves temperatures above 2200°F (1205°C), showed improved properties over material fabricated at temperatures below 2200°F. The creep-rupture properties of FS-85 and Cb-752 were improved by annealing at 2900°F (1595°C) for 1 hr prior to testing. Pretest annealing at higher temperature resulted in inferior properties. The creep-rupture properties of unalloyed tantalum, Ta–10 W, T-111 (Ta–8 W–2 Hf), and T-222 (Ta–9.6 W–2.4 Hf–0.01 C) were evaluated over the temperature range of 1000 to 1650°C. This study showed that the tantalum-base alloys all have similar properties over the temperature range investigated, suggesting that the primary strengthening mechanism is solid-solution hardening rather than precipitate-dislocation interactions.

TRW Equipment Laboratories has completed one program[103] and is conducting another[104,105] for NASA to generate long-term creep data on refractory alloys at elevated temperatures. The materials of interest are molybdenum-base TZC (Mo–1.2 Ti–0.25 Zr–0.15 C) and TZM (Mo–0.5 Ti–0.08 Zr–0.02 C) alloys and tantalum-base T-111 and ASTAR 811C (Ta–8 W–1 Re–0.7 Hf–0.025 C) alloys. Creep tests are conducted in a vacuum environment ($<1 \times 10^{-8}$ torr) at 1600 to 2600°F (870 to 1425°C) under stresses to provide 0.5 to 1.0% creep in 100 to 15,000 hr. Analysis of the data using the Larson–Miller parameter indicates that at higher stress levels and lower temperatures, a specially processed lot of TZM having a somewhat higher than normal carbon content is superior to TZC in the stress-relieved condition, whereas at higher temperatures and lower stresses, the two materials have comparable creep behavior. Tests with T-111 showed that significant variations in creep strength can occur between different heats. The low measured creep strength of T-111 alloy was thought to be the result of fine grain size. ASTAR 811C showed creep properties that were superior to those of T-111.

Investigators at Oak Ridge[33e] have been studying the properties of wrought tungsten produced by chemical-vapor deposition (CVD). The deformation characteristics, recrystallization temperature, and ductile–brittle transition temperature (DBTT) of CVD tungsten sheet containing 25 ppm fluorine and rolled at temperatures between 400 and 1000°C to reductions of 40 to 95% were determined. When specimens were reduced 80% by rolling above 500°C, the columnar grain structure was completely destroyed and a fine cellular substructure developed. These samples did not recrystallize in 1 hr below 1800°C and recrystallized completely only after annealing above 2100°C, which is significantly higher than the 1100 to 1400°C recrystallization temperatures of conventionally produced tungsten. A fine distribution of gas bubbles smaller than 400 A in diameter was observed in the substructure of samples annealed between 1400 and 1800°C. Additional samples, preannealed at 1800 and 2500°C to precipitate larger bubbles before rolling, recrystallized at much lower temperatures. The data show that the gas bubbles smaller than 400 A in diameter, unprecipitated fluorine-impurity clusters, or both are responsible for retarding recrystallization in this material.

A study was made at NASA–Lewis[106] of the mechanical properties of vacuum arc-melted tungsten and W–Re alloys at 77 to 810°K to elucidate the mechanism by which rhenium additions lower the DBTT of tungsten. The temperature and strain-rate dependence of the yield stress of tungsten is reduced by alloying with rhenium. This is shown to be because of a reduction in the Peierls stress. The reduction of the transition temperature is attributed to the reduced Peierls stress through its effect on the mobility and rate of multiplication of dislocations.

Other work at NASA on W–Re alloys has shown[107] that alloys containing 20 to 28 at.% rhenium may be considered superplastic. Alloys in this composition range exhibited elongations of over 200% in tensile tests at 2000°C. Rapid grain growth in these alloys, relative to W–Re alloys with lesser rhenium contents, and continuous recrystallization during tensile testing signified the occurrence of enhanced diffusion processes. Strain-rate sensitivities generally ranged between 0.2 and 0.3 for these alloys, but strain-rate sensitivities as high as 0.8 were observed immediately following initial recrystallization.

It was determined in a program at Battelle–Northwest[108] that technetium has the same ability to impart ductility to recrystallized tungsten as does rhenium. For example, the addition of 3.5 at.% technetium lowered the DBTT of pure recrystallized tungsten from 675°C to 280°C. Technetium additions

in the range of 3.5 to 20 at.% were found to be most effective.

The effects of composition, heat-treatment, and substructure on the strength and ductility of W–Hf–C alloys have been studied at NASA–Lewis.[109] These alloys exhibit a sevenfold strength improvement over unalloyed tungsten at 3500°F (1925°C) that is related to the precipitation-stabilized, fine dislocation structure formed within the cell boundaries. The compositions of the alloys ranged from 0.23 to 1.76 at.% for hafnium and from 0.179 to 0.942 at.% for carbon, with carbon-to-hafnium ratios from 0.17 to 2.80 and calculated amounts of hafnium carbide up to 1.5 vol.%. The high-temperature tensile strengths of swaged, recrystallized, solution-annealed-and-aged W–Hf–C alloys increased with increasing hafnium carbide contents up to approximately 0.5 vol.%, after which further additions caused a slight decrease in strength. The strongest alloys contained equiatomic amounts of carbon and hafnium, with approximately 0.3 to 0.4 at.% considered optimum. The 3500°F tensile strength of swaged material was a linear function of the inverse square root of the cell size. Limited tensile and microstructural studies indicated that the alloys are heat-treatable. The stress for a 3500°F, 100-hr rupture life of the material as swaged was approximately 14,000 psi. A solution-annealed-and-aged specimen tested in 3500°F step-load creep tests required a stress of approximately 20,000 psi for a minimum creep rate of 6×10^{-7} sec^{-1}, corresponding approximately to a 100-hr rupture life.

The use of refractory metals in the as-sintered condition has been discouraged by the belief that useful engineering properties could not be obtained in unworked alloys. At Minnesota Mining[110] a study was conducted to compare the tensile properties of wrought recrystallized W–25 Re with those of unwrought as-sintered rod converted directly from elemental powders. The results of this work indicated that at comparable grain sizes there need be no marked difference in properties. After exposure to very high temperatures, the sintered material was actually superior to the wrought recrystallized material as a result of the differences in grain-growth characteristics.

Although it has been known that niobium and tantalum are capable of absorbing large amounts of nitrogen, oxygen, and carbon in dissolved form at higher temperatures, the alpha solid solution has usually been neglected in the corresponding systems. This is partially due to the lack of data available. Recently the alpha-solid-solution regions for the gas–metal systems of niobium and tantalum have been studied in more detail. At the Max-Planck Institute,[111] the data necessary for the thermodynamic analysis of these systems have been compiled. Equilibrium pressures of N_2, CO, O_2, O, NbO, NbO_2, TaO, and TaO_2 are given as functions of the temperature and concentration over the solid-solution region of niobium and tantalum. From this, it is possible to estimate the role that is played by individual gas-absorption and degasification reactions over various pressure and temperature ranges.

German investigators[112] have noted the strong influence of titanium concentration on the creep and stress-rupture behavior of V–Ti and V–Ti–Nb alloys above 650°C. At titanium concentrations above 1 wt.%, the stress-rupture strength is lowered with increasing titanium content, whereas the ultimate tensile strength increases. This effect is not altered by changing the niobium content. The time to rupture at high stresses is increased with increased niobium content. At low stresses the influence of the niobium content decreases, so that the 10,000-hr stress-rupture strength of the vanadium alloys is only slightly dependent on the niobium concentration. The strongest vanadium-base alloys show outstanding stress-rupture strengths in the temperature range between 650 and 800°C. The activation energy for creep in the temperature range 650 to 700°C is strongly influenced by the titanium content, whereas it is not at all sensitive to the niobium content. The creep and stress-rupture behavior of the vanadium-base alloys, even at higher titanium concentrations, seems to depend most strongly on the interaction between the titanium and interstitial impurities. (J. H. Peterson)

Nonfueled Refractories

Preparation and Fabrication

Manning and Stoops[113] have examined the compatibility, wetting, and fabrication characteristics of several refractory metal–ceramic material combinations. Refractory oxides (Y_2O_3-stabilized HfO_2 and ZrO_2, ThO_2, CeO_2), carbides (HfC, NbC, TaC, and ZrC), borides (NbB_2 and TaB_2), and HfN were examined for stability in contact with refractory metals of Groups VIA and VIIA. Thermodynamic calculations were made to predict stability up to 2500°K between the ceramic oxides and carbides in contact with molybdenum, rhenium, and tungsten. Reaction studies showed that Mo–40 Re, rhenium, and

tungsten are stable in contact with the carbides, nitrides, and oxides to 2450°C, with two exceptions: CeO_2 in contact with tungsten at 1700°C and Mo–40 Re in contact with WC. The Mo–40 Re and rhenium also reacted with NbB_2 and TaB_2 above 2200°C to form very hard single-phase compounds. The results are summarized in Table III-14.

Sessile-drop contact angles between liquid Cr, V, Pt, Rh, Mo, and Mo–Re alloy and solid ThO_2, HfO_2, ZrO_2, HfC, TaC, and ZrC were measured[114] at

Table III-14 Results of Compatibility Studies of Refractory Metals with Ceramics[113]

Metal	Ceramic	Temp., °C	Exposure time, min	Atm	Reaction
		Oxides			
Mo–40 Re	ThO_2	2350	120	Vacuum	No
Re	ThO_2	2350	120	Vacuum	No
W	ThO_2	2350	120	Vacuum	No
Mo–40 Re	91 HfO_2 + 9 Y_2O_3	2350	120	Vacuum	Slight
Re	91 HfO_2 + 9 Y_2O_3	2350	120	Vacuum	Slight
W	91 HfO_2 + 9 Y_2o_3	2350	120	Vacuum	Slight
Mo–40 Re	91 HfO_2 + 9 Y_2O_3	2350	120	Vacuum	Slight
Re	91 HfO_2 + 9 Y_2O_3	2350	120	Vacuum	Slight
W	91 HfO_2 + 9 Y_2O_3	2350	120	Vacuum	Slight
W	91 HfO_2 + 9 Y_2O_3	2525	60	Helium	Slight
		Nitrides			
Mo–40 Re	HfN	2500	60	Helium	No
Re	HfN	2500	60	Helium	No
W	HfN	2500	60	Helium	Slight
		Borides			
Mo–40 Re	TaB_2	2000	60	Vacuum	No
Mo–40 Re	TaB_2	2350	60	Vacuum	Yes
Re	TaB_2	2000	60	Vacuum	No
Re	TaB_2	2350	60	Vacuum	Yes
Re	NbB_2	2250	60	Vacuum	Yes
		Carbides			
Mo–40 Re	HfC	2450	60	Vacuum	No
Mo–40 Re	HfC	2500	15	Vacuum	Yes
Mo–40 Re	HfC	2500	15	Helium	Yes
Re	HfC	2500	60	Helium	No
W	HfC	2600	180	Vacuum	Slight
Mo–40 Re	NbC	2450	60	Vacuum	No
Mo–40 Re	NbC	2600	11	Vacuum	Yes
Re	NbC	2500	60	Vacuum	No
W	NbC	2500	240	Vacuum	No
Mo–40 Re	TaC	2450	60	Vacuum	No
Mo–40 Re	TaC	2500	15	Vacuum	Yes
Mo–40 Re	TaC	2500	15	Helium	Yes
Re	TaC	2500	60	Vacuum	No
W	TaC	2600	180	Vacuum	No
W	TaC	2600	60	Helium	No
Mo–40 Re	ZrC	2450	60	Vacuum	No
Mo–40 Re	ZrC	2500	15	Helium	Yes
Re	ZrC	2500	60	Vacuum	No
W	ZrC	2500	120	Helium	No

temperatures up to 2800°C in helium. Little wetting occurred between any of the metals and the refractory oxides, but molybdenum and the Mo–Re alloy did wet the refractory carbides. Microscopic examination of the metal–ceramic interfaces showed that HfC–(Mo–40 Re) and ZrC–(Mo–40 Re) had highly desirable wetting and solubility characteristics for making cermets. Specimens were fabricated from these two systems with 25 and 50 vol.% metal by cold pressing and sintering and by hot pressing. The microstructures of these cermets consisted of small, uniformly dispersed carbide particles in Mo–Re matrices. The hardnesses and transverse rupture strengths of these cermets, as illustrated in Table III-15, indicate that they have considerable promise for high-temperature applications.

Ultrafine particles (100 to 1000 A) of TaC, NbC, TiC, and TaN have been prepared by Neuenschwander[115] by means of plasma-reaction processes. Free carbon has been noted in the carbide compounds, as well as oxygen contents comparable to those in conventionally prepared powders.

Russian investigators[116] have developed procedures for obtaining ZrC on a semiindustrial scale which include the use of an electric resistance furnace with a hydrogen atmosphere at 2200°C. Other Soviet studies[117] have examined the conditions for obtaining spherical granules of WC employing tumbling methods. Samsanov, Vitryanyuk, and Sysov[118] investigated conditions for obtaining materials with high porosity from titanium and zirconium carbides directly during soot reduction of the oxides in a vacuum. The porosities of the resulting bodies were 68 to 74% for zirconium carbide and 69 to 77% for titanium carbide. It was shown that introducing some carbides into the initial charge of oxides and soot regulates the porosity and relative volumetric shrinkage because the carbide particles serve as recrystallization nuclei and activate sintering.

German investigators[119] have succeeded in producing solid solutions of several carbides by an auxiliary-metal-bath technique. The resulting mixed carbides were pure—low in oxygen and nitrogen—and well crystallized. Miscibility gaps were reported at low temperatures in carbide systems that up to now have been considered as completely miscible.

Chemical activation was investigated[120] as a means of sintering ZrB_2 to produce bodies of almost zero porosity. Activated sintering occurs when ZrO_2 and boron are added to the ZrB_2. At sintering temperatures the ZrO_2 is reduced by the carbon in the ZrB_2 grain boundaries, leaving highly active zirconium atoms that react with the free boron atoms to form finely divided ZrB_2. The excess energy of the latter accelerates the diffusion processes, and this, aided by the high surface tension, promotes densification of the ZrB_2 crystals. Basically, activated sintering is a volume-diffusion process, which accounts for the fact that the carbon, distributed in the original boride grain boundaries throughout the crystal volume, was completely eliminated during the activated sintering.

It was established by the Soviets[121] that niobium or tantalum diboride with a composition close to that of stoichiometric NbB_2 or TaB_2 could be obtained by heating Nb_2O_5 or Ta_2O_5 with elemental boron at 1650°C in vacuo for 1 hr. Similar treatments of V_2O_3

Table III-15 Properties of (Mo–40 Re)-Bonded Carbides[114]

Composition, vol.%	Processing conditions: Sintering temp., °C	Processing conditions: Time at max. temp., min	Density, g/cm³	Density, % of theoretical	Hardness, Rockwell A	Transverse rupture strength, psi
(Mo–Re)	2300	120	14.00	99.2	52 to 53	
25(Mo–Re)–75 HfC	2300	120	12.42	95.4	81	100,100
25(Mo–Re)–75 HfC	2300	120	12.45	95.7	81	106,600
50(Mo–Re)–50 HfC	2300	120	12.41	93.1	79	169,000
50(Mo–Re)–50 HfC	2300	120	12.50	93.7	79	180,000
50(Mo–Re)–50 HfC	2300	120	12.54	94.0	79	161,000
25(Mo–Re)–75 ZrC	2500	4	8.14	95.2	87 to 88	96,100
25(Mo–Re)–75 ZrC	2500	4	8.21	96.0	86 to 87	100,600
25(Mo–Re)–75 ZrC	2160*	0.5	8.17	95.4	88 to 89	98,700
50(Mo–Re)–50 ZrC	2300	120	9.77	94.9	79 to 80	120,900
50(Mo–Re)–50 ZrC	2500	2	9.39	91.3	78	90,200

*Hot pressed.

with boron metal did not give a single-phase product but yielded a mixture of VB_2 and VB. A method for the chemical analysis of NbB_2 and TaB_2 samples was proposed.

A detailed French study[122] revealed that the properties of plasma-sprayed borides and nitrides were generally quite different from those of similar materials produced by sintering. The Japanese[123] used a transport-type plasma torch to produce tantalum nitride from metallic tantalum and nitrogen plasma. X-ray analysis revealed that the bulk of the product was the TaN that was sought.

Phase Equilibria

Researchers at the University of Vienna[124] have investigated the miscibility of cubic multicomponent carbides. The miscibility gap within the systems TiC–(ZrC, HfC) and VC–(NbC, TaC) was determined experimentally in the region from 1200°C up to the temperature of the critical point. Other university researchers[125] have determined the phase diagrams of the systems VC–ZrC and VC–HfC. The mutual solubilities of the monocarbides VC–ZrC and VC–HfC, respectively, were determined by X-ray methods in the corresponding pressed-and-sintered powder mixtures. In the system VC–ZrC at 2270°C, they were 1.7 mole % VC and 0.3 mole % ZrC; at the eutectic temperature of 2550°C, 8.1 mole % VC and 7.0 mole % ZrC. In the system VC–HfC at 2270°C, they were 3.4 mole % VC and 4.5 mole % HfC; at the eutectic temperature of 2650°C, 8.8 mole % VC and 14.3 mole % HfC. The constitution of the two pseudobinary systems was determined by means of a simple Seger-cone method. It was found that these are simple eutectic systems, and the supposition that the miscibility gap in the solid state is closed at high temperatures is thus not confirmed for the two carbide pairs.

The ternary systems Ta–Mo–C and Nb–Mo–C were investigated by Aerojet-General[126,127] utilizing X-ray, melting point, DTA, and metallographic methods on chemically and thermally characterized specimens; phase diagrams for temperatures from 1500°C through the melting range were established. At high temperatures the cubic monocarbides TaC and α–MoC_{1-x}, as well as the hexagonal subcarbides Ta_2C and Mo_2C, form continuous series of solid solutions. Below 1960°C the homogeneity range of the cubic Mo–C phase is temperature dependent. At 2230°C the ternary subcarbide solid solution disproportionates into metal and monocarbide alloys. The sublattice order–disorder transformation temperatures in both subcarbides are lowered by the mutual exchange. The ternary range of the η–MoC_{1-x} phase is very restricted, and the metastable ξ–Ta–C phase is stabilized in the ternary. Seven isothermal reactions occur in the system in the range from melting to 1500°C; two further isotherms between 1400 and 1500°C are indicated to result from the order–disorder transition of Mo_2C. Calculated equilibria in the Ta–Mo–C system, based on existing literature data for the thermodynamic properties of the binary carbides, are in good agreement with experimental observations.

The ternary-alloy system Nb–Mo–C is very similar[127] to the system Ta–Mo–C above 1500°C. Dimolybdenum carbide dissolves up to 44 mole % Nb_2C (2240°C), whereas the maximum solid solubility of Mo_2C in Nb_2C does not exceed 5 mole %. The order–disorder transformation temperatures in Mo_2C and Nb_2C are lowered by the mutual metal exchanges. Six invariant (p = constant) reactions occur in the ternary system; three correspond to four-phase reactions involving a liquid phase, one to a eutectoid reaction, and two further isotherms are associated with limiting tie lines. Thermodynamics indicate that the low relative stability of the binary subcarbides, together with the large stability differences between niobium and molybdenum carbides, is responsible for the stable equilibrium between the monocarbide and the metal phase in the ternary region.

Phase equilibria in the system of V–Cr–C at 1000°C have been established,[128] and a compound of the approximate composition of VCr_2C_2 was found. The solid solubility of chromium in VC is 30 at.% and in V_3C, 32 to 33 at.%. In the systems Nb–Cr–C and Ta–Cr–C, phase equilibria were established at 1050 and 1000°C. The ternary carbide Nb_3Cr_3C was not found.

A phase formation accompanying the interaction of transition metals with carbon in thin (20 to 50 μ) layers obtained by the condensation in vacuo (5×10^{-5} torr) of Nb, Zr, Ta, Hf, and Ti vapors on the surface of graphite at 1500 to 2200°C was examined.[129a] The diffusion processes in such layers possess a number of specific features that could be used for growing compounds within a narrow composition range. The occurrence of one or another phase in the layers was found to bear a definite relation to the manner of obtaining the layers, depending on base-layer temperature, supersaturation of the metal vapors, and the time of layer formation. Under certain conditions all the carbide phases were observed simultaneously within the layers, and the corresponding metal appeared on the outer surface of the layer. Compounds of the type

MeC_x were isomorphous with known MeC carbides and had smaller lattice parameters. From data on the dependence of the niobium carbide lattice parameter on carbon content in NbC_x, it was found that $0.8 > x > 0.7$. In the system Ti–C, compounds of the type MeC_x were not found, though possibility of such a compound in this system cannot be excluded.

A constitution diagram was constructed by the Soviets[130] for the Zr–ZrC–ZrN system at 1600°C. The melting points of alloys in the $ZrC_{0.923}$–$ZrN_{0.818}$ cross section were measured. The results apparently were in good agreement with isobar–isothermal potentials calculated for constitution diagrams of ZrC–ZrN and $ZrC_{0.923}$–$ZrN_{0.818}$.

Other Russian investigators studied the W–Cr–B and W–Mo–B systems[131] and the Ta–Ti–B and Ta–Mo–B systems.[132] In the system W–Cr–B, the ternary compound $W_{3.2}Cr_{1.8}B_3$ exists in the solid state and has a crystal structure of the Cr_5B_3 type ($a = 5.600 \pm 0.003$ A, $c = 10.88 \pm 0.01$ A, $c/a = 1.91$). The compound W_2B dissolves 61 at.% of chromium, whereas the compound CrB dissolves 37 at.% of tungsten. The continuous solid solution W_2B–Mo_2B exists in the system of W–Mo–B. The compound TaB dissolves 10 at.% of titanium; likewise, the compound TiB dissolves 10 at.% of tantalum. In the system Ta–Mo–B the compounds Ta_3B_2 and TaB dissolve 40 at.% of molybdenum, and the compound Mo_2B dissolves 10 at.% of tantalum. The lattice parameters of binary boride compounds correspond to the atomic radii of the constituents.

Thermodynamic Properties

The dependence of carbon activity on composition and temperature in nonstoichiometric vanadium and titanium carbides was determined[129b] in the range 973 to 1223°K. Carbon activity was determined by investigating gaseous equilibria in the system H_2–CH_4–C (in the carbide). It was found that, when the atomic ratio of carbon to metal changes within the homogeneity region, the carbon activity changes by more than two orders of magnitude. In vanadium carbide at 1000°K, for example, the carbon activity increases by a factor of 500 when the ratio of carbon atoms to vanadium atoms changes from 0.6 to 0.93. From an analysis of the temperature dependencies, it was established that the change in carbon activity within the homogeneity region of the vanadium and titanium carbides was influenced by both the enthalpy and the entropy terms. The partial molar free energy of the carbon in vanadium and titanium carbides was calculated, and the Gibbs–Duhem equation was used to estimate the partial molar free energies of the vanadium and titanium. The total free energies of the vanadium and titanium carbides were calculated and compared with published data for nonstoichiometric carbides of Nb, Th, U, and Hf.

The integral and partial configuration entropies for solid solutions of carbides were calculated by the Soviets.[129c] Analysis of data on the magnetic susceptibility, electronic heat capacity, ordering, and characteristic temperature in systems of carbides of transition metals in groups IV through VI showed that nonconfigurational (i.e., electronic, magnetic, and vibrational) contributions to entropy may be ignored for solutions formed by carbides of metals of a single group in the periodic system, or for dilute carbide solutions. In another investigation[133] the enthalpies of three compositions of zirconium carbide were determined in the homogeneity domain at 1300 to 2500°K by means of a vacuum calorimeter device, and equations relating enthalpy and heat capacity to temperature were developed.

Tables III-16 and III-17 show thermodynamic properties of TaC and WC based on calorimetric measurements of heat capacities to 1700 and 2700°K, respectively.[134]

Physical Properties

French researchers have published a report[135] concerning the high-temperature mechanical properties of some refractory carbide materials. A study of tensile strength as a function of temperature showed differences between the different carbides and also differences between these carbides and graphite. Only tantalum carbide shows a real advantage over graphite from room temperature to 3200°C. Its thermal-shock resistance was intrinsically low but could be improved by impregnating the carbide with metals such as copper or silver which have a good thermal conductivity.

In a study of the groups IVB and VB monocarbides,[136] the thermal expansion of theoretically dense test samples prepared by liquid-state carburization was found to be inversely related to their melting points. As shown in Figs. III-28 and III-29, the microhardness increased with increasing stoichiometry (C : Hf ratio) in the group IVB monocarbides and decreased in the group VB monocarbides. The yield strength as a function of temperature is shown in Figs. III-30 and III-31. Hafnium carbide had the highest yield stress and VC the lowest. The HfC material was noted to contain about 1.5 wt.% zirconium and had

Table III-16 Thermodynamic Properties[1 3 4] of TaC

Temp., °K	Heat capacity (C_p), cal/(mole)(°C)	Enthalpy above 298°K (H_T-H_{st}), cal/mole	Entropy above 298°K (S_T-S_{st}), cal/mole	Free-energy function $\left(-\frac{G_T-H_{st}}{T}\right)$, cal/mole
298	4.38	0	0.00	5.05
	(4.34)*			(5.03)
400	4.83	476	1.37	5.23
500	5.33	993	2.52	5.58
600	5.60	1,540	3.52	6.00
700	5.79	2,112	4.40	6.43
800	5.93	2,700	5.18	6.85
900	6.02	3,299	5.89	7.27
1000	6.10	3,903	6.53	7.68
1100	6.16	4,514	7.11	8.06
1200	6.23	5,133	7.65	8.42
1300	6.29	5,759	8.13	8.75
1400	6.34	6,398	8.62	9.10
1500	6.38	7,046	9.07	9.42
	(6.42)	(6,984)	(9.07)	(9.40)
2000	(6.71)	(10,329)	(10.96)	(10.85)
2500	(7.06)	(13,766)	(12.50)	(12.04)
3000	(7.42)	(17,375)	(13.82)	(13.08)
3500	(7.88)	(21,221)	(15.00)	(13.99)
4000	(8.48)	(25,348)	(16.10)	(14.81)

*Values in parentheses are extrapolated.

Table III-17 Thermodynamic Properties[1 3 4] of WC

Temp., °K	Heat capacity (C_p), cal/(mole)(°C)	Enthalpy above 298°K (H_T-H_{st}), cal/mole	Entropy above 298°K (S_T-S_{st}), cal/mole	Free-energy function $\left(-\frac{G_T-H_{st}}{T}\right)$, cal/mole
298	4.18	0	0.00	4.15
400	4.72	454	1.31	4.33
500	5.16	950	2.41	4.66
600	5.47	1,482	3.38	5.06
700	5.71	2,042	4.24	5.47
800	5.89	2,623	5.02	5.89
900	6.02	3,218	5.72	6.29
1000	6.13	3,822	6.36	6.69
1100	6.21	4,430	6.94	7.06
1200	6.29	5,053	7.48	7.42
1300	6.37	5,682	7.98	7.76
1400	6.44	6,320	8.45	8.09
1500	6.52	6,966	8.90	8.41
1600	6.59	7,621	9.32	8.71
1700	6.65	8,265	9.72	9.01
1800	6.72	8,951	10.11	9.28
1900	6.78	9,627	10.47	9.55
2000	6.85	10,306	10.82	9.82
2100	6.91	10,996	11.16	10.07
2200	6.98	11,692	11.48	10.32
2300	7.05	12,391	11.79	10.55
2400	7.11	13,105	12.09	10.80
2500	7.18	13,816	12.39	11.01
2600	7.24	14,536	12.67	11.23
2700	7.31	15,263	12.94	11.44
	(7.40)*	(15,270)	(12.95)	(11.44)
3000	(7.70)	(17,515)	(13.73)	(12.04)

*Values in parentheses are extrapolated.

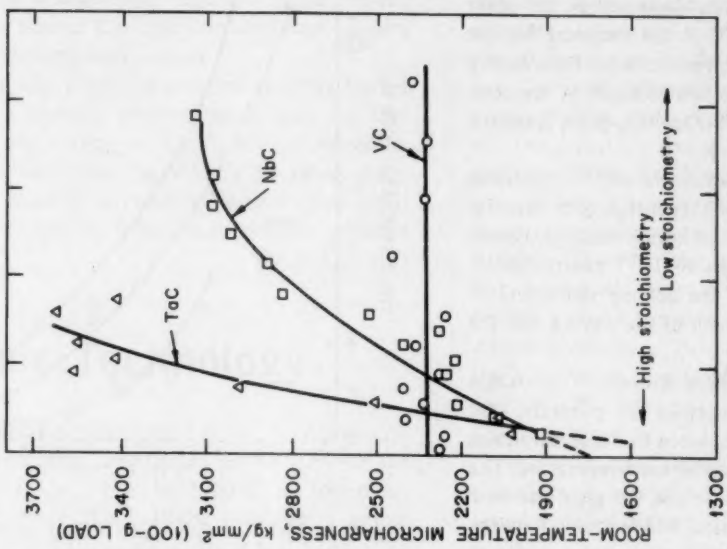

Fig. III-29 Effect of stoichiometry on microhardness of the group VB monocarbides.[136] (VC—2300°C, 144 min; NbC—2850°C, 100 min; TaC—2600°C, 330 min.)

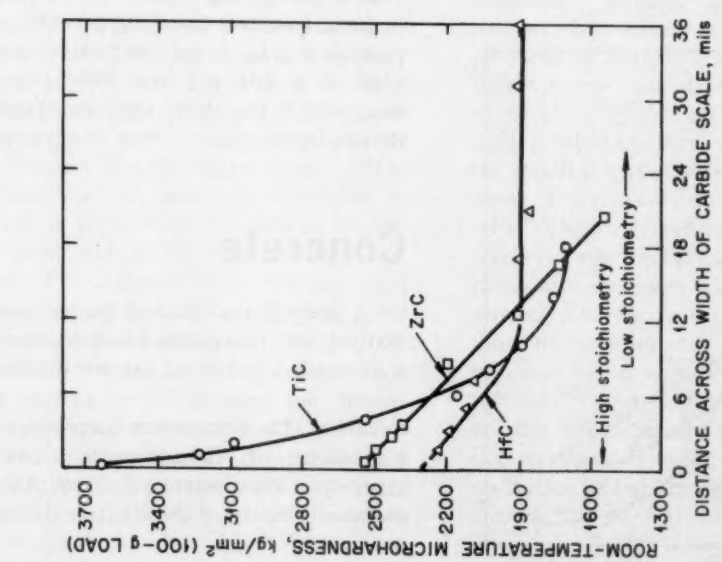

Fig. III-28 Effect of stoichiometry on microhardness of the group IVB carbides.[136] (TiC—2300°C, 144 min; ZrC—2800°C, 27 min; HfC—3000°C, 100 min.)

only one-third the grain size of the others, which probably accounts for its superior strength. Susceptibility to strain hardening decreased in the order TaC, NbC, HfC, ZrC, TiC, VC. It was proposed that the carbides derive their room-temperature hardness from a high Peierls force, whereas their strength at temperatures greater than one-half the melting point is related to metal diffusion.

In Soviet irradiation experiments,[137] diffusion carbide coatings on high-melting metals (Nb, Mo, Ta, and W) cracked and diffusion boride coatings disintegrated under radiation doses of 10^{20} neutrons/cm^2. The radiation resistance of the coating was found to depend on the relative growth of the coating and the base.

Investigators at Gulf General Atomic,[138] in studies of the structure and properties of pyrolytic SiC deposited in a fluidized bed, noted that internal strains decreased with increasing deposition temperature. The degree of preferred orientation and the grain size were fairly insensitive to deposition temperatures between 1300 and 1600°C, but both increased sharply between 1700 and 1800°C. The deposits, characterized by columnar grains, were predominantly beta SiC with traces of alpha SiC and excess carbon. The (1 1 1) planes tended to lie parallel to the deposition surface. Room-temperature modulus of rupture and Young's modulus of beta SiC deposited at 1400 to 1600°C were about 134×10^3 and 62×10^6 psi, respectively. The mean thermal-expansion coefficient between 22 and 1000°C of beta SiC deposited at 1300 to 1800°C was $(4.94 \pm 0.12) \times 10^{-6}$/°C. The thermal conductivity of 1400°C material was 0.07 to 0.15 cal/(cm)(°C)(sec) at room temperature, decreasing by 40% over the temperature interval 22 to 600°C. Material deposited at 1400 to 1800°C had over 99% of the theoretical density (3.212 g/cm^3), with the 1800°C material showing 99.9%. (W. C. Chard)

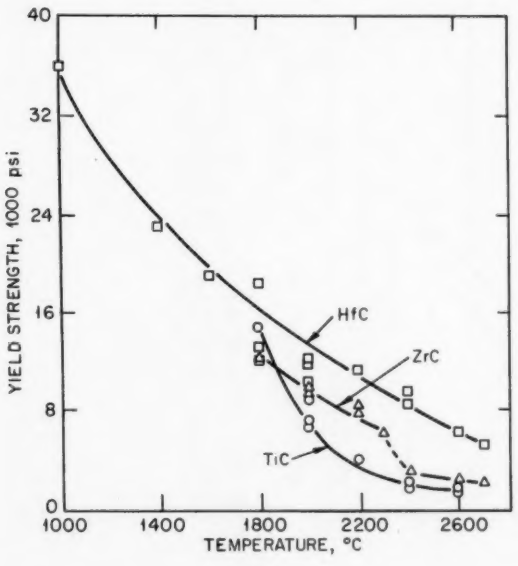

Fig. III-30 Yield strength (0.2% offset) of the group IVB monocarbides.[136] Strain rate = 0.02 min^{-1}.

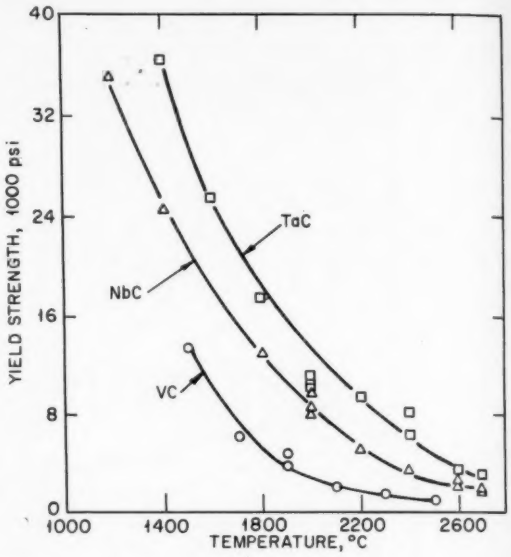

Fig. III-31 Yield strength (0.2% offset) of the group VB monocarbides.[136] Strain rate = 0.02 min^{-1}.

Concrete

A study of the effect of thermal exposure up to 500°F (260°C) on portland-cement concrete as related to its use in a prestressed-concrete pressure vessel for a reactor was reported[139] by workers at Battelle–Columbus. The influence of temperature on the compressive strength, flexural strength, and modulus of elasticity of the concrete was shown to depend on the moisture content of the concrete during heating or testing.

Concrete specimens in which the moisture was retained during heating exhibited significantly poorer structural properties than concrete heated under conditions in which the moisture was free to evaporate. The

deterioration of structural properties in wet concrete subjected to sustained heating was attributed to the occurrence of hydrothermal reactions in the cement phase which altered the highly cementitious calcium silicate hydrates originally present.

Evidence was presented to show that the heated portion of a concrete pressure vessel does not lose moisture during heating, so that its strength would be substantially below that indicated by laboratory specimens tested in air at atmospheric pressure. This fact is of vital importance to designers of concrete pressure vessels. (D. R. Lankard)

Ceramic Technology

The mechanical properties of press-forged polycrystalline alumina were investigated at AVCO over the temperature range −196 to 1700°C in four-point bending.[140] Since this material possessed a strong crystallographic texture, the study served to identify any dependence of brittle and plastic properties on orientation. Tests in the brittle range failed to exhibit a significant effect on strength of the orientation of load to the predominant basal plane in these polycrystalline specimens. Thus it was inferred that basal slip or basal twinning had little or no role in crack nucleation. The existence of a constant strength–grain size (2 to 10 μ) relation at −196 and 1200°C was attributed mainly to grain-boundary "character" that could include many factors, but the special twist character of the grain boundaries parallel with the tensile axis of loading and the special character of pore-boundary interfaces were thought to dominate. The high-temperature (1300 to 1700°C) deformation was essentially independent of orientation and is substantially the same as for hot-pressed or sintered materials of comparable grain size. The relation $\sigma = K\dot{\epsilon}m$ holds, with $m = 0.6$ to 0.9, which was interpreted as representing a diffusional creep mechanism with an added component due to grain-boundary sliding; σ is stress, $\dot{\epsilon}$ is rate of strain, and K is a constant.

Room-temperature fracture studies were conducted on polycrystalline magnesia, and the results were compared with those of previous studies conducted under liquid nitrogen (−196°C) to establish the effects of surface condition and atmosphere. Magnesia was tested in four-point bending at a strain rate of 5×10^{-3} min^{-1}. Tests were conducted in moist air and in dry argon after outgassing in vacuum for 1 hr at 900°C. Surface conditions investigated included the following: 500-grit diamond ground, chemically polished, mechanically polished, and annealed 8 hr at 1200°C in air. Magnesia was sensitive to the perfection of surface structure, indicating that fracture is related to the critical flaw length by the Griffith criterion. Annealing was the most effective surface treatment, and the average fracture stress of annealed specimens was about 1.6 times that of the specimens that had diamond-ground surfaces. There was no conclusive evidence of stress corrosion at room temperature (17°C) since tests in dry argon and moist air gave nearly identical fracture strengths. However, the strength of magnesia at 17°C was dependent on surface condition, and the dependence correlated well with the presence of mobile surface dislocations. This, together with the absence of stress corrosion, suggested that dislocation crack nucleation is the dominant fracture mode in magnesia at this temperature.

Polycrystalline alumina was tested by the same procedure as was the magnesia. Surface conditions tested included 500-grit diamond grinding, mechanical polishing, and annealing for 16 hr at 1300°C in vacuum. Polycrystalline alumina exhibited striking evidence of stress corrosion, which limited the strength to 0.7 of a baseline level for a given microstructure on specimens with a surface produced by 500-grit diamond grinding. In the absence of stress corrosion (tested in liquid nitrogen or in dry argon after vacuum outgassing), annealed specimens were consistently stronger than specimens that had a surface finish produced by 500-grit diamond grinding, although the difference was not statistically significant for tests conducted at 17°C in dry argon. Strengths for mechanically polished specimens were nearly the same as those for annealed specimens when tested at 17°C in dry argon. This result did not agree with earlier work at −196°C, which showed a slight decrease in strength for specimens with mechanically polished surfaces as compared with specimens with 500-grit diamond-ground surfaces. The discrepancy between these results and those for single crystals, where mechanical polishing increased the strength by 80%, was tentatively attributed to intergranular cracking in both diamond grinding and mechanical polishing of the polycrystalline specimens. However, the dependence of strength on surface perfection, which was found in this study and in the previous study conducted at −196°C, supports a Griffith crack-failure mechanism in polycrystalline alumina. The present study also showed that there was no correlation of the strength of alumina at 17°C with the percentage of transgranular fracture. Thus the transgranularity of fracture appears to be a

stronger function of the inherent grain-boundary strength than of the stress level at which fracture was initiated.

Johnson and Muan reported[141] on phase-equilibrium studies in the systems Si–O and Cr–O. The research indicated that at high temperatures no stable intermediate compounds exist between the metal and oxides, SiO_2 or Cr_2O_3. A large concentration range of coexistence of two liquid phases above liquidus temperature was found in both systems.

The effects of exposure to water vapor on the fracture stress and Young's modulus of polycrystalline MgO were studied by Janowski and Rossi.[142] The rate and extent of degradation, which was attributed to chemical attack, were found to be dependent on the amount and nature of porosity. After 12 months' exposure to laboratory atmosphere, the Young's modulus of a 10% porous specimen had decreased by 33%, whereas that of a 5% porous specimen had decreased 25%. Strength was much less adversely affected.

ManLabs reports[143,144] on a multiorganizational effort aimed at developing modified diboride materials exhibiting improved oxidation resistance, strength, and thermal-stress resistance without sacrificing high-temperature stability. A program was evolved in which several hundred diboride specimens ranging from 2-in.-diameter to 6-in.-square billets were fabricated, principally by conventional hot pressing of HfB_2 or ZrB_2 powders alone or with silicon carbide, graphite, and other additives in the form of powder, whiskers, or yarn. Hot forging, plasma spraying, and sintering were explored as alternative means of producing dense diboride specimens. Compositionally the specimens varied from pure diboride material up to 30 wt.% SiC or 50 wt.% carbon.

It was found that ceramic additives in HfB_2 or ZrB_2 enhanced densification and fabrication (by hot pressing) of fine-grained crack-free billets. Oxidation screening evaluations conducted at temperatures of 1700 to 2200°C showed that SiC is effective in reducing diboride oxidation and in increasing the adherence characteristics and temperature limits of the formed protective oxide coatings. The incorporation of graphite in the diborides improved their thermal-stress resistance but detracted from their oxidation resistance. Mechanical screening tests showed that the fine-grained fully dense diboride composites had improved high-temperature bend strengths of 40,000 to 60,000 psi (at 1800°C) and moduli of elasticity of 70 to 80×10^6 psi (at 1400°C). The SiC additions to ZrB_2 of HfB_2 did not adversely affect the composite moduli, whereas porosity and graphite substantially reduced the Young's modulus. Temperature and strain-rate dependence tests showed a limited plasticity in bending at 1800°C for all the compositions tested. Steady-state thermal-stress resistance measurements on hollow cylindrical specimens indicated that sufficient plastic strain occurred at 1275°C to prevent fracture due to thermal stresses.

It is claimed, on the basis of the results obtained, that diboride materials can be recommended with greater confidence as monolithic ceramic bodies for application in environments that produce thermal stresses and surface oxidation. These materials are recommended for applications, such as reactor control rods, which require that their specific geometry be retained in service for long periods of time. It is also claimed that the success of the ceramic-additive approach has eliminated the need for the consideration of low-melting metal additives as a means of enhancing consolidation.

Workers at Montecatini–Edison[145] examined phase relations in the ZrO_2–Al_2O_3 system. They found that above 1930°C, up to 1 wt.% ZrO_2 is soluble in Al_2O_3, giving hexagonal crystals with $a_0 = 7.849$ and $c_0 = 16.183$. The eutectic, at 57.4 wt.% Al_2O_3, was found to be at 1710°C. The ZrO_2-rich side of the diagram, where considerable solid solution is known to exist, was not reexamined. (H. D. Sheets, Jr.)

Diffusion Studies

Bibliographies and General Theory

Oak Ridge has compiled a list[146] of useful references that include U. S. and foreign papers issued between 1962 and 1967 dealing with diffusion in transition metals (groups IV to VI). Los Alamos has also published a compilation[147] of over 50 references and abstracts concerned with the diffusion of gold and silver, with emphasis on the effects of plastic deformation.

An ample supply of recent literature is available dealing with diffusion in general, theories of diffusion, and methods for measuring and calculating diffusivity. In his book on the subject,[148] Manning discusses atomic diffusion processes in terms of the random-walk concept and derives equations for diffusion from these considerations. Random-walk theory is reviewed in detail, and the random-walk diffusion equations are derived, then modified for correlation effects and for cases in which diffusion is enhanced by various driving

forces, such as atom- and vacancy-concentration gradients, electric fields, chemical-potential gradients, and temperature gradients. A description of how other driving forces such as stress gradients and physical accelerations can be incorporated into general equations for diffusion is presented.

Several papers have proposed modifications to Boltzmann–Matano solutions for cases of multicomponent diffusion systems in which volume change on mixing is significant[149,150] and in which a discontinuous diffusion profile occurs at the boundary of a moving interface.[151] An alternative method for predicting ternary diffusion interactions from solubility relations in systems involving two-phase equilibria has been suggested.[152] Three cases of two-phase equilibrium are discussed, and an example case using the Al–Si–Mg system is considered. Dayananda[153] has proposed a method for determining atomic mobilities of all components in multicomponent systems directly from a single diffusion couple, provided thermodynamic parameters are known. The method is based on an atomic-mobility model developed with diffusion fluxes referred directly to the composition of the Kirkendall interface and assumes that (1) the diffusion flux of each component at the interface is dependent only on its chemical-potential gradient; (2) the interface composition is constant, and the interface moves at a parabolic rate; (3) local equilibrium conditions prevail in the diffusion zone; and (4) the atomic mobilities are independent of concentration gradients. Tanzilli and Heckel[154] described a numerical method to solve the two-phase, diffusion-controlled, moving-interface problem involving finite boundaries. Solutions were obtained for planar, cylindrical, and spherical interfaces. The authors indicate that these results permit other investigators to estimate the behavior of similar two-phase diffusion systems.

A simplified method described[155] for measuring small diffusion coefficients (on the order of 10^{-12} cm/sec) by chemical sectioning permits fast and accurate determinations. In the experiments reported, radioactive silver ions were introduced into a crystal of pure AgBr from a radioactive silver nitrate solution. Successive layers of the crystal were dissolved, 2 to 5 μ at a time, onto a velvet cloth impregnated with a 0.1*M* solution of KCN. The residual activity in the crystal was measured with a scintillation counter.

Diffusion in Metallic Fuel Systems

Self-diffusion of plutonium in the epsilon phase was studied[156] using ^{240}Pu tracers. After diffusion annealing, layers of the welded couple were ground off, intensities were measured with a scintillation counter, and concentration–penetration curves were analyzed by the generalized Gruzin method. The diffusivity of plutonium in the epsilon phase was found to be 10^{-7} cm^2/sec between 500 and 620°C, and fitted the Arrhenius-type equation $D = 2 \times 10^{-2}$ exp $(-18{,}500/RT)$ cm^2/sec. Both the frequency factor and activation energy for self-diffusion are considered to be anomalously low and could not be traced to grain-boundary diffusion or surface diffusion.

Cerium diffusion was measured in couples of delta-stabilized Pu–Ce alloys[157] made by hot pressing together alloys containing 3.74 and 7.17 wt.% cerium, diffusion annealing at 403 to 528°C for 8 to 76 days, and analyzing by electron microprobe. Diffusivities were on the order of 10^{-11} cm^2/sec. The data followed the Arrhenius-type equation $D = 1.31 \times 10^{-2}$ exp $(-29{,}600/RT)$ cm^2/sec.

Diffusion of uranium in tungsten between 1760 and 2730°C was found[158] by mass-spectrometric analysis to follow the relation $D_{U-W} = 1.8 \times 10^{-2}$ exp $(-93{,}000/RT)$ cm^2/sec.

Diffusion in Refractory-Metal Systems

Self-diffusion studies[159] of niobium in its alloys with tungsten were reported in the Russian literature. The ^{95}Nb traces were incorporated on the alloy surfaces and diffusion annealed at 1600 to 2000°C for as long as it took to obtain diffusion zones 200 to 500 μ thick. Successive layers 5 to 10 μ thick were ground off, and the residual activity was determined. The authors found that small alloy contents (of tungsten) of about 5 wt.% increased the activation energy appreciably, from 113 to 310 kcal/gram atom, and increased the frequency factor from 28.12 to over 2300 cm^2/sec. These increases are discussed in terms of bond-strengthening processes and possible polarization of the internal orbits of niobium.

Diffusion of rhenium and molybdenum in tungsten and tungsten-base alloys was examined by Russian investigators.[160] For the W–Re study, tungsten and tungsten alloys were fabricated by casting, hot rolling, and annealing. After electrolytic deposition of ^{186}Re onto specimen surfaces, the specimens were diffusion annealed in purified argon at temperatures between 2000 and 2400°C for periods of 2 to 48 hr. Diffusion coefficients were determined by serial sectioning and measuring the integral activity of each section. The temperature dependence of diffusion of rhenium into polycrystalline tungsten was given by the equation

$D = 19.5$ exp $(-141{,}000/RT)$ cm^2/sec. Diffusion of rhenium into the tungsten alloy, W–27 Re–0.2 Ti, was described by the similar equation, $D = 9.2 \times 10^{-3}$ exp $(-94{,}000/RT)$ cm^2/sec.

The diffusivity of molybdenum was examined in single-crystal tungsten, in polycrystalline tungsten, and in W–Mo alloys ranging from W–5 Mo to W–55 Mo. The tracer, ^{99}Mo, was electrolytically deposited on the surfaces and diffusion annealed at the same conditions used to study the W–Re system. The temperature-dependent diffusivity of molybdenum into single-crystal tungsten was described by the equation $D = 5 \times 10^{-2}$ exp $(-121{,}000/RT)$ cm^2/sec and that into polycrystalline tungsten by the equation $D = 3.7 \times 10^{-3}$ exp $(-110{,}000/RT)$ cm^2/sec. Temperature-dependent equations for two of the five W–Mo alloy systems were given as D_{Mo} (in W–44 Mo) $= 1.7 \times 10^{-1}$ exp $(-107{,}000/RT)$ cm^2/sec, and D_{Mo} (in W–55 Mo) $= 1.2 \times 10^{-1}$ exp $(-103{,}000/RT)$ cm^2/sec. The effect of molybdenum concentration in the W–Mo alloy on diffusivity of ^{99}Mo at 1900°C is shown in Fig. III-32.

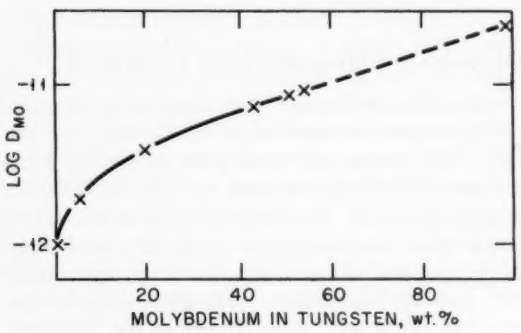

Fig. III-32 Diffusivity in the W–Mo system.[160]

In another Soviet study[161] the diffusivities of molybdenum and niobium in yttrium were determined at 1300°C to be, respectively, $D_{Mo-Y} \leqslant 1.8 \times 10^{-8}$ cm^2/sec and $D_{Nb-Y} \leqslant 1.4 \times 10^{-8}$ cm^2/sec.

Diffusion in Miscellaneous Metallic Systems

Using mass spectrometry, Schwegler[158] found that ruthenium diffuses in beta zirconium between 880 and 1030°C according to the relation $D = 8.8 \times 10^{-4}$ exp $(-36{,}700/RT)$ cm^2/sec. For ruthenium in alpha zirconium, diffusion followed the relation $D = 1.17 \times 10^{2}$ exp $(-61{,}000/RT)$ cm^2/sec between 760 and 863°C. However, after the Ru–Zr sample was cycled through the alpha–beta phase change, the diffusion equation became $D = 1.3 \times 10^{-2}$ exp $(-41{,}500/RT)$ cm^2/sec. Thin filaments of the solvent metals containing low concentrations of the solute material were used as ion sources in a mass spectrometer. The solute atoms evaporated from the filament as soon as they diffused to the surface. The ions thus accelerated were analyzed, and diffusion coefficients were calculated from ionic current rates. This method is limited in the temperature range in which measurements can be obtained.

For the diffusion of zirconium in yttrium, the Soviets[161] found that $D_{Zr-Y} = 4 \times 10^{-3}$ exp $(-38{,}000/RT)$ cm^2/sec between 1000 and 1300°C.

In a report concerned with the influence of surface films on the mechanical behavior of metals,[162] diffusion rates of copper and chromium into titanium and of copper into aluminum were determined. Thin films were evaporated onto substrates of titanium and aluminum, the titanium specimens were diffusion annealed at 1700°F (925°C) for 2 hr, and the aluminum specimens were diffused at 900°F (480°C) for 2 hr; the specimens were then examined by electron-microprobe analysis. Diffusivities for the various couples were calculated to be 3.9×10^{-9} cm^2/sec for Cu–Ti specimens, 8.9×10^{-9} cm^2/sec for Cr–Ti specimens, and 4.8×10^{-8} cm^2/sec for the Cu–Al specimens. In the Cu–Ti specimen, a Cu–Ti intermetallic compound was formed near the surface but was not identified. The diffusion of beryllium into iron and nickel has been investigated[163] at temperatures from 1100 to 1350°C for Be–Fe couples and from 1020 to 1400°C for the Be–Ni couples using ^{7}Be as the radioactive tracer. Diffusion of beryllium in iron was described by the Arrhenius-type equation $D_{Be-Fe} = 0.1$ exp $(-56{,}600/RT)$ cm^2/sec, and for beryllium into nickel the data followed the equation $D_{Be-Ni} = 0.019$ exp $(-46{,}200/RT)$ cm^2/sec.

A continuing program at Savannah River Laboratory to provide data for the design, fabrication, and operation of ^{60}Co heat sources includes studies of ^{60}Co diffusion into potential encapsulation material. Experiments were carried out[164] on Inconel 600 and on pure cobalt, each plated with ^{60}Co and heated at 1000°C for 100 hr. Two methods were used to measure activity profiles, one counting characteristic gamma radiations and the other counting the beta activity. Good agreement was obtained by the two methods, as shown in Table III-18. In the Inconel 600 samples, two specimens having two different grain sizes

Table III-18 Comparison of ^{60}Co Diffusion Coefficients at 1000°C Obtained by Two Counting Methods[164]

	400-channel analyzer		Beta–gamma counter	
	Diffusion coefficients, cm^2/sec		Diffusion coefficients, cm^2/sec	
Material	Volume	Grain boundary	Volume	Grain boundary
Inconel 600	1.3×10^{-11}	2.3×10^{-6}	1.5×10^{-11}	1.8×10^{-6}
Cobalt	1.4×10^{-11}	1.6×10^{-6}	1.9×10^{-11}	1.4×10^{-6}

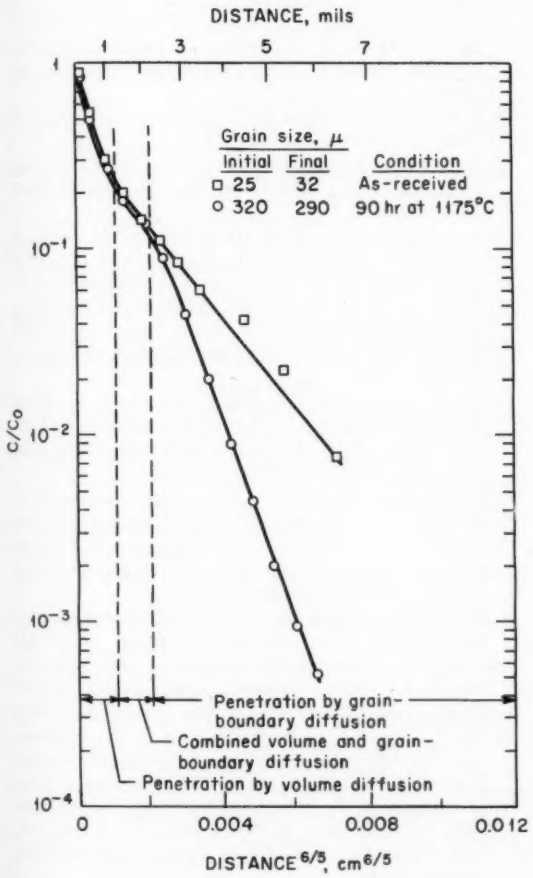

Fig. III-33 Effect of grain size[164] on diffusion of cobalt in Inconel 600. Diffusion anneal—100 hr at 1000°C.

(25 μ and 320 μ) were tested. The experiments showed that grain-boundary diffusion of ^{60}Co was more rapid in the smaller grained material, as illustrated in Fig. III-33. (A. N. Ashurst)

References

1. S. G. Young, Cavitation Damage of Stainless Steel, Nickel, and an Aluminum Alloy in Water for ASTM Round Robin Tests, Report NASA-TM-X-1670, National Aeronautics and Space Administration, Lewis Research Center, October 1968.
2. W. B. Cottrell, ORNL Nuclear Safety Research and Development Program, Bimonthly Report for July–August 1968, USAEC Report ORNL-TM-2368, Oak Ridge National Laboratory, November 1968.
3. G. V. Karpenko, V. I. Pokhmurs'kiy, V. G. Protsik, and S. I. Rusin, On the Corrosion of Metals in Freon, Report NASA-TT-F-11864 (N68-30221) [translated from *Dopov. Akad. Nauk Ukr. RSR, Ser. A*, No. 2: 178-180 (1968)].
4. C. V. Taylor and J. G. Goodwin, The Effect of Temperature and Time on Zircaloy Oxide Formation and Its Removal by Pickling, USAEC Report WAPD-TM-786, Westinghouse Electric Corporation, Bettis Atomic Power Laboratory, September 1968.
5. Atomic Energy of Canada Limited, unpublished, October 1968.
6. C. J. Rosa, Oxidation of Zirconium—A Critical Review of the Literature, *J. Less-Common Metals*, **16**(3): 173-201 (November 1968).
7. G. P. Marino, Hydrogen Behavior in Zirconium-Based Alloys (LWBR Development Program), USAEC Report WAPD-TM-759, Westinghouse Electric Corporation, Bettis Atomic Power Laboratory, June 1968.
8. Atomic Energy of Canada Limited, unpublished, July 1968.
9. F. H. Megerth (Comp.), Zircaloy-Clad UO_2 Fuel Rod Evaluation Program, Quarterly Progress Report No. 3, May–July 1968, USAEC Report GEAP-5667, General Electric Company, Nuclear Fuels Department, August 1968.
10. E. M. Hornsveld, Corrosion of Carbon Steel, Norwegian Report KR-127, May 1968.
11. E. R. Michaud and J. W. Seifert, Tube Bend Erosion Study, USAEC Report BAW-1280-53, The Babcock & Wilcox Co., June 24, 1968.
12. D. J. Duquette and H. H. Uhlig, Effect of Dissolved Oxygen and NaCl on Corrosion Fatigue of 0.18% Carbon Steel, *ASM (Amer. Soc. Metals), Trans. Quart.*, **61**(3): 449-456 (September 1968).
13. F. W. Cole, J. B. Padden, and A. R. Spencer, Oxidation

Resistant Materials for Transpiration Cooled Gas Turbine Blades. II, Wire Specimen Tests, Report NASA-CR-1184, The Bendix Corporation, September 1968.

14. J. S. Wolf and G. D. Sandrock, Some Observations Concerning the Oxidation of the Cobalt-Base Superalloy L-605 (HS-25), Report NASA-TN-D-4715 (N68-29954), National Aeronautics and Space Administration, Lewis Research Center, August 1968.
15. P. Kofstad and A. Z. Hed, Oxidation Behavior of Co–25 Cr and Co–35 Cr Alloys, Report NASA-CR-72420, Battelle–Columbus, June 4, 1968.
16. J. S. Sheasby, Oxidation of Niobium in the Temperature Range 450 to 720°C, *J. Electrochem Soc.*, **115**: 695-700 (July 1968).
17. H. Inouye, Interactions of Refractory Metals with Active Gases in Vacua and Inert Gas Environments, USAEC Report ORNL-4312, Oak Ridge National Laboratory, October 1968.
18. G. Geschwind, Oxidation of Refractory Metals, *Scr. Met.*, **2**: 519-524 (1968).
19. W. L. Acherman, J. P. Carter, and D. Schlain, Corrosion Properties of the TZM and Molybdenum-30 Tungsten Alloys, USAEC Report BM-RI-7169, Bureau of Mines, College Park Metallurgy Research Center, August 1968.
20. K. Friendrich, Oxidation of Molybdenum, Tungsten, and Rhenium Powders at Room Temperature in Air of Different Humidities, *J. Less-Common Metals*, **16**: 147-156 (1968).
21. J. Ferrante and G. C. Barton, Low-Energy Electron Diffraction Study of Oxygen Adsorption on Molybdenum (111) Face, Report NASA-TN-D-4735, National Aeronautics and Space Administration, Lewis Research Center, August 1968.
22. T. E. Madey and J. T. Yates, Jr., Desorption by Electron Impact: Oxygen Adsorbed on Tungsten, *Surface Sci.*, **11**: 327-351 (July 1968).
23. General Electric Company, Advanced Products Operation, Sodium Components Development Program, Mass Transfer Investigations in Liquid Metal Systems, Quarterly Progress Report No. 5, March–May 1968, USAEC Report GEAP-5648, pp. 36-37, 56-59, July 1968.
24. E. R. Astley, Fast Flux Test Facility, Quarterly Progress Report, April–June 1968, USAEC Report BNWL-880, (*a*) pp. 4.49-4.60, (*b*) p. 4.120, Battelle–Northwest, October 1968.
25. T. L. Hoffman, Corrosion Experience with Type 316 Stainless Steel in Sodium–Potassium Eutectic Alloy at 1400°F, USAEC Report IN-1185, Idaho Nuclear Corporation, October 1968.
26. H. U. Borgstedt, Study of the Transfer of Carbon Through Molten Sodium from Unstabilized to Stabilized Austenitic Stainless Steel (in German), *Corros. Sci.*, **8**: 405-412 (June 1968).
27. A. F. Brown and D. J. Hayes, Observations on the Decarburisation and Graphitisation of Steels by Sodium, *J. Nucl. Mater.*, **27**: 187-193 (1968).
28. Argonne National Laboratory, Reactor Development Program Progress Report, October 1968, USAEC Report ANL-7513, (*a*) pp. 124-126, (*b*) pp. 91-92, Nov. 27, 1968.
29. General Electric Company, Advanced Products Operation, Sodium-Cooled Reactors, Fast Ceramic Reactor Development Program, Twenty-Sixth Quarterly Report, January–April 1968, USAEC Report GEAP-5631, pp. 96-99, June 1968.
30. F. B. Litton and J. H. Bender, Removal of the Sodium Bond from Sintered (U,Pu)C Pellets, *Nucl. Appl.*, **5**: 299-301 (November 1968).
31. R. L. Eichelberger, The Solubility of Oxygen in Liquid Sodium: A Recommended Expression, USAEC Report AI-AEC-12685, Atomics International, Nov. 1, 1968.
32. G. J. Lamprecht and P. Crowther, Solubility of Metals in Liquid Sodium: The Systems Sodium–Silver, Sodium–Zinc, and Sodium–Cerium, *Trans. Met. Soc. AIME*, **242**: 2169-2171 (October 1968).
33. P. Patriarca and W. O. Harms (Comps.), Fuels and Materials Development Program Quarterly Progress Report for Period Ending June 30, 1968, USAEC Report ORNL-4330, (*a*) pp. 78-82, (*b*) pp. 104-110, (*c*) pp. 141-142, (*d*) pp. 142-146, (*e*) pp. 286-294, Oak Ridge National Laboratory, Metals and Ceramics Division, November 1968.
34. E. M. Simons, Corrosion by Nonaqueous Liquids, *Reactor Mater.*, **11**(3): 169 (Fall 1968).
35. G. M. Loiacono and B. Michelman, Growth and Properties of $K_4Nb_6O_{17}$, *J. Amer. Ceram. Soc.*, **51**: 542-543 (Sept. 21, 1968).
36. V. J. Tennery and K. W. Hang, Heats of Transition in $NaNbO_3$, *J. Amer. Ceram. Soc.*, **51**: 469 (Aug. 21, 1968).
37. D. H. Jansen, J. H. DeVan, C. W. Cunningham, L. C. Fuller, and R. E. MacPherson, Niobium–1% Zirconium Boiling-Potassium Forced-Circulation Loop Test, USAEC Report ORNL-4301, Oak Ridge National Laboratory, December 1968.
38. W. F. Brehm, Jr., J. L. Gregg, and Che-uy Li, Grain Boundary Penetration of Niobium (Columbium) by Lithium, *Trans. Met. Soc. AIME*, **242**: 1205-1210 (July 1968); also USAEC Report NYO-3228-12.
39. C. E. Johnson, Fast Reactor Systems for Space Power, in Proceedings of the National Topical Meeting on Fast Reactor Systems, Materials, and Components, Cincinnati, Ohio, April 2–4, 1968, pp. 41-60, USAEC Report CONF-680419, American Nuclear Society.
40. Gulf General Atomic, Inc., Research and Development on Fission-Heated Thermionic Cells for Application to Nuclear Space Power Systems (unclassified title), Summary Report for Period October 1, 1967–June 30, 1968, USAEC Report GA-8924, p. 5, Aug. 2, 1968. (Classified)
41. Yu. F. Bychkov, I. D. Laptev, and A. N. Rozanov, Corrosive Influence of Diphenyl on Metals and Oxides, Report FTD-MT-66-23 (AD-670944) (translated from Investigation of the Application of Organic Heat-Transfer Media as Moderators in Power Reactors, pp. 151-163, State Committee for the Use of Atomic Energy of USSR, Moscow, 1964).
42. J. C. Hesson, J. L. Anderson, and R. O. Ivins, Chemloc-II: A Computer Program Describing the Core Heating and Cladding-Steam Reaction for a Water-Cooled Power Reactor Following a Loss of Coolant, USAEC Report ANL-7361, Argonne National Laboratory, April 1968.
43. Argonne National Laboratory, Reactor Development Program Progress Report, September 1968, USAEC Report ANL-7500, (*a*) pp. 131-133, (*b*) p. 100, Oct. 29, 1968.
44. J. J. Holmes, Tensile Properties of 25% Cold-Worked and

Annealed Austenitic Stainless Steels After Fast Reactor Irradiation, *Trans. Amer. Nucl. Soc.*, **11**(2): 484-485 (November 1968).

45. H. Böhm and H. Hauck, Investigation of the Influence of Cold-Working and Thermomechanical Treatment on the Radiation-Induced, High Temperature Embrittlement of Austenitic Steels, *Trans. Amer. Nucl. Soc.*, **11**(2): 482 (November 1968).
46. Argonne National Laboratory, Reactor Development Program Progress Report, July 1968, USAEC Report ANL-7478, pp. 56-57, Aug. 28, 1968.
47. H. J. Laue, H. Böhm, and H. Hauk, Multiaxial In-Reactor Stress-Rupture Strength of Stainless Steels and a Nickel Alloy, German Report KFK-814, August 1968.
48. General Electric Company, Missile and Space Division, AEC Fuels and Materials Development Program Progress Report No. 74, USAEC Report GEMP-1006, pp. 37-40, June 29, 1968.
49. H. Busboom, W. Kimball, A. Withop, and F. Comprelli, A Technique for Measurement of Circumferential Ductility of Irradiated Tubing, *Trans. Amer. Nucl. Soc.*, **11**(2): 483-484 (November 1968).
50. Atomics International, AEC Unclassified Programs. Quarterly Technical Progress Report, January–March 1968, USAEC Report AI-AEC-12680, pp. 127-131.
51. J. J. Holmes and H. R. Brager, Fast Reactor-Induced Swelling by Void Formation in Type 304L Stainless Steel, *Trans. Amer. Nucl. Soc.*, **11**(2): 479 (November 1968).
52. T. Lauritzen, G. Ferguson, L. Seacrist, and F. Comprelli, Density Changes in Several Austenitic Stainless Steels After Irradiation in EBR-II, *Trans. Amer. Nucl. Soc.*, **11**(2): 479-480 (November 1968).
53. H. R. Brager and R. E. Robbins, Stabilized Cavities in Irradiated Austenitic Stainless Steel, *Trans. Met. Soc. AIME*, **242**(9): 2010-2011 (September 1968).
54. H. R. Brager, R. E. Robbins, and G. L. Kulcinski, Anomalous Behavior of Bubbles in AISI Type 304 Stainless Steel Irradiated in the ETR, *Trans. Amer. Nucl. Soc.*, **11**(2): 502-503 (November 1968).
55. L. Ljungberg, Transmutations in Fast Reactor Cladding and an Experiment To Simulate Their Effects in an Incoloy 800 Type of Alloy, Swedish Report S-384, 1968.
56. K. Veevers and W. B. Rotsey, Effect of Irradiation on Strain Aging in Annealed Zircaloy-2, *J. Nucl. Mater.*, **27**: 108-111 (July 1968).
57. J. J. Cadwell, D. R. deHalas, R. E. Nightingale, and D. C. Worlton, Battelle–Northwest, unpublished, August 1968.
58. S. Peterson (Comp. and Ed.), Metals and Ceramics Division Annual Progress Report for Period Ending June 30, 1968, USAEC Report ORNL-4370, (*a*) p. 118, (*b*) pp. 238-239, (*c*) pp. 60-61, Oak Ridge National Laboratory, October 1968.
59. C. L. Younger and G. N. Wright, Effect of 10^{20} Neutron-per-Square-Centimeter Irradiation on Embrittlement of Polycrystalline Tungsten, Report NASA-TN-D-4661 (N68-28818), National Aeronautics and Space Administration, Lewis Research Center, July 1968.
60. L. E. Steel, J. R. Hawthorne, C. Z. Serpan, Jr., and U. Polapous, Irradiation Effects on Reactor Structural Materials, Quarterly Progress Report, February 1–April 30, 1968, Report NRL-Memo-1872, Naval Research Laboratory, May 15, 1968.
61. C. Z. Serpan, Jr., Notch Ductility and Tensile Property Evaluation of the PM-2A Reactor Pressure Vessel, Report NRL-6739, Naval Research Laboratory, Apr. 22, 1968.
62. S. M. Ohr, Work Hardening Characteristics of Neutron Irradiated Iron, *Scr. Met.*, **2**: 213-216 (April 1968).
63. A. S. Sastri and D. G. Walker, The Effect of Fast Neutron Irradiation on the Tempering of Plain-Carbon Steels, *J. Aust. Inst. Metals*, **13**(3): 163-168 (August 1968).
64. L. E. Katz, H. Herman, and A. C. Damask, Precipitation in Neutron-Irradiated Aluminum-Base Copper, *Acta Met.*, **16**: 939-945 (July 1968).
65. H. Kissinger, Unit Cell and Dimensional Changes in Irradiated Single-Crystal Rhenium, *Phil. Mag.*, **17**: 871-873 (April 1968).
66. G. L. Kulcinski, The Effect of Hydrostatic Pressure on the Recovery of Electrical Properties of Irradiated Molybdenum, USAEC Report BNWL-844, Battelle–Northwest, July 1968.
67. G. L. Kulcinski and H. E. Kissinger, The Effect of Hydrostatic Pressure on the Recovery of Unit Cell Dimensions in Irradiated Molybdenum, USAEC Report BNWL-845, Battelle–Northwest, August 1968.
68. G. L. Kulcinski and B. Mastel, Hydrostatic Pressure Induced Annealing of Defect Clusters in Irradiated Molybdenum, USAEC Report BNWL-846, Battelle–Northwest, September 1968.
69. G. L. Kulcinski, The Effect of Hydrostatic Pressure on the Recovery of Irradiation Induced Hardness in Molybdenum, USAEC Report BNWL-847, Battelle–Northwest, September 1968.
70. M. J. Makin, Electron Displacement Damage in Copper and Aluminum in a High-Voltage Electron Microscope, British Report AERE-R-5821, July 1968.
71. M. Ruehle, Electron Microscopy of Small Defect Clusters in Irradiated Metals. II. Investigations on Neutron- and Ion-Irradiated Copper and Neutron-Irradiated Nickel, British Report AERE-Trans-1087 [translated from *Phys. Status Solidi*, **19**: 279-295 (1967)].
72. B. Mastel and J. L. Brimhall, Development of Voids in Nickel During Irradiation, USAEC Report BNWL-SA-1768 (Rev.), Battelle–Northwest, Aug. 20, 1968.
73. R. C. Rau, R. L. Ladd, and J. Moteff, Radiation Damage in Vanadium, USAEC Report GEMP-612, General Electric Company, Missile and Space Division, September 1968.
74. J. D. Elen, Direct Observation of Damage in Neutron Irradiated Vanadium, Dutch Report RCN-96, December 1967.
75. G. P. Seidel, The Effect of Neutron Irradiation on the Plastic Deformation of Single Crystals of Iron with Different Carbon Content. I. The Yield Stress at the Beginning of Deformation, USAEC Report ORNL-tr-1932 [translated from *Phys. Status Solidi*, **25**: 175-188 (1968)].
76. G. E. Russcher, Calculations of Vacancy Cluster Production in Iron for EBR-II, DFR, FTR, and ETR, USAEC Report BNWL-819, Battelle–Northwest, September 1968.
77. H. Kellerer and G. Piatti, The Time/Temperature Dependence of the Hardness of Dispersion-Strengthened Aluminum Alloys, *J. Nucl. Mater.*, **27**: 245-256 (1968).

78. D. Gualandi, D. Gelli, P. Jehenson, L. Mori, and M. Paganelli, Dispersion Strengthened Aluminum for Nuclear Purposes, with Particular Emphasis on Correlation Between Creep Strength and Microstructure Parameters, Report EUR-4035*e*, June 20, 1968.
79. J. T. Blucher, P. Knudsen, and N. J. Grant, Effect of Strain Rate and Temperature at High Strains on Fatigue Behavior of SAP Alloys, *Trans. Met. Soc. AIME*, **242**: 1605-1611 (August 1968).
80. W. Engelmaier, Fatigue Behavior and Crack Propagation in 2024-T3 Aluminum Alloy in Ultrahigh Vacuum and Air, *Trans. Met. Soc. AIME*, **242**: 1713-1718 (August 1968).
81. H. E. Evans, The Mechanism of Void Growth and Factors Affecting the Onset of Intergranular Failure During Creep of Magnox Al80, British Report RD/B/N-1009, February 1968.
82. P. Bowring, P. W. Davies, and B. Wilshire, The Strain-Dependence of Density Changes During Creep, *Metal Sci. J.*, **2**: 168-171 (September 1968).
83. J. Hull and H. Conrad, Thermally Activated Deformation of Alpha Zirconium and Alpha Zircaloy, LWBR–LSBR Development Program, USAEC Report TID-24570, Franklin Institute Research Laboratories, August 1967.
84. D. Mills and G. B. Craig, The Plastic Deformation of Zirconium–Oxygen Alloy Single Crystals in the Range 77 to 950°K, *Trans. Met. Soc. AIME*, **242**: 1881-1890 (September 1968).
85. D. H. Baldwin and R. Reed-Hill, Some Effects of Oxygen on the Tensile Deformation of Polycrystalline Zirconium, *Trans. Met. Soc. AIME*, **242**: 661-669 (April 1968).
86. W. R. Tyson and G. B. Craig, Deformation of Zr–N Alloys, *Can. Met. Quart.*, **7**(3): 119-126 (July–September 1968).
87. Y. Mishima, S. Tshino, and S. Nakajima, A Resistometric Study of the Solution and Precipitation of Hydrides in Unalloyed Zirconium, *J. Nucl. Mater.*, **27**: 335-344 (1968).
88. R. P. Marshall, Directional Strain and Hydride Orientation in Zircaloy, USAEC Report DP-1138, Savannah River Laboratory, October 1968.
89. I. A. El-Shanshoury, I. M. Voronin, V. A. Rudenko, and M. N. Bassin, The Effect of Hydrogen and Extension Rates on the Mechanical Properties of Zr–1% Nb Alloy Over the Temperature Range of 30 to 600°C, *J. Nucl. Mater.*, **27**: 102-107 (July 1968).
90. T. E. Michaels, Acoustic Emission of Zircaloy-2 During Tensile and Fatigue Loading, USAEC Report BNWL-727, Battelle–Northwest, August 1968.
91. Zirconium Based Materials to be Utilized in Nuclear Reactors, French Patent 1,448,044, Apr. 9, 1965.
92. G. F. Slattery, The Effect of Cooling Rate on the Beta–Alpha Transformation in the Zr/2 At.% Cr/0.16 At.% Fe Alloy, British Report TRG-Report-1683(S), 1967.
93. B. J. S. Wilkins, J. Chater, and A. R. Reich, The Internal Oxidation of Zirconium–Yttrium Alloys, Canadian Report AECL-2717, August 1968.
94. G. E. Lien (Ed.), *Behavior of Superheater Alloys in High Temperature, High Pressure Steam*, American Society of Mechanical Engineers, 1968.
95. L. K. Singhal and J. W. Martin, The Growth of $M_{23}C_6$ Carbide on Grain Boundaries in an Austenitic Stainless Steel, *Trans. Met. Soc. AIME*, **242**: 814-819 (May 1968).
96. J. F. Eckel and T. B. Cox, Temperature Dependence of the Solid Solubility of Nitrogen in AISI Type 304 Stainless Steel, *J. Mater.*, **3**(3): 605-613 (September 1968).
97. R. R. Benson, Jr., R. K. Dann, and L. W. Roberts, Jr., Hydrogen Embrittlement of Stainless Steel, *Trans. Met. Soc. AIME*, **242**: 2199-2205 (October 1968).
98. R. V. Hart and H. Gayter, Recovery of Mechanical Properties in Nickel Alloys by Reheat-Treatment, *J. Inst. Metals*, **96**: 338-344 (October 1968).
99. G. P. Sullivan, G. A. Webster, and B. J. Piearcey, The Effect of Stress Cycling on the Creep Behavior of a Wrought Nickel-Base Alloy at 955°C, *J. Inst. Metals*, **96**: 274-281 (September 1968).
100. G. H. Karchner and E. T. Stephenson, A Microstructural Study of the Role of Vanadium in Decreasing the Toughness of 0.5% Mo–B Steels, *ASM (Amer. Soc. Metals), Trans. Quart.*, **61**: 457-467 (September 1968).
101. B. M. Kapadia, R. M. Brown, and W. J. Murphy, The Influence of Nitrogen, Titanium, and Zirconium on the Boron Hardenability Effect in Constructional Alloy Steels, *Trans. Met. Soc. AIME*, **242**: 1689-1694 (August 1968).
102. R. L. Stephenson, The Creep-Rupture Properties of Some Refractory Metal Alloys, *J. Less-Common Metals*, **15**(4): 395-424 (August 1968).
103. J. C. Sawyer and E. A. Steigerwald, Generation of Long-Time Creep Data of Refractory Alloys at Elevated Temperatures, Report NASA-CR-93193, TRW Equipment Laboratories, June 6, 1967.
104. J. C. Sawyer and K. D. Sheffler, Generation of Long-Time Creep Data on Refractory Alloys at Elevated Temperatures, Report NASA-CR-72319, TRW Equipment Laboratories, Aug. 1, 1967.
105. K. D. Sheffler and E. A. Steigerwald, Generation of Long-Time Creep Data on Refractory Alloys at Elevated Temperatures, Report NASA-CR-72391, TRW Equipment Laboratories, Dec. 14, 1967.
106. P. L. Raffo, Yielding and Fracture in Tungsten–Rhenium Alloys, Report NASA-TN-D-4567, National Aeronautics and Space Administration, Lewis Research Center, May 1968.
107. M. Garfinkle, Superplasticity in Tungsten–Rhenium Alloys, Report NASA-TN-D-4728, National Aeronautics and Space Administration, Lewis Research Center, August 1968.
108. R. G. Nelson and D. P. O'Keefe, Study of Tungsten–Technetium Alloys, USAEC Report BNWL-865, Battelle–Northwest, September 1968.
109. L. S. Rubenstein, Effects of Composition and Heat Treatment on High-Temperature Strength of Arc-Melted Tungsten–Hafnium–Carbon Alloys, Report NASA-TN-D-4379, National Aeronautics and Space Administration, Lewis Research Center, February 1968.
110. A. Milner, Tensile Evaluation of Unworked Tungsten–25 Percent Rhenium Alloys Consolidated by Sintering Elemental Powders, *Powder Met.*, **11**: 56-62 (Spring 1968).
111. E. Fromm, Thermodynamic Analysis of the Solid Solution of Carbon, Nitrogen, and Oxygen in Niobium and

Tantalum, *J. Less-Common Metals*, **14**(1): 113-125 (January 1968); also ORNL-TR-1942.

112. H. Böhm and M. Schirra, Creep and Stress Rupture Behavior of Vanadium–Titanium and Vanadium–Titanium–Niobium Alloys, *Z. Metallk.*, **59**: 715-723 (September 1968).
113. C. R. Manning, Jr., and R. F. Stoops, High-Temperature Cermets I. Compatibility, *J. Amer. Ceram. Soc.*, **51**: 411-415 (Aug. 21, 1968).
114. C. R. Manning, Jr., and R. F. Stoops, High-Temperature Cermets II. Wetting and Fabrication, *J. Amer. Ceram. Soc.*, **51**: 415-419 (Aug. 21, 1968).
115. E. Neuenschwander, Preparation and Characterization of Ultrafine Carbides, Nitrides, and Metals, *J. Less-Common Metals*, **11**: 365-375 (1966).
116. R. G. Shumilova and R. Ya. Kosalapova, Obtaining Zirconium Carbide on a Semi-Industrial Scale, *Porosh. Met., Akad. Nauk Ukr. SSR*, No. 4: 86-89 (April 1968).
117. G. I. Zakharova, N. G. Kalinina, and V. S. Neshpor, Investigation of Conditions for Obtaining the Spherical Granules of Tungsten Carbide, *Porosh. Met., Akad. Nauk Ukr. SSR*, No. 5: 1-5 (May 1968).
118. G. V. Samsonov, V. K. Vitryanyuk, and P. D. Sysov, Obtaining High-Porous Materials from Titanium and Zirconium Carbides, *Porosh. Met., Akad. Nauk Ukr. SSR*, No. 4: 22-28 (April 1968).
119. G. Jangg, R. Kieffer, and L. Usner, Production of Mixed Carbides by Auxiliary Metal Bath, *J. Less-Common Metals*, **14**: 269-277 (March 1968).
120. G. A. Meerson and A. E. Gorbunov, Activated Sintering of Zirconium Boride, *Izv. Akad. Nauk SSSR, Neorg. Mater.*, **4**: 320-324 (March 1968).
121. P. Peshev, L. Leyarovska, and G. Bliznakov, Borothermic Preparation of Some Vanadium, Niobium, and Tantalum Borides, *J. Less-Common Metals*, **15**: 259-267 (July 1968).
122. L. Lecrivain and G. Provost, Properties of Plasma-Sprayed Borides and Nitrides, *Ber. Deut. Keram. Ges.*, **45**: 347-351 (July 1968).
123. O. Matsumoto and Y. Hayakawa, Preparation of Tantalum Nitride by Means of Nitrogen Plasma Jet, USAEC Report MLM-1475(tr) [translated from *Denki Kagaku*, **34**: 775-779 (1966)].
124. R. Kieffer, H. Nowotny, A. Neckel, P. Ettmayer, and L. Usner, Miscibility of Cubic Multicomponent Carbides, *Monatsh. Chem.*, **99**: 1020-1027 (May–June 1968).
125. P. Ettmayer, R. Kieffer, and L. Usner, Phase Diagrams of the Systems VC–ZrC and VC–HfC, *Planseeber. Pulvermet*, **16**: 108-113 (July 1968).
126. E. Rudy, C. E. Brukl, and S. Windisch, Constitution of Ternary Ta–Mo–C Alloys, *J. Amer. Ceram. Soc.*, **51**: 239-250 (May 21, 1968).
127. E. Rudy, C. E. Brukl, and S. Windisch, Constitution of Niobium–Molybdenum–Carbon Alloys, *Trans. Met. Soc. AIME*, **239**: 1796-1808 (November 1967).
128. T. F. Federov, N. M. Popova, L. V. Gorshkova, L. V. Skolozdra, and Yu. B. Kuzma, The Phase Equilibria in the Systems of Vanadium–Chromium–Carbon, Niobium–Chromium–Carbon and Tantalum–Chromium–Carbon, *Porosh. Met., Akad. Nauk Ukr. SSR*, No. 3: 42-48 (March 1968).
129. *Thermodynamics of Nuclear Materials*, Symposium Proceedings, Vienna, 1967, International Atomic Energy Agency Vienna, 1968 (STI/PUB/162).
    a. A. A. Babad-Zakhryapin, L. M. Gert, and V. D. Rogozin, Phase Formation Accompanying the Interaction of Transition Metals with Carbon in Thin Layers, pp. 427-434.
    b. V. I. Alekseev, Thermodynamic Properties of Non-Stoichiometric Vanadium and Titanium Carbides, pp. 435-447.
    c. R. A. Andrievskii, V. N. Zagryazkin, and R. A. Lyutikov, Calculation of Configurational and Excess Entropies in Metal Carbide Solution Transition, pp. 449-456.
130. I. N. Danisina, Yu. N. Vil'k, R. G. Avarbe, Yu. A. Omel'chenko, and T. P. Ryzhkova, Constitution Diagram for the Zirconium–ZrN–ZrC System, *Zh. Prikl. Khim.*, **41**: 492-500 (March 1968).
131. W. S. Telegus and Yu. B. Kuz'ma, Phase Equilibria in the Systems of W–Cr–B and W–Mo–B, *Porosh. Met., Akad. Nauk Ukr. SSR*, No. 2: 68-75 (February 1968).
132. A. S. Sobolev, Yu. B. Kuz'ma, T. E. Soboleva, and T. F. Federov, Phase Equilibria in the Systems Tantalum–Titanium–Boron and Tantalum–Molybdenum–Boron, *Porosh. Met., Akad. Nauk Ukr. SSR*, No. 1: 62-67 (January 1968).
133. A. G. Turchanin and V. V. Fesenko, Enthalpy and Heat Capacity of Zirconium Carbide in the Homogeneity Domain over the Temperature Range 1300 to 2500°K, *Porosh. Met., Akad. Nauk Ukr. SSR*, No. 1: 88-90 (January 1968).
134. Y. A. Chang, Thermal Properties of Tantalum Monocarbide and Tungsten Monocarbide, *Trans. Met. Soc. AIME*, **239**: 1685-1691 (November 1967).
135. A. Hivert and J. Poulignier, Mechanical Properties at High Temperatures of Some Ultrarefractory Carbides, *Rev. Int. Hautes Temp. Refract.*, **5**: 55-61 (January–March 1968).
136. W. F. Brizes, Mechanical Properties of the Group IVB and VB Transition Metal Monocarbides, Report NASA-CR-95887 (N68-30720), University of Pittsburgh, July 11, 1968.
137. V. V. Ogorodnikov, M. S. Koval'chenko, A. G. Krainii, and A. P. Epik, Neutron Irradiation Effects on Diffusion Carbide and Boride Coatings on High-Melting Metals, *Fiz.-Khim. Mekh. Mater.*, **4**: 36-38 (1968).
138. R. J. Price, Structure and Properties of Pyrolytic Silicon Carbide, USAEC Report GA-8883, Gulf General Atomic Incorporated, Oct. 22, 1968.
139. D. R. Lankard, D. L. Birkimer, F. F. Fondriest, and M. J. Snyder, The Effects of Moisture Content on the Constitution and Structural Properties of Portland Cement Concrete Exposed to Temperatures up to 500°F, preprint of paper presented at the 1968 Fall Convention, American Concrete Institute, Memphis, Tenn., Nov. 3–8, 1968.
140. W. H. Rhodes, D. J. Sellers, R. M. Cannon, A. H. Heuer, W. R. Mitchell, and P. Burnett, Microstructure Studies of Polycrystalline Refractory Oxide, Report AVSSD-0098-68-RR, AVCO Corporation, May 1968.
141. R. E. Johnson and A. Muan, Phase Diagrams for the Systems Si–O and Cr–O, *J. Amer. Ceram. Soc.*, **51**(8): 430-433 (August 1968).
142. K. R. Janowski and R. C. Rossi, Mechanical Degradation

of MgO by Water Vapor, *J. Amer. Ceram. Soc.*, **51**(8): 453-455 (August 1968).

143. E. V. Clougherty, D. Kalish, and E. T. Peters, Research and Development of Refractory Oxidation Resistant Diborides, Report AFML-TR-68-190, ManLabs, Inc., July 1968.
144. E. V. Clougherty, R. L. Pober, and L. Kaufman, Synthesis of Oxidation Resistant Metal Diboride Composites, *Trans. Met. Soc. AIME*, **242**: 1077-1082 (June 1968).
145. G. Cevales, Phase-Equilibrium Diagram of Al_2O_3–ZrO_2 and Examination of a New Phase 99 Percent Al_2O_3–1 Percent ZrO_2 (e Alumina), *Ber. Deut. Keram. Ges.*, **45**: 216-219 (May 1968).
146. Oak Ridge National Laboratory, Groups IV, V, and VI Transition Metals. Supplement No. 1. Selected References on Preparation, Structure, Physical Properties, Metallography, and Transport Properties, USAEC Report ORNL-RMIC-8, 1967.
147. J. Furnish (Comp.), Solid State Diffusion of Gold and Silver: A Literature Search, USAEC Report LA-3806, Los Alamos Scientific Laboratory, Sept. 5, 1967.
148. J. R. Manning, *Diffusion Kinetics for Atoms in Crystal*, D. Van Nostrand Co., Inc., Princeton, N. J., 1968.
149. M. A. Dayananda, A Practical Coordinate for Multicomponent Diffusion, *Scr. Met.*, **2**(2): 117-120 (February 1968).
150. J. J. van der Broek, Determination of Ternary Diffusion Coefficients, *Scr. Met.*, **2**(10): 561-564 (October 1968).
151. M. Appel, Solution for Fick's Second Law with Variable Diffusivity in a Multiphase System, *Scr. Met.*, **2**(4): 217-222 (April 1968).
152. R. C. Doward, Predicting Ternary Diffusion Interactions from Solubility Relationships, *Trans. Met. Soc. AIME*, **242**: 1470-1472 (July 1968).
153. M. A. Dayananda, Atomic Mobilities in Multicomponent Diffusion and Their Determination, *Trans. Met. Soc. AIME*, **242**: 1369-1372 (July 1968).
154. R. A. Tanzilli and R. W. Heckel, Numerical Solutions to the Finite, Diffusion-Controlled, Two-Phase, Moving-Interface Problem (with Planar, Cylindrical, and Spherical Interfaces), *Trans. Met. Soc. AIME*, **242**: 2313-2321 (November 1968).
155. R. F. Steiger and T. R. Steel, A Chemical Sectioning Method for the Measurement of Small Diffusion Coefficients in Solids, USAEC Report UCRL-18345, University of California, Lawrence Radiation Laboratory, July 1968.
156. M. Dupuy and D. Calais, Self-Diffusion in Plutonium Epsilon Phase (BCC), *Trans. Met. Soc. AIME*, **242**: 1679-1683 (August 1968).
157. M. R. Harvey, A. L. Rafalski, and D. H. Riefenberg, Cerium Diffusion in Delta Stabilized Pu–Ce Alloys, *ASM (Amer. Soc. Metals), Trans. Quart.*, **61**: 629-631 (September 1968).
158. E. C. Schwegler, Jr., Mass Spectrometric Measurement of the Diffusion of Uranium in Tungsten at High Temperatures, Thesis, Rensselaer Polytechnic Institute, 1967.
159. V. D. Lyubimov, P. V. Gel'd, G. P. Shveybin, and Yu. A. Sutina, Self-Diffusion of Niobium in Its Alloys with Tungsten, *Russian Met. (Engl. Transl.)*, No. 2: 40-43 (1967).
160. V. E. Lashkarev (Ed.), Diffusion of Rhenium and Molybdenum in Tungsten and Tungsten-Based Alloys, USAEC Translation AEC-tr-6869/6 [from *Ukr. Fiz. Zh.*, **12**(6): 973-977 (June 1967)].
161. V. D. Rogozin, L. M. Gert, and A. A. Babad-Zakhryapin, Diffusion of Zirconium, Molybdenum, and Niobium in Metallic Yttrium at Temperatures of 1000 to 1300°C (in Russian), *Izv. Akad. Nauk SSSR, Metal.*, No. 3: 228-231 (May–June 1968).
162. I. R. Kramer, Study of the Influence of Solid Films on the Mechanical Behavior of Metals, Report MCR-67-398 (Issue 5), Martin Marietta Corporation, July 30, 1968.
163. G. V. Grigor'ev and L. V. Pavlinov, Diffusion of Beryllium into Iron and Nickel, *Fiz. Metal. Metalloved.*, **25**: 836-839 (May 1968).
164. H. S. Hilborn (Comp.), Savannah River Laboratory Isotopic Power and Heat Sources. Part I. ^{60}Co, Quarterly Progress Report, April–June 1968, USAEC Report DP-1169-1, Savannah River Laboratory, July 1968.

Section
IV
Reactor Materials

Special Fabrication Techniques

Melting, Casting, and Fabrication of Cast Structures

Atomics International[1] has prepared and characterized fuel samples for tests of radiation-induced swelling in tungsten-doped uranium monocarbide. Details are given on the arc melting and casting and the zone-melting processes used to prepare the 0.33-in.-diameter fuel slugs. Tungsten was added, and the carbon-to-metal (uranium + tungsten) stoichiometry was controlled by a zone-leveling procedure. The purpose of the tungsten addition was to provide a dispersion of very fine particles to trap fission-gas bubbles and limit swelling. Electron micrographs are presented which show the presence of fine particles. The unirradiated fuel samples have been further characterized by chemical analysis, optical metallography, length measurement, and density determination.

The French[2] have produced a nuclear fuel with improved chemical-corrosion resistance, thermal conductivity equal to that of uranium, and mechanical properties superior to those of UC or USi, by arc melting a stoichiometric or reaction-balanced mixture of USi and UC under an inert gas at approximately 25 volts and 600 amp. The fused mass is placed in a mold, arc melted for about 1 min at 1000 amp, and drop cast. The product is a nonequilibrium phase that, upon being heat-treated at approximately 1650°C for 50 to 100 hr, is stated to have the composition $U_3C_3Si_2$.

Fuel rods of Al–10 Pu* alloy were fabricated by an injection casting process and encapsulated in Zircaloy-2 tubing at Battelle–Northwest.[3] Casting was accomplished by inserting one end of a 0.610-in.-ID by 42-in.-long pyrex-glass mold into the molten alloy and then evacuating the mold. The diameter of the cast rods was 0.600 ± 0.001 in., with an average length of 38 in. Each element contained two or more of the fuel rods, totaling 47.75 in. in length. Unheated pyrex molds produced higher quality castings than unheated mild-steel molds, heated pyrex-glass molds, or heated mild-steel molds. The melt homogeneity was improved significantly by changing from intermittent melt stirring to continuous melt stirring prior to casting.

The Japanese[4] have examined the metallographic features of the cast structures of electron-beam-melted niobium-alloy ingots by microscopic observation, autoradiograph, X-ray microanalysis, and X-ray-diffraction analysis. Contrary to expectations, the cast structure of the ingots consisted of equiaxed grains, and the beta solid solution was retained at room temperature. Microsegregation of zirconium was noticed at grain boundaries and inside the equiaxed grains, forming a subgrain boundary-like structure. According to X-ray microanalysis the estimated zirconium concentration of the segregated zone was nearly equal to the zirconium concentration of the final liquid in the freezing process of the alloys. Zirconium was also concentrated macroscopically at the outer surface of the ingot, showing sharp inverse segregation. This inverse segregation was attributed principally to the effect of outgassing pressure on the zirconium-rich melt in the freezing transient layer.

Marked differences in room-temperature ductility between electron-beam-melted ingots of Nb–Zr (NZ) alloy and Nb–Zr–Ti (NZT) alloy were observed.[5] That is, the NZ alloy fractured in a brittle manner at room temperature, unlike the ductile-fracture behavior of the NZT alloy ingot, and repeated twin formation was noticed for only the NZT alloy ingot during tensile tests. The Charpy-impact-test transition temperature of the NZ alloy ingot was about 250°C, which is 250 to 330°C higher than that of the NZT alloy ingot. The room-temperature ductility of the Nb–Zr alloy ingot was influenced strongly by the zirconium concentration, and an abnormal brittle fracture was observed for only the Nb–30 Zr alloy ingot. There was no good

*Unless otherwise designated, all compositions are understood to be by weight percent.

correlation between the oxygen content and the ingot ductility.

An electron-beam zone refiner was developed at Oak Ridge[6] to produce high-purity zirconium and other refractory metals for use in high-field galvanomagnetic studies. A quadrupole gas analyzer was used to monitor the gas composition over various metals during zoning. Resistance ratios ($R_{300°K}/R_{4.2°K}$) and chemical analysis provided indications of purity levels. Zirconium was successfully zone refined, using up to 65 zone passes for oxygen removal. The low partial pressures in the system made these lengthy operations possible without excessive contamination. Resistivity ratios of up to 1300 in zirconium and 300 in hafnium were achieved.

Consumable-electrode arc melting and nonconsumable-electrode skull arc melting were investigated as possible manufacturing processes for the preparation of hypereutectic zirconium and hafnium carbide alloys at Battelle–Columbus.[7] Numerous experimental consumable-electrode runs, resulting in castings up to 5 in. in diameter, were performed. Persistent cracking in castings forced abandonment of the consumable-electrode process in favor of the nonconsumable-electrode skull arc-melting process. Techniques were developed for preparing satisfactory castings up to 3½ in. in diameter by this latter process. The developed process consisted of two steps: prealloying and drop casting.

Over 1500 skull arc-melting and casting runs were performed which yielded castings suitable for over 175 environment-test specimens and 275 property-test specimens. The thermal conductivity, thermal expansion, and heat capacity of specimens of ZrC + C alloys (19.7 to 24.4 wt.% carbon) were measured over the temperature range 70 to 4500°F (20 to 2480°C) and of HfC + C alloys (13.5 to 15.8 wt.% carbon) over the temperature range 70 to 5000°F (20 to 2760°C). Tensile tests, compression tests, and dynamic-modulus measurements were also performed on these alloys at 70, 3500, and 4500 or 5000°F. Data obtained in these measurements are presented.

Materials Research Corp.[8] has conducted an experimental program on the melting of aluminum nitride. They estimated that a nitrogen pressure less than 200 atm would be required to keep nitrogen in the compound. Two approaches were used to melt this compound. Resistance-heated crucibles of tungsten, rhenium, and graphite were tried first, but all reacted with the aluminum nitride, contaminating the melt so that the melting point of the compound could not be determined. This technique did result in a stable melt in equilibrium with the pressurized-nitrogen atmosphere. Arc melting on a water-cooled crucible was tried to prevent contamination of the melt. However, the high pressure required a high-current-density arc, and the thermal gradients in the charge prevented a pressure-stabilized melt. Distillation of aluminum was also a problem. On the basis of these experiences, the investigators suggested that aluminum nitride might be melted by a submerged-arc technique that would cause self-resistance melting.

NASA–Lewis[9] has extruded thin-wall tungsten tubing in lengths of 7.5 to 10.6 ft using the floating-mandrel techniques. Tubing diameters were either ½ or ⅜ in., and the nominal wall thickness was 0.020 in. Extrusion temperatures were 1925 to 2230°C, and reduction ratios were from 20 to 26. In most of the tubes, variations in diameter and wall thickness over a length of 8 to 10 ft were less than 0.020 and 0.008 in., respectively. The feasibility of warm-drawing (700°C) the extruded tubing was demonstrated. Drawing greatly improved tubing surface finish and dimensional tolerances.

Three dispersion-strengthened tantalum-base alloys for use in advanced space power systems have been developed by Westinghouse.[10-12] The processing compositions are Ta–8 W–1 Re–1 Hf (ASTAR-811), Ta–7 W–1 Re–1 Hf–0.012 C–0.012 N (ASTAR-811CN), and Ta–8 W–1 Re–0.7 Hf–0.025 C (ASTAR-811C). Primary breakdown of the 4-in.-diameter consumable-electrode-melted ingots was by upset or side forging at 2250°F (1400°C). The ingots were then rolled to 0.040-in. sheet.

Tensile properties were determined over the temperature range −320 to 3000°F. As-TIG-welded sheet specimens of ASTAR-811 and ASTAR-811CN were ductile when bent over a radius of 1t at −320 and −225°F, respectively. As-rolled sheet, 33% prior reduction, of both compositions was completely recrystallized after heating for 1 hr at 1600°C. Postweld anneals of 1-hr duration at temperatures ranging from 1800 to 2600°F (980 to 1425°C) resulted in an increase in the ductile–brittle transition temperature of TIG-welded ASTAR-811CN, but the transition temperature of TIG-welded ASTAR-811 remained below −320°F. Phase-identification studies on ASTAR-811CN indicated that the hexagonal close-packed tantalum dimetal carbide is the precipitate that occurs during processing to 0.04-in. sheet and short-time anneals. The face-centered cubic carbonitride phase occurs at the expense of the dimetal carbide during longer (>16 hr) anneals at temperatures of about 2400°F (1315°C) and higher. The effect of grain size and annealing tempera-

tures on the creep properties of ASTAR-811, ASTAR-811CN, and ASTAR-811C were also determined. Grain-size data were obtained on these alloys as a function of annealing time and temperature.

The effects of various factors on the capacity for deep drawing of commercial-grade sintered molybdenum and several Soviet molybdenum alloys (TsM-2 and Vm-1) were investigated by the Russians.[13] The specimens were flat, 6 mm wide and 0.5 and 0.8 mm thick, cut from rolled sheets at 0, 45, and 90° angles to the direction of rolling. Test specimens in the annealed or strain-hardened condition were tested at temperatures up to 500°C. The minimum drawing temperature of all the investigated materials except recrystallized sheet was below room temperature, indicating that satisfactory parts can be produced by drawing at room temperature. The capacity for deep drawing depended mainly on the impurity content, the microstructure, and the deformation rate. Raising the drawing temperature to 100 to 120°C significantly decreased the susceptibility to exfoliation and cracking and appreciably extended the workability of the investigated metals. Static uniaxial tension tests did not adequately reveal the capacity of molybdenum sheet for deep drawing because of the anisotropy of mechanical properties in the sheet plane and because of the difference in behavior of molybdenum at linear and plane modes of the stressed state. However, the capacity for deep drawing was satisfactorily characterized by biaxial static tension tests with a fluid (in burst tests) or a rigid punch. The capacity of sheet molybdenum for deep drawing increased with increasing (to 70 to 90%) prestraining by cold or warm rolling. The experimental results showed the feasibility of progressive multioperation deep drawing of thin-wall parts from molybdenum and molybdenum-alloy sheets, with or without intermediate stress relieving. Depending on the sheet thickness, the direction of rolling, and the heat-treatment prior to drawing, the optimum temperature of drawing was between 220 and 350°C.

A 4-in.-diameter ingot of V–10 Cr alloy weighing about 10 kg was double consumable arc melted at Argonne.[14] The furnace pressure was approximately 400 torrs in both melting operations, and chromium losses were below 0.2%. The ingot was nearly free of second phase, and no evidence of the cored structure characteristic of vanadium-alloy castings containing titanium was found. The ingot was made into an extrusion billet and double extruded at 1150°C. The billet was reduced 3.8 to 1 in primary extrusion and 10 to 1 in secondary extrusion to produce a bar of square cross section measuring $\frac{5}{8}$ in. on a side. The extruded bar could not be rolled at room temperature. Very light reductions produced very severe transverse cracking. A 1-hr heat-treatment at 800°C, followed by a reduction of 20 to 30% at 300°C, permitted further reduction at room temperature to more than 60%.

A preliminary investigation[15] was made to ascertain the factors that govern the coextrusion of rods, tubes, and cans from combinations of dissimilar metals. The results obtained showed that the flow of metal during coextrusion was dependent on the relative extrudabilities, disposition, and dimensions of the dissimilar metals in the original billet, and on the die geometry. The coextrusion of rods appeared to be limited to metals of fairly similar extrusion characteristics, and the loss of useful product due to dissimilar flow appeared to be less if the billet was made such that the material of higher strength was wholly enclosed by material of the lower strength. No metallurgical bonding was achieved under the conditions of test at room temperature. (D. E. Stellrecht)

Powder-Metallurgy Materials and Techniques

Review Publications

German investigators[16] have considered the theoretical aspects of the sintering process. Their review includes the definition and delineation of the concept of sintering, stages of sintering, possible mechanisms of material transport, and factors affecting material transport. Sintering of multicomponent systems without solubility of the components, with mutual solubility of the components, with the formation of new phases (reaction sintering), with oxide mixtures, and with sintering processes in the presence of a liquid phase is discussed. Hot pressing of large articles is described. A listing of 385 references is included.

A British review[17] discusses control-material manufacture, production of tungsten alloys, stainless-steel filters, impurity effects, magnesium alloys, dispersion-strengthened ferritic steels, SAP, and mixed-oxide and particle fuels.

The Germans have published three additional reviews on assorted topics in the powder-metallurgy field. In the first review,[18] techniques for the powder-metallurgy preparation of Fe, Cu, Ni, Co, low-melting heavy metals, refractory metals, and metal carbides are

discussed. The second review[19] deals with the production of electric-contact materials. Particular subjects discussed are: the production and physical characteristics of powders, methods for evaluation, mixing and blending, compacting, sintering, and impregnation. Materials described include copper and silver alloys, metals with metal carbides, and systems of metals and metalloids. The third review[20] is concerned with the application of high-speed procedures in powder metallurgy. Techniques such as the application of explosive material, underwater sparks, compressed gas, and magnetism for the deformation or treatment of metals are discussed. The high-speed procedures have been utilized for the consolidation of powder. A detailed report is given on experiments on the consolidation of metal and ceramic powders.

Powder Production

The Indians[21] have investigated the preparation of micron-size zirconium-metal powder by the calciothermic reduction of ZrO_2 in the presence of $CaCl_2$ (added as a heat sink to prevent sintering). The influence of variables such as initial particle size of ZrO_2, proportion of calcium excess and $CaCl_2$ in the charge, and temperature of reduction has been studied to arrive at the optimum conditions. A metal-powder yield of over 90% of theoretical, with particles predominantly 2 μ in size, has been obtained at 950°C with −325-mesh ZrO_2, a calcium excess of 50%, and 0.5 mole $CaCl_2$/mole ZrO_2 in the charge.

The Bulgarians[22] have devised a continuous method for producing molybdenum powder. A paramolybdate material is progressively reduced as it passes through a tubular rotating furnace. The final product is a moderately fine molybdenum powder of excellent quality.

Fabrication of All-Metal Products

The development of thin-walled tungsten and tungsten-alloy tubing[23a] continues at Oak Ridge. The experimental data for extrusions produced during the last 2½ years are summarized.

Recent work is directed toward developing large-diameter tubular products by the floating-mandrel process. Tube shells 1⅜ to 1⅞ in. in outside diameter and ¾ to 1 in. in inside diameter are obtained by the primary extrusion of 3-in.-diameter billets. Recently, larger tubes 2¼ in. in outside diameter and 1¼ in. in inside diameter have been produced by 4-in.-diameter billets. Two 6-in.-diameter billets were extruded to a 3⅜-in. outside diameter and 2⅜-in. inside diameter by the tube-shell extrusion technique. The finished tube shells were approximately 6 ft long and are the largest tube-shell extrusions of tungsten made to date.

In another investigation[24] at Oak Ridge, three 4-in.-diameter spheres were fabricated from very uniform, high-density, unalloyed, gas-pressure-bonded tungsten. These components were fabricated for use in an experiment designed to provide a more precise value of Newton's gravitational constant. The tungsten-powder billets were consolidated at autoclave conditions of 2900°F (1695°C) and 13,000 psi for 8 hr. Two of the spheres were lapped to a sphericity of better than 5 μin. and a background surface finish of 3 μin. peak to valley. The average density of the spheres, which varied less than 300 $\mu g/cm^3$ between themselves, was 19.074 g/cm^3.

Fabrication of Fiber-Strengthened and Dispersion-Strengthened Products

At Lewis Research Center,[25] refractory-oxide particles of UO_2 and ZrO_2 were added to a tungsten matrix and elongated into fibers by hot extrusion. The extrusion temperatures ranged from 3200 to 4000°F (1760 to 2205°C). The oxide fibers appeared to be ellipsoidal, with the major axis aligned in the extrusion direction. Oxide-matrix deformation characteristics were related to the extrusion parameters by comparing measured oxide-fiber strains with the deformations of the composite extrusions.

In another investigation[26] at Lewis Research Center, the fibering of oxides by hot deformation in metal matrices was carried out with ThO_2, ZrO_2, MgO, or Al_2O_3 particles dispersed in unalloyed niobium or tantalum. Composites were prepared by conventional powder-metallurgy techniques and extrusion. The resulting composites exhibited improved high-temperature (to 1650°C) tensile strengths and ratios of tensile strength to density, as well as improved stress-rupture properties, when compared with additive-free matrix materials. They also compared favorably in mechanical properties with some commercial alloys.

The Italians[27] have been concerned with the fabrication of tubular containers from a sintered SAP alloy. The production process involves pulverizing high-purity aluminum and then grinding the powder in the presence of oxygen and a silicone as a grinding or lubricating agent to partially oxidize the aluminum to Al_2O_3. Sintering and subsequent extrusion stages are required to complete the tubes. In another Italian paper[28] the technology of producing drawn SAP pipes

of large size is discussed. The starting material contained 10 wt.% Al_2O_3.

The Canadians[29] have investigated the structure and properties of dispersions of fused and sized yttria particles in zirconium produced by a powder-metallurgy technique in which particle-free matrix volumes are efficiently broken up in an intermediate stage of rehydriding and recrushing. Stress-rupture tests at 500°C on specimens so processed showed no effect of the yttria particles for concentrations up to 2 vol.%. At higher concentrations the properties improved progressively, culminating in a 10-fold increase in rupture time at 5 vol.% yttria. Specimens were rolled at 950°C after sintering at 1200 or 1000°C. The hot-rolled specimens, which were also rehydrided and resintered, showed more complex behavior wherein the rupture time first decreased to a minimum at about 2 vol.% yttria and then increased again. At 5 vol.% yttria, the rupture times were, respectively, 3 and 50 times greater than those for hot-rolled-and-sintered zirconium without yttria.

Corresponding tests using selected zirconium alloys instead of pure zirconium as the matrix showed that the best hot-rolled dispersions had rupture properties comparable to those of hot-rolled Zircaloy-2 or annealed Zr–2.5 Nb. The dispersions were still much inferior, however, to ultrahigh-strength alloys such as annealed Zr–1.5 Al–0.5 Mo. (C. A. MacMillan)

Chemical Plating

Tensile strength and microhardness of 20 ± 5 μ-thick nickel and iron films were measured by Palatnik, Il'inskiy, and Ravlik.[30] Films were prepared by vacuum vaporization at a rate of 0.2 to 0.3 μ/min. Because of the brittleness of iron films at ordinary temperatures, the tensile strength of these films was investigated only at high temperature. Nickel films were characterized by considerable longtime stability of strength at room temperature.

Niobium, tungsten, molybdenum, and tantalum were deposited[31] on ceramic and metallic substrates by reduction of their chlorides with zinc and cadmium in the gaseous phase at 500 to 700°C. Deposition of less volatile subchlorides of niobium, tungsten, and tantalum was not observed. Tests with molybdenum were still in progress. Two methods of the process were explored. In the first method, zinc and niobium pentachloride (for example) were evaporated separately and their vapors brought into contact in the reaction chamber using argon as the carrier gas. In the second approach a mixture of zinc powder with chlorides of the metals to be deposited was allowed to fall into the reaction chamber to evaporate and react. The latter arrangement was considered particularly suitable for the deposition of alloys.

A study to determine the effect of deposition parameters on the characteristics of SiC deposits (i.e., deposit density, surface appearance, phases present, hardness, and deposition rate) produced by chemical-vapor deposition from $SiCl_4$–CH_4–H mixtures was conducted at Oak Ridge.[32] The deposition rate was a function of temperature and gas composition. Decreasing the pressure within the range 1 to 180 torrs reduced the deposition rate. The surface morphology of the deposits varied markedly with deposition temperature and was also a function of the gas composition. X-ray-diffraction analysis showed that deposits that were formed below approximately 1250°C contained free silicon. At and above 1250°C, only SiC was formed for certain ranges of Si–C and H–Si ratios. At temperature above 1350°C and for low Si–C ratios, the deposit contained free graphite. The bulk of the SiC was the cubic beta phase, with small amounts of one or more of the hexagonal alpha phases present.

Tungsten–rhenium alloy sheet[23b] for metallurgical- and mechanical-properties evaluation was deposited by the hydrogen reduction of WF_6 and ReF_6. Alloys were deposited on the surfaces of resistance-heated stainless-steel or molybdenum strips or cylinders contained within a 4-in.-ID by 24-in.-long water-cooled chamber. The gas flow was along the axes of the substrates, which were loaded in tension to maintain straightness. Deposition temperatures were varied from 600 to 950°C at about 10 torrs. The hydrogen/(WF_6 + ReF_6) volume ratio was maintained constant at 15, the WF_6/ReF_6 ratio was adjusted to deposit nominally 5 to 25% rhenium alloys (presumably atomic percent). Nominally 5 at.% rhenium alloys were generally uniform in composition along the length and had smooth surfaces. Nominally 25 at.% rhenium alloys were more uniform in composition when deposited at 750°C. These alloys had smooth surfaces when deposited on sheet substrates but were nodular on ¼-in.-OD substrates. Periodic reversal of the gas flow improved the thickness uniformity of the deposits. It was thought that fine-grained W–25 at.% Re alloy without nodular growths might be obtained by vapor deposition of layers of tungsten and rhenium or W–Re alloy with subsequent diffusion treatment.

A process for the deposition of chromium on entrained ThO_2 particles by hydrogen reduction of

CrI_2 was developed at Battelle–Columbus.[33] The process development included design and construction of laboratory-scale apparatus for continuous feeding of controlled amounts of ThO_2 particles and CrI_2 to the coating chamber, effective reduction of CrI_2 with hydrogen in the presence of entrained ThO_2, and collection of the powder product. Small amounts (5 to 16 g/batch) of $Cr–ThO_2$ powder were obtained with a ThO_2 content within about 0.5 wt.% of the desired composition and of low C, N, S, and metallic-impurity content. Analyses of nonthoriated chromium showed the oxygen content to be less than 1145 ppm. The $Cr–ThO_2$ powder was consolidated by hot isostatic pressing into dispersions with interparticle spacing in the range of 3.0 to 5.1 μ at ThO_2 concentrations of 2, 3, and 5 vol.%. Metallographic examination of specimens heat-treated at 2400 and 2600°F (1315 and 1425°C) for 100 hr indicated that individual ThO_2 particles and clumps of ThO_2 particles present in the as-consolidated material became spheroidized during the heat-treatment. Migration of individual particles was either minimal or did not occur.

The system parameters that control deposition rates and etch rates in the radio-frequency sputtering process were studied by Vossen and O'Neill.[34] Since crystalline oxides of low chemical-bond strength can be reduced chemically by argon discharges in the process, 18 different oxides were studied experimentally, resulting in a tabulation that can be used to determine whether or not reduction will occur in a given material. Additional changes in stoichiometry that can occur as a result of sublimation from the target or substrate when one of the constituents is highly volatile were also investigated, using the system $Cd_xNb_2O_{5+x}$ as a vehicle.

Adhesion of aluminum chemically vapor deposited on steel was investigated by Redmond and Bazzarre.[35] Triisobutylaluminum was used as the source of aluminum, and nitrogen was the carrier gas. Isobutylene was added to decrease the formation of the undesirable diisobutylaluminum hydride. The bonding on oxide-covered substrates was found to be primarily mechanical in nature. Deposition-process parameters had a significant effect on adhesion; surface cleaning was less important.

The formation of discontinuities in aluminum-base cementation coatings on iron-, nickel-, and cobalt-base superalloys was tackled by Brill-Edwards and Epner.[36] Three main classes of defects were observed in the coatings on each of these alloys and were attributed, respectively, to irregular vapor diffusion through the pack, selective reaction and nucleation at the substrate surface, and nonuniform solid-state diffusion through the coating. Irregularities in the physical and chemical structure of the pack led to macroscopic variations of coating thickness, whereas low processing temperatures and low aluminum-supply rates promoted irregular nucleation and growth at high-energy sites on the substrate surface. Low aluminum-supply rates promoted entrapment of pack powder particles.

The vacuum metal-pack, vacuum slip-pack, and slurry-fusion processes for the application of high-temperature protective coatings on conventional superalloys and TD nickel were discussed by Gadd, Nejedlik, and Graham.[37] The specific coating elements included Al, Cr, W, Mo, and Ta applied separately or in combinations. Coating parameters, coating-formation mechanisms, and protective capabilities of the different types of coatings were given.

A new process for aluminum-coating steel sheet or strip was described by Sugano, Mori, and Inoue.[38] The process consisted in applying atomized aluminum powder to the surface of an adhesive-treated steel strip, drying the adhesive, compacting the powder into a solid layer by rolling, and then sintering the aluminum layer and bonding it to the steel substrate by heat-treatment. The coating had good adhesion on bending and satisfactory corrosion resistance.

The application, structure, and physical properties of high-temperature, oxidation-resistant Sn–Al–Mo coatings for tantalum alloys were described by Sama and Reznik.[39] The processes involved in the application and formation of fused silicide coatings for refractory metals were discussed by Sama and Priceman.[40] Chemistry, crystal structure, and morphology of these coatings were given. Both types of coatings were tested in a number of severe tests and were applied also to large, intricate hardware.

The production and the structure of a composite kind of protective coating for unalloyed molybdenum and molybdenum TZM alloy consisting of a porous $MoSi_2$ layer impregnated with a low-melting Sn–Al alloy were reported by Stecher and Lux.[41] The SnAl phase, which was liquid at oxidation temperatures, formed a protective Al_2O_3 film and conferred self-healing properties to the coating in case fissures occurred. The protective $MoSi_2$ coating, combined with a SnAl phase, appeared to be particularly promising in view of its increased reliability with respect to possible failures from local defects after short oxidation times. However, a loss of the protective effect during longer time oxidation was attributed to structural modifications within the coating.

Three types of coating—$MoSi_2$, modified $NbSi_2$, and silicide-glaze composite—were developed by Restall[42] for the protection of high-strength niobium alloys intended for turbine-blading operation up to 1300°C. The performance of these coatings was compared with that of coatings developed elsewhere. Silicide-base coatings contained microcracks that had an important effect on oxidation and impact behavior of niobium alloys. In the silicide-glaze coating, the glaze filled the microcracks in the silicide coating and acted as an oxidation-resistant coating in its own right, rendering the silicide-glaze coatings superior to silicide-base coatings in laboratory tests. Two multiphase coatings, one based on Cr–Ti–Si and the other proprietary, called R513, behaved similarly to the silicide-glaze coating in oxidation and creep tests. Oxidation tests in the temperature range 1100 to 1300°C showed all three coatings to be superior to silicide-base coating on F48 alloy. The Cr–Ti–Si coating tended to embrittle F48 alloy impact-test pieces at room temperature. (J. Zupan)

Explosive Metalworking

One of the newest applications of explosive metalworking is in the fabrication of composite materials. A very interesting flat composite plate, consisting of tungsten wire in a copper matrix, was fabricated by Jarvis and Slate[44] using this approach. Alternate layers of copper foil and small tungsten wires were placed in a heavy steel grooved plate covered with a metal plate and a layer of explosive. The detonation of the explosive progressed in the longitudinal direction of the wires and produced a sound composite. The volume fraction of fibers obtained was 17%, and the alternate copper layers were well bonded to each other. A sample was tested and was found to have the theoretically predicted ultimate strength.

Although the explosive-compaction process has been in use since 1955, the process has several rather severe limitations for use as a laboratory tool. For this reason, Hagemeyer and Regalbuto,[45] working at General Dynamics, designed and built a high-velocity compaction device that has the advantages of small size, simplicity of operation, and safety. The apparatus employs a projectile accelerated by a gunpowder charge to impact a small cylindrical sample of the powder under study. In the work reported, a series of 16 metal powders, listed in Table IV-1, were impacted at various velocities. It was found that samples which were "underhit" were whole and had high green strengths but were of low density. "Overhit" samples were shattered and cracked. The samples were evaluated for density and hardness, and the optimum results

Table IV-1 Density and Hardness Values for Green Compacts Produced by Impact[45]

Sample	Particle size*	Sample weight, g	Impact velocity, ft/sec	Impact energy, ft-lb/g of powder	Compact density, g/cm^3	Density, % of theoretical	Hardness, DPH
Aluminum, pure	−325	2.0	590.	119.	2.70	99.+	54
Aluminum, 2024	−325	2.0	650.	142.	2.76	99.+	140
Aluminum, 6061	−325	2.0	560.	114.	2.69	99.+	104
Aluminum, 7075	−325	2.0	650.	142.	2.78	99.+	160
Chromium	−100	5.0	1030.	145.	6.70	94.	596
Cobalt	−170, +200	5.9	875.	90.	8.09	93.	293
Copper, irregular	−325	6.3	730.	58.	8.77	98.	129
Copper, dendritic	−325	5.0	800.	88.	8.81	99.	168
Iron, carbonyl	10 μ	5.0	875.	104.	7.72	98.	218
Molybdenum	−325	6.0	980.	88.	9.39	92.	286
Nickel	2 to 5 μ	4.0	940.	155.	8.62	97.	349
Niobium	−100	5.0	1030.	145.	8.26	96.	178
Tantalum	−200	10.0	780.	38.	16.25	99.	202
Titanium	−100	3.0	1030.	242.	4.33	96.	150
Zirconium	−100	5.0	1030.	145.	6.42	99.	364
304 stainless steel	−100	5.0	780.	75.	7.67	97.	322

*Mesh size except where otherwise noted.

for each of the materials are shown in the table. Several of the materials had hardnesses and structures indicative of extensive cold working. It was demonstrated that densities greater than 90% of theoretical could be obtained by this technique.

The use of a related device for compaction of brittle ceramic oxides is discussed in a U. S. patent.[46] The powder is compacted by a heavy, pneumatically driven, rapidly moving ram (the ram weighs about 1 ton and is capable of traveling at 35 to 75 ft/sec) that impacts the sample contained in a suitable holder. Even though this technique has been in use for some time, the production of crack-free items from brittle materials has not been possible. In this patent the oxide to be compacted is contained in a graphite can that is then surrounded with a loose granular material (e.g., magnesium oxide). This assemblage is placed in an impaction container, then placed in the die, heated, evacuated, and impacted. By this technique it was possible to obtain 0.6-in.-diameter by 1-in.-long crack-free cylinders of fine-grained BeO and BeO–25 vol.% UO_2 having densities of 95% of theoretical or better.

Powders can be compacted by high-energy-rate techniques in two ways—impaction (discussed above) and direct explosive compaction. A paper by Leonard[47] presents the current state of the art of the direct compaction of powders by explosives. Most of the research in this area is of the "cut-and-try" method since a theoretical analysis of the behavior of a cylindrical sample contained in a metal tube surrounded by an explosive charge is very difficult at present. Qualitatively, however, the process can be described. A sound compact can be produced by balancing the two competing shock-wave actions that occur as the shock wave moves in toward the center of the sample. These two actions are the attenuation of the shock impulse due to the energy absorbed during void collapse and the increase in shock pressure due to convergence. If shock attenuation is overriding, incomplete densification occurs; if the shock pressures generated at the center are too high, cracking or melting will occur. The limitations and applications of the process are presented, and representative materials and shapes that have been fabricated are shown. The effects of changing the process variables—initial powder density, container size or material, and explosive type or amount—are discussed.

A U. S. patent[48] discusses the use of explosives to weld tubes into tube sheets (as used, for example, in heat exchangers). In the method an open-ended tube is placed in the hole in the tube sheet, a close-fitting plastic cartridge containing the explosive charge is positioned in the tube, and the charge is detonated. The position relative to the surface and the length of the metallurgical bond produced between the tube and tube sheet could be controlled quite closely by careful placement of the explosive charge.

A somewhat similar patent[49] describes a very similar operation. In this patent, tubes are expanded and locked into position in a tube sheet by explosive means. A length of detonating explosive cord is contained in a plastic holder positioned within the tube to be expanded. Although the joints so produced were evidently not metallurgically bonded, they exhibited pull-out strengths of the order of 6000 lb.

A program has been instituted at Oak Ridge[50] to study the high-energy-rate forming behavior of selected materials. The response of beryllium, titanium, tungsten, and their alloys will be investigated using a Dynapak to impact form the materials. High-energy-rate techniques are being utilized in place of conventional techniques because of the increased strength and ductility attainable with these methods. Billets of commercial and hot isostatically pressed beryllium 2.5 in. in diameter by 4 in. long were impacted at 650°C and various impact energies. It was found that 25% reduction was attained with one impact of 30,000 ft-lb, but that a second strike at the same energy fractured the billet. (D. Laber)

Welding and Brazing

Welding

A new chamber for inert-gas tungsten-arc welding of Zircaloy fuel pins was developed recently at Risø in Denmark.[51] This small chamber is designed to weld very long rods (6 ft and longer) with only the end of the rod placed in the chamber. The welding setup prevents the formation of pockets in the welding zone by reducing heat input and by automatically regulating chamber pressure. It also provides a system for automatic evacuation and helium filling of the pins, thus speeding up the production rate.

Inert-gas tungsten-arc welding procedures have also been developed at Los Alamos,[52] where researchers have designed a welding fixture and power supply for encapsulating plutonium. This fixture, without using large vacuum-"inertable" glove boxes, provides a high-quality inert atmosphere in the encapsulating container while keeping the outside surface of the container free from contaminants. The power supply provides programmed welding current from less than 10 amp to

more than 200 amp. Welding procedures are reported for a variety of end-cap designs and materials (stainless steel, mild steel, Ta, Cu, Ni, Au, and W).

Battelle–Northwest[53] has developed electron-beam welding procedures to encapsulate radioisotopes. A 6-kva welder was used for welds in 1-in.-thick 304 stainless steel. Single-pass bead-on-plate and butt welds with 100% penetration were made under the following conditions:

Beam potential	100 kva
Beam current	23 ma
Weld speed	10 in./min
Beam focus	½ in. below surface

The same welder has been used to join molybdenum liners to carbon steel and to weld tantalum to 304 stainless steel. Under the microscope, sections of the latter welds where the beam had penetrated the tantalum resembled brazed joints, the stainless steel having wetted and flowed around the tantalum.

Solar[54] has completed a program on diffusion bonding of various refractory metals and superalloys using resistance welding equipment. Two processes were developed: yield-stress-controlled diffusion bonding and continuous-seam diffusion bonding. For the former, a resistance welder was modified to allow the use of hot, refractory-metal electrodes. Typical welding procedures using the modified equipment require 10 sec of heating and hold time, usually under constant pressure during the hold cycle. Reproducible, high-quality joints were made in niobium alloys (D43, B66, Cb-752, and D36), tantalum alloys (T111 and T222), TZM molybdenum, and superalloys (TD nickel and TD nickel–chromium). Tooling principles were developed for straight and curved T-joints, lap joints, and more complex configurations.

The continuous-seam process, using a modified seam welder, was developed to increase bonding speed. Welding speeds up to 13 in./min were demonstrated on Ti–6 Al–4 V alloy. Excellent joint quality was obtained in these welds, with strength equal to that of the parent metal in both the as-bonded and heat-treated conditions.

The effect of welding on properties of tungsten and W–Re alloys was investigated recently at Oak Ridge.[23c] These studies indicate that a minimum preheat of 150°C is necessary to produce crack-free, one-pass butt welds in $^{1}/_{16}$-in.-thick unalloyed tungsten sheet. Higher preheats apparently were not beneficial in these joints but may be helpful in designs involving more severe stress concentrations or larger parts.

It was also shown that weldment quality depends on the tungsten fabrication method. Weldments in arc-cast and electron-beam-melted base metals were essentially free from porosity. However, weldments in powder-metallurgy tungsten were subject to embrittlement, with gross porosity occurring, particularly along the fusion line. The embrittling was attributed to the large grain size of the welds and the adjacent recrystallized heat-affected zone. The effects of time and temperature on the hardness of bead-on-plate welds in unalloyed powder-metallurgy tungsten are shown in Fig. IV-1. These welds were made using W–26 Re filler wire.

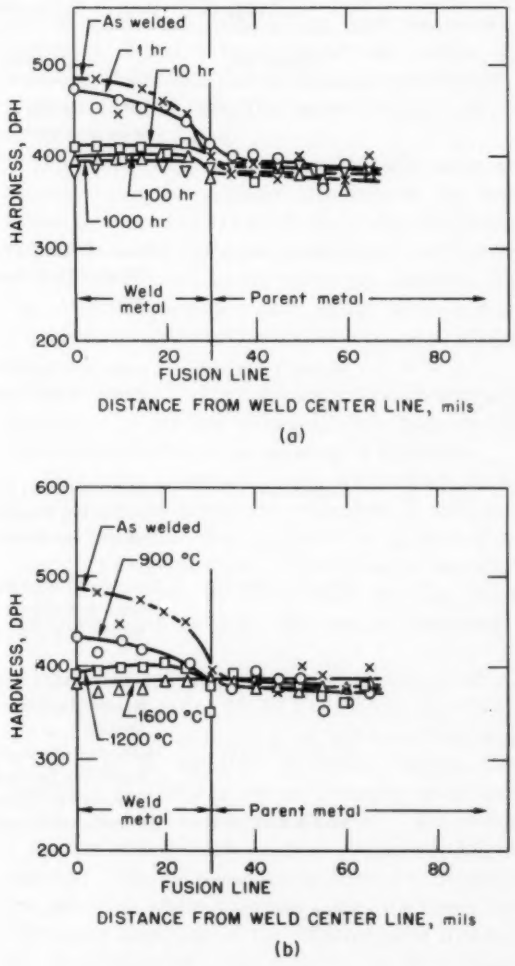

Fig. IV-1 Hardness of powder-metallurgy tungsten welded with W–26 Re filler wire.[23c] (*a*) Effect of time at 1200°C. (*b*) Effect of temperature for 100 hr.

Computer programs of interest to welding engineers have been developed at the Union Carbide Y-12 plant.[55] These programs provide guidance in making practical use of heat-transfer equations that describe the thermal history at the weld heat-affected zone. Solutions for four types of problems are now available:

1. Determination by thermal mapping of the "temperature hill" enveloping the welding heat source on a semi-infinite plate.

2. Determination of the peak temperature at some distance from the weld center line on the bond line.

3. Determination of the peak surface temperature at an edge of a plate parallel to the weld.

4. Determination of the peak temperature on the bottom side of plates having partial-penetration welds.

Some recently issued patents, mostly French, concerning fuel-element end-closure welding are summarized in Table IV-2.

Brazing

Northrup[56] has developed a procedure, called thin-film diffusion brazing, for joining titanium alloys. This method uses copper plating and thermal cycling to produce both solid- and liquid-state diffusion. The

Table IV-2 Recent Patents Related to Fuel-Element End Closures

Patent No.	Subject	Brief description
French 1,423,478	Closure Welding of Nuclear Reactor Fuel Elements Having a Very Thin Sheath	A method of welding a flexible metal sheath less than 0.1 mm thick using a plug and a metal ferrule. All three components are welded together to seal the sheath
French 1,431,278	Closure Welding of Nuclear Reactor Fuel Element Sheath	Argon-arc welding of end caps with the normal V-shape groove connected at its bottom with annular groove to form a Y-shaped groove
French 1,429,797	Closure Welding of Nuclear Reactor Fuel Elements	End capping of pin-type fuel elements using peripheral argon-arc welding, swaging of the end, and helium-arc closure welding
French 1,411,641	Closure Method for the Ends of Nuclear Fuel Elements of the Dispersion Type	Consists of hot pressing, e.g., 2742°F (1450°C), 200 ksi (140 kg/cm^2), 1 hr, a disk to a fuel bar
French 1,486,856	Closure of Fuel Elements for Nuclear Reactors Having a Sheath of Fritted Aluminum	Pressure welding of end plugs by circumferential hammering (5 sec at shock frequency of 3000/min) at 932°F (500°C)
French 1,355,939	Closure Welding of Nuclear Reactor Fuel Element Sheaths	Welding of annular end caps to tubular sheaths
U. S. 3,392,438	Method of Closing Ends of Protective Tubes for Nuclear Reactor Fuel Elements	Pin-type fuel elements closed by swaging and welding
British 1,118,104	Production and Testing of Weld Seams	Circular weld seams on fuel-rod end caps are made by rotating the rod about its axis, so that the weldment moves adjacent to the welding electrode. The weld is continuously irradiated by focused X-ray beams, which are also received by a detector to indicate weld quality

surfaces to be joined are plated with a thin film of copper, abutted, and then heated at 500°F/min to 1700°F (280°C/min to 925°C), held for 20 min, cooled rapidly to 1450°F (790°C), and held for 15 min. Reproducible test specimens were produced in Ti–8 Al–1 Mo–1 V using this method. These specimens exhibited higher strength and greater resistance to stress-corrosion cracking and thermal exposure than did as-received material or uncoated specimens subjected to the same thermal cycle.

Oak Ridge researchers[23d] have investigated the use of the Ti–Zr–Ge system for brazing refractory metals. Many alloys in this system were studied, all of which wet satisfactorily. Some were superior, however. For example, sound joints with excellent filleting were produced in tantalum and molybdenum with the Ti–20 Zr–8 Ge alloy. The Ti–20 Zr–15 Ge alloy was shown to be outstanding for joining graphite.

Brazing refractory metals to copper or steel normally requires plating the refractory metal with copper and nickel and heat-treatments in a vacuum. At Risø a method for brazing tantalum or niobium to copper or stainless steel has been developed[51] which involves electrolytic copper plating of the tantalum or niobium. No further details are given in their report.

(J. E. Mortland and R. M. Evans)

Nondestructive Testing

Ultrasonic Techniques

Continued development at the Research Division of Automation Industries[57] has resulted in a wheel-type probe using the Delta technique. The wheel is capable of inspecting aluminum butt welds at the rate of 50 ft/hr. The method shows many advantages over radiography in detecting lack of penetration of a 0.030- by 0.060-in. size, lack of fusion as narrow as 0.025 in., and microfissuring (a laminar, shrinkage-type defect that cannot be detected by radiography). Destructive tests showed that the Delta method detected 80% of tight lack-of-penetration defects, compared with only 36% detected by radiography in 18 ft of weld. It is surprising that so little use has been made of the Delta technique by industry, considering the advantages of the method. The advantages stem from the relative insensitivity to defect orientation. The detected signal is produced by reflection, reradiation, or mode conversion caused by the defect. Energy due to at least one of these phenomena is directed toward the receiving transducer which is located directly over the defect region.

Common practice in testing bonded lap joints for lack of bond using ultrasonic through-transmission techniques involves scanning the bonded area and indicating those areas which produce a signal level either above (good area) or below (poor area) an arbitrary signal level. Workers at Los Alamos[58] have taken what appears to be a better approach. They use a voltage-to-frequency converter to convert the analog gate signal of conventional equipment to a frequency that corresponds to the amplitude of the voltage of the received signal. The method is used to inspect brazed lap joints in tubing. The tubing is rotated and the number of cycles in one revolution of the tubing is registered on a counter.

The transmitting transducer is $\frac{3}{4}$ in. in diameter and focussed. It is located 2 in. from the receiving transducer, which is located inside the tubing. The receiver is 0.060 by 0.060 in. and is mounted inside a 0.100-in.-diameter tube. The transducer axis is normal to the axis of the tubing.

An error will result when multiple scans are necessary to cover a brazed area because any overlapped area is counted twice. Shifts in alignment during inspection would also cause errors. Both these sources of error are inherent in any integrating technique. The Los Alamos approach would appear to be a more acceptable method than the common go, no-go integration.

Oak Ridge[23e] has adapted ultrasonic-resonance equipment to produce strip-chart recordings of wall thicknesses of tubing to an accuracy of 0.0001 in.

Oak Ridge personnel[23f] also are studying the use of reflection holograms for evaluation of surface as well as subsurface discontinuities in metals and ceramics. The workpiece is a shock-mounted aluminum block 45 in. long by 29 in. wide by 3 in. thick. Maximum depth of field with present equipment is 9 in.

Initiation of fatigue cracks extending around notched specimens of 2014-T6 aluminum alloy, 5 Al–2.5 Sn–Ti alloy, maraging steel, and cobalt-base alloy L-605 can be detected at depths ranging from 0.0005 in. to 0.004 in. by an ultrasonic pulse–echo method used at Lewis Research Center.[59] The method makes use of commonly available equipment. A $\frac{1}{2}$-in.-diameter, 7-Mc/sec transducer is clamped to the end of the specimen, where it remains during the fatigue test. The signal amplitude of the reflected pulse is plotted by an oscillograph. The intensity of the reflected energy is a function of the total area of the intercepted portion of the ultrasonic beam and the average intensity of the beam over the intercepted area. The

plot of the signal amplitude, therefore, can be presented as a function of depth of penetration of the fatigue crack. (D. Ensminger)

NDT Techniques Other Than Ultrasonic

Studies of Am–Cm–Be as a possible nonreactor neutron source for neutron radiography have been completed at Argonne.[60] The authors conclude:

> 1. Direct-exposure neutron radiography is practical using an Am–Cm–Be source. (Graphs and figures are available relating source yield, collimation, exposure, image quality, etc.)
>
> 2. Transfer-method neutron radiography is practical, but, for a 10^9-neutron/sec source and the existing simple dysprosium foil–KK film image recording, the collimation would be limited to collimator ratios of 1 : 10 (aperture-to-length) or poorer. Higher source strengths would, of course, allow correspondingly improved characteristics.
>
> 3. No apparent advantage is gained by using beryllium oxide rather than water as a moderator for systems with Am–Cm–Be as the neutron source.

Investigators at Oak Ridge have continued their basic analytical work using computer methods for solution of eddy-current inspection and design problems.[61] For several different coil/work configurations, references or curves are given showing coil impedance, defect sensitivity, and phase and amplitude of voltage. Curves are given relating coil impedance and cladding thickness for certain metal-layer combinations. Data given on the effects of specimen thickness permit the choice of optimum parameters to obtain maximum sensitivity over a particular thickness range. Signals can be derived mathematically from a defect sensitivity factor, a defect shape-and-orientation factor, and the defect volume. Data are given for a spheroidal flaw. Experiments with a coil and single conducting plane give excellent agreement between measured and calculated values within experimental error. Coil-resolution studies and approaches to probe-coil temperature compensation are also reported.

Investigators at Battelle–Northwest[62] are reporting results from their studies of acoustic-emission phenomena. In one study, noise spectra and useful instrument details resulting from measurements on a reactor during start-up are presented. Although the investigators point out that acoustic-emission methods are limited to detection of a dynamic condition and will not detect a static flaw or discontinuity, this reviewer believes that in spite of this the method could eventually become very important for purposes of in-service reactor inspection. The study is summarized by the investigators as follows:

> Acoustic noise data were collected from various locations on the Dresden I nuclear power reactor during start-up and subsequent increase to full power during June, 1968. The purpose of these measurements was to provide initial definition of the reactor system noise problem. The problem must be overcome if acoustic emission sensing is to be utilized to detect flaw formation and growth in pressure boundaries during operation.
>
> In all cases but one, the significant elements of the noise spectrum appeared below 500 kHz, and especially below 200 kHz. One condition during start-up, where high flow was routed through a 6-in. bypass line by throttling a main valve, produced a noise spectrum with significant amplitudes to 1 MHz. This, however, was a transient condition that did not appear to affect the spectrum at other monitor points. Above 1 MHz, up to the approximately 3.5 MHz response limit of the measurement system, the level of signals observed was essentially that of the normal electronic noise of the monitor system. There was no significant change in the noise spectrum detected on the primary recirculation system as a function of increasing temperature, i.e., full cold flow produced the same spectral distribution as did similar flow at full power level.
>
> The noise spectrum observed on the Dresden I reactor contains a "window" from about 750 kHz to 3 MHz which could be available for detection of acoustic emission. Current laboratory-test work on high-frequency detection of acoustic emission has shown good detector response in this region. There is little incentive to work above 3 MHz for field application purposes because the signal attenuation with increasing frequency rises very rapidly for ferrous materials above that point. This would lead to an excessive number of sensing points in order to provide complete system coverage.
>
> The results of this test are considered encouraging . . . because they indicate a useable frequency range for the detection of acoustic emission on nuclear power plants; . . . however . . . they cannot be considered conclusive.

Acoustic-emission data for crack detection and pipe bursts have also appeared in print recently.[63] The author makes the now widely known comments: "As just one non-nuclear example, it might be used to provide early warning of fatigue in critical aircraft components. We have already flown acoustic-emission monitoring equipment with this in mind, and found that the aircraft structures we examined emit signals similar to those described under in-flight stress. These signals are readily isolated from normal aircraft noises." (A. F. Leatherman)

References

1. A. C. Hott, Preparation of UC and UC–W Specimens for an Irradiation Test of the Value of a Fine-Particle Dispersion in the Control of Fission Gas Swelling, USAEC Report NAA-SR-12629, Atomics International, May 31, 1968.

2. P. Blum, P. Guinet, and H. Vaugoyeau, Nuclear Fuel Material and Method of Preparation, British Patent 1,124,810, Dec. 2, 1964.
3. G. E. Miller, Injection Casting Aluminum–10 Wt.% Plutonium Fuel Elements, *Nucl. Appl.*, **5**: 68-73 (August 1968).
4. T. Takaai, The Electron Beam Melting of the Refractory Metals. 10. Cast Structure of Electron-Beam Nb Alloy Ingots, *Nippon Kinzoku Gakkaishi*, **32**: 796-802 (August 1968).
5. T. Takaai, The Electron Beam Melting of the Refractory Metals. 11. Ductility of Electron Beam Melted Nb Alloy Ingots, *Nippon Kinzoku Gakkaishi*, **32**: 802-807 (August 1968).
6. D. S. Easton and J. O. Betterton, Jr., Ultrahigh-Vacuum Zone Purification of Zirconium with Analysis of Partial Pressures, USAEC Report ORNL-4309, Oak Ridge National Laboratory, December 1968.
7. E. L. Foster, Jr., S. G. Nelson, D. P. Moak, D. E. Price, N. M. Griesenauer, J. Lagedrost, Jr., and J. M. Allen, Development of a Subscale Manufacturing Process for the Fabrication of Hypereutectic Transition-Metal Carbide Composites, Report AFML-TR-68-255, Battelle–Columbus, September 1968.
8. W. Class, An Aluminium Nitride Melting Technique, Report NASA-CR-1171 (N68-33335), Materials Research Corp., September 1968.
9. C. P. Blankenship and C. A. Gyergak, Extrusion of $\frac{1}{2}$ and $\frac{3}{8}$ Inch Diameter Thin-Wall Tungsten Tubing in Lengths Near 10 Feet, Report NASA-TM-X-1638 (N68-32977), National Aeronautics and Space Administration, Lewis Research Center, August 1968.
10. R. W. Buckman, Jr., and R. C. Goodspeed, Development of Dispersion Strengthened Tantalum Base Alloy, Quarterly Progress Report, August 20–November 20, 1966, Report NASA-CR-72316 (N68-13625), Westinghouse Electric Corporation, Astronuclear Laboratory.
11. R. W. Buckman, Jr., and R. C. Goodspeed, Development of Dispersion Strengthened Tantalum Base Alloy, Quarterly Progress Report, November 20, 1966–February 20, 1967, Report NASA-CR-72306 (N68-13630), Westinghouse Electric Corporation, Astronuclear Laboratory.
12. R. W. Buckman, Jr., and R. G. Goodspeed, Development of Dispersion Strengthened Tantalum Base Alloy, Quarterly Progress Report, February 20–May 20, 1967, Report NASA-CR-72326 (N68-18131), Westinghouse Electric Corporation, Astronuclear Laboratory.
13. V. N. Korolev and L. A. Shofman, Deep Drawing of Molybdenum and Its Alloys, *Kuznechno-Shtampovochnoe Proizvod.*, No. 10: 17-23 (1967).
14. Argonne National Laboratory, Reactor Development Program Progress Report, October 1968, USAEC Report ANL-7513, pp. 92-93, Nov. 27, 1968.
15. E. Whitfield, Preliminary Study of the Coextrusion of Dissimilar Metals, Report NP-17605, National Engineering Laboratory, January 1967.
16. F. Thuemmler and W. Thomma, Sintering Process, *Met. Rev. (Publ. in Metals Mater.)*, **115**: 69-108 (1967).
17. R. Paris and V. A. Tracy, Discussion on the Role of Powder Metallurgy in Nuclear Technology, *Powder Met.*, **11**: 203-211 (Spring 1968).
18. F. Eisenkolb, Latest Results and Present State of Powder Metallurgy, Part II, Construction Materials, *Neue Huette*, **13**: 39-45 (January 1968).
19. H. Schreiner, *Powder Metallurgy of Electrical Contacts*, Vol. 20, Springer-Verlag, Berlin, 1964.
20. G. Gentzsch, Application of High-Speed Procedures in Powder Metallurgy, *Klepzig Fachber.*, **75**: 313-322 (May 1967).
21. C. V. Sundaram, P. K. Ray Chaudhuri, L. V. P. Roman, and T. S. Krishnan, Preparation of Zirconium Metal Powder by Calciothermic Reduction of Zirconium Oxide, *Trans. Indian Inst. Metals*, **20**: 187-190 (December 1967).
22. D. Dhak'ron, V. Visarionov, K. V'lchev, and G. Khristov, Producing Molybdenum Powder in a Tubular Rotating Furnace, *Rubodobiv Met.*, **22**: 57-60 (September 1967).
23. P. Patriarca and W. O. Harms (Comps.) and D. J. Rucker (Ed.), Fuels and Materials Development Program, Quarterly Progress Report for Period Ending June 30, 1968, USAEC Report ORNL-4330, (*a*) p. 272, (*b*) pp. 281-284, (*c*) pp. 295-300, (*d*) pp. 352-354, (*e*) p. 357, (*f*) p. 306, Oak Ridge National Laboratory, November 1968.
24. J. H. Nash, A. C. Neeley, and P. J. Steger, High-Density Tungsten Spheres, USAEC Report Y-1654, Union Carbide Corporation, Nov. 18, 1968.
25. C. P. Blankenship, Oxide Deformation and Fiber Reinforcement in a Tungsten Metal Oxide Composite, Report NASA-TN-D-4475 (N68-18610), National Aeronautics and Space Administration, Lewis Research Center, March 1968.
26. R. W. Jeck, J. W. Weeton, and R. A. Signorelli, Fibering of Oxides in Refractory Metals, *ASTM Spec. Tech. Publ.*, No. 427: 91-106 (1967).
27. D. Gualandi and P. Jehenson, Al–Al_2O_3 Structures and Process for Obtaining Same, British Patent 1,123,394, Aug. 14, 1968.
28. F. Bertazzoli, A. Anselmi, C. Belvedere, and W. Buergers, The Technology of the Manufacture of Semifinished Products of Sintered Aluminum–Alumina Material (SAP), *Met. Ital.*, **60**: 535-547 (June 1968).
29. J. Reyek and B. G. Childs, Structure and Properties of Yttria–Zirconium Dispersions, *J. Nucl. Mater.*, **26**: 285-299 (1968).
30. L. S. Palatnik, A. I. Il'inskiy, and A. G. Ravlik, Strength of Nickel and Iron Films Obtained by Vacuum Condensation, Report NASA-TT-F-11447 (N68-31981) [translated from *Fiz. Metallov. Metalloved.*, **19**(2): 310-311 (February 1965)].
31. F. Brossa, H. W. Schleicher, and H. Venker, Deposition of Nb, Ta, Mo, and W by Reduction of the Corresponding Chloride with Zn Vapor, in *Protection Against Corrosion by Metal Finishing* (in German), Report CONF-661138, pp. 148-150.
32. J. E. Spruiell, Chemical Vapor Deposition of Silicon Carbide from Silicon Tetrachloride–Methane–Hydrogen Mixtures, USAEC Report ORNL-4326, Oak Ridge National Laboratory, December 1968.
33. N. D. Veigel, J. L. McCall, K. E. Meiners, and J. M. Blocher, Jr., Chemical Vapor Deposition of Chromium on ThO_2, Report NASA-CR-72404, Battelle–Columbus, June 30, 1968.
34. J. L. Vossen and J. J. O'Neill, Jr., R-F Sputtering Processes, *RCA Rev.*, **29**(2): 149-179 (June 1968).
35. J. P. Redmond and D. F. Bazzarre, Adhesion of Chemically

Vapor Deposited Aluminum on Steel, *Electrochem. Technol.*, 6(9-10): 336-337 (September–October 1968).

36. H. Brill-Edwards and M. Epner, Effect of Material Transfer Mechanisms on the Formation of Discontinuities in Pack Cementation Coatings on Superalloys, *Electrochem. Technol.*, 6(9-10): 299-307 (September–October 1968).
37. J. D. Gadd, J. F. Nejedlik, and L. D. Graham, Vacuum Pack and Slurry Coating Processes for Coating Superalloys, *Electrochem. Technol.*, 6(9-10): 307-315 (September–October 1968).
38. G. Sugano, K. Mori, and K. Inoue, A New Aluminum Coating Process for Steel, *Electrochem. Technol.*, 6(9-10): 326-329 (September–October 1968).
39. L. Sama and B. D. Reznik, Tin–Aluminum–Molybdenum Oxidation Protective Coatings for Tantalum Alloy Aerospace Parts, *Electrochem. Technol.*, 6(3-4): 113-119 (March–April 1968).
40. S. Priceman and L. Sama, Reliable, Practical, Protective Coatings for Refractory Metals Formed by the Fusion of Silicon Alloy Slurries, *Electrochem. Technol.*, 6(9-10): 315-326 (September–October 1968).
41. P. Stecher and B. Lux, Oxidation Protection of Molybdenum Through a $MoSi_2$/SnAl Protective Coating, *J. Less-Common Metals*, 14(4): 407-426 (April 1968).
42. J. E. Restall, The Development and Testing of Protective Coatings on F48 and SU16 Niobium Alloys, *J. Less-Common Metals*, 16(1): 11-36 (September 1968).
43. Reference deleted.
44. C. V. Jarvis and P. M. B. Slate, Explosive Fabrication of Composite Materials, *Nature*, 220: 783-784 (Nov. 23, 1968).
45. J. W. Hagemeyer and J. A. Regalbuto, Dynamic Compaction of Metal Powders with a High Velocity Impact Device, *Int. J. Powder Met.*, 4: 19-25 (July 1968).
46. J. R. Hague and D. W. Brite, Fabrication of High Energy Rate Impaction, U. S. Patent 3,344,209, to USAEC, Sept. 26, 1967.
47. R. W. Leonard, Direct Explosive Compaction of Powder Materials, *Battelle Tech. Rev.*, 17(10): 13-17 (November–December 1968).
48. C. C. Simons and R. J. Carlson, Method of Explosively Welding Tubes to Tube Plates, U. S. Patent 3,409,969, to Westinghouse Electric Corporation, Nov. 12, 1968.
49. I. Berman and B. S. Thakkar, Explosive Expansion of Tubes into Tube Sheets, U. S. Patent 3,411,198, Nov. 19, 1968.
50. Oak Ridge National Laboratory, Y-12 Development Activities Progress Report, May–July 1967, USAEC Report Y-1652, pp. C54-56, Jan. 20, 1969. (Classified)
51. Metallurgy Department Annual Progress Report for the Period Ending March 31, 1968, Danish Report RISO-179, July 1968.
52. J. W. Anderson and J. R. Nichols, Encapsulation of Plutonium and Other Radioactive Materials in Welded Containers, USAEC Report LA-3937, Los Alamos Scientific Laboratory, April 1968.
53. K. Drumheller (Ed.), Division of Isotope Development Programs, Quarterly Report, August–September, 1968, USAEC Report BNWL-924, Battelle–Northwest, November 1968. (Classified; material cited is unclassified.)
54. A. G. Metcalfe and F. K. Rose, Production Tool for Diffusion Bonding, Report AFML-TR-68-231, International Harvester Co., Solar Division, August 1968.
55. R. A. Huber, D. Bradway, C. M. Wiedemann, and P. W. Turnor, Computer Programs for Calculating Peak Temperature Distribution in Welding, USAEC Report Y-1627, Union Carbide Corporation, Oct. 16, 1968.
56. T. A. Krinski, Thin Film Diffusion Brazing of Titanium Alloys, Part II, Report MRG-66-01, Northrup Corp., Norair Division, July 1966.
57. K. J. Hannah, B. T. Cross, and W. M. Tooley, Development of the Ultrasonic Delta Technique for Aluminum Welds and Materials, Report NASA-CR-61952 (N68-34770), Automation Industries, Inc., Research Division, May 15, 1968.
58. N. B. Edenborough, Integration of Ultrasonic Bond Signals, USAEC Report LA-DC-9383, Los Alamos Scientific Laboratory, October 1968.
59. S. J. Klima and J. C. Freche, Ultrasonic Detection and Measurement of Fatigue Cracks in Notched Specimens, Report NASA-TN-D-4782 (N68-35071), National Aeronautics and Space Administration, Lewis Research Center, September 1968.
60. Argonne National Laboratory, Reactor Development Program Progress Report, September 1968, USAEC Report ANL-7500, pp. 100-101, Oct. 29, 1968.
61. S. Peterson (Comp. and Ed.), Metals and Ceramics Division Annual Progress Report for Period Ending June 30, 1968, USAEC Report ORNL-4370, pp. 125-129, Oak Ridge National Laboratory, October 1968.
62. P. H. Hutton, Nuclear Reactor System Noise Analysis, Dresden I Reactor, Commonwealth Edison Company, USAEC Report BNWL-867, Battelle–Northwest, October 1968.
63. D. C. Worlton, Recent Nondestructive Testing Advances at Battelle–Northwest Laboratory, USAEC Report BNWL-SA-1772 (Pt. I), Battelle–Northwest, May 1, 1968.

LEGAL NOTICE

This journal was prepared under the sponsorship of the U. S. Atomic Energy Commission. Neither the United States, nor the Commission, nor any person acting on behalf of the Commission:

A. Makes any warranty or representation, expressed or implied, with respect to the accuracy, completeness, or usefulness of the information contained in this journal, or that the use of any information, apparatus, method, or process disclosed in this journal may not infringe privately owned rights; or

B. Assumes any liabilities with respect to the use of, or for damages resulting from the use of any information, apparatus, method, or process disclosed in this journal.

As used in the above, "person acting on behalf of the Commission" includes any employee or contractor of the Commission, or employee of such contractor, to the extent that such employee or contractor of the Commission, or employee of such contractor prepares, disseminates, or provides access to, any information pursuant to his employment or contract with the Commission, or his employment with such contractor.

Nuclear Science Abstracts

The U. S. Atomic Energy Commission, Division of Technical Information, publishes *Nuclear Science Abstracts (NSA)*, a semimonthly journal containing abstracts of the literature of nuclear science and engineering.

NSA covers (1) research reports of the U. S. Atomic Energy Commission and its contractors; (2) research reports of government agencies, universities, and industrial research organizations on a worldwide basis; and (3) translations, patents, books, and articles appearing in technical and scientific journals.

Complete indexes covering subject, author, source, and report number are included in each issue. These indexes are cumulated and sold separately.

Availability of NSA

SALE *NSA* is available on subscription from the Superintendent of Documents, U. S. Government Printing Office, Washington, D. C. 20402, at $42.00 per year for the semimonthly abstract issues and $38.00 per year for the cumulated-index issues. Subscriptions are postpaid within the United States, Canada, Mexico, and all Central and South American countries, except Argentina, Brazil, Guyana, French Guiana, Surinam, and British Honduras. Subscribers in these Central and South American countries, and in all other countries throughout the world, should remit $52.50 per year for subscriptions to semimonthly abstract issues and $47.50 per year for the cumulated-index issues. The single-copy price for the abstract issues is $1.75 postpaid, with this exception: Add one-fourth of $1.75 for mailing to the countries to which the $52.50 subscription rate applies.

EXCHANGE *NSA* is also available on an exchange basis to universities, research institutions, industrial firms, and publishers of scientific information. Inquiries should be directed to the Division of Technical Information Extension, U. S. Atomic Energy Commission, P. O. Box 62, Oak Ridge, Tennessee 37830.

UNITED STATES
ATOMIC ENERGY COMMISSION
P.O. BOX 62
OAK RIDGE, TENNESSEE 37830

OFFICIAL BUSINESS

POSTAGE AND FEES PAID
U.S. ATOMIC ENERGY COMMISSION

MR. R.E. CHAPIN 1
DIRECTOR OF LIBRARIES
MICHIGAN STATE UNIVERSITY
EAST LANSING, MICHIGAN 48823

DOCUMENTS
JUN 14 1969
MICHIGAN STATE UNIVERSITY
LIBRARIES

TECHNICAL PROGRESS REVIEWS may be purchased from Superintendent of Documents, U. S. Government Printing Office, Washington, D.C. 20402. *Nuclear Safety* at $3.50 per year (six issues) for each subscription or $0.60 per issue, each of the other journals at $2.50 per year (four issues) or $0.70 per issue. The use of the order form below will facilitate the handling of your order.

POSTAGE AND REMITTANCE: Postpaid within the United States, Canada, Mexico, and all Central and South American countries except Argentina, Brazil, Guyana, French Guiana, Surinam, and British Honduras. For these Central and South American countries and all other countries: add, for each annual subscription, $1.00 for *Nuclear Safety* and $0.75 for each of the other journals; for single issues, add one-fourth of the single-issue price. Payment should be by check, money order, or document coupons, and MUST accompany order. Remittances from foreign countries should be made by international money order or draft on an American bank payable to the Superintendent of Documents or by UNESCO book coupons.

---

order form

SUPERINTENDENT OF DOCUMENTS
U. S. GOVERNMENT PRINTING OFFICE
WASHINGTON, D. C. 20402

Please send	1, 2, or 3 years
☐ Isotopes and Radiation Technology	____
☐ Nuclear Safety	____
☐ Reactor and Fuel-Processing Technology	____
☐ Reactor Materials	____

Enclosed: document coupons ☐ check ☐ money order ☐

Charge: Superintendent of Documents No._____

SUPERINTENDENT OF DOCUMENTS
U. S. GOVERNMENT PRINTING OFFICE
WASHINGTON, D. C. 20402

(Print clearly)

_____
Name

_____
Street

_____
City, State, ZIP Code